Investigation of an Adsorption System for the Seasonal Storage of Heat Applied to Residential Buildings

Maria Mottillo

A Thesis

in

The Department

of

Building, Civil and Environmental Engineering

Presented in Partial Fulfillment of the Requirements
for the Degree of Master of Applied Science (Building Engineering) at
Concordia University
Montréal, Québec, Canada

January 2006

CONCORDIA UNIVERSITY

School of Graduate Studies

This is to certify that the thesis prepared

By: Maria Mottillo

Entitled: Investigation of an Adsorption System for the Seasonal Storage of Heat Applied to Residential Buildings

and submitted in partial fulfillment of the requirements for the degree of

Master of Applied Science (Building Engineering)

complies with the regulations of the University and meets the accepted standards with respect to originality and quality.

Signed by the final examining committee:

_____ Chair

_____ Examiner

_____ Examiner

_____ Examiner

_____ Supervisor

Approved by _____

Chair of Department or Graduate Program Director

_____ 20___ _____

Nabil Esmail, Dean of Engineering & Computer Science

ABSTRACT

Investigation of an Adsorption System for the Seasonal Storage of Heat Applied to Residential Buildings

Maria Mottillo

Residential fuel cell cogeneration systems are being targeted as energy–efficient alternatives to conventional power plants to heat and power our homes. However, when a fuel cell is controlled to meet a house's electrical load, there may be an excess amount of heat that is available in the summer when a house's thermal requirements are minimal. The objective of this work is to investigate the feasibility of coupling an adsorption system to a residential fuel cell cogeneration system for the seasonal storage of the fuel cell's surplus thermal output. A mathematical model of an adsorption storage system is developed, by applying first principles, and implemented into the ESP-r building energy simulation program. The model is validated using published data and verified using a sensitivity analysis technique. Finally, the predicted annual energy performance of a house served by a fuel cell cogeneration system coupled to an adsorption storage system is compared to the predicted annual energy performance of two alternate heating systems using ESP-r, taking into account the dynamic nature of the house's electrical and thermal loads. For the set of operating conditions considered in the study, the adsorption storage unit is able to improve the overall energy performance of the residential fuel cell cogeneration system in the winter but not in the summer. Simulation results show that factors such as the utility grid's generation source and the capacity of the adsorption storage unit influence whether the energy performance of the residential fuel cell cogeneration system surpasses the energy performance of a conventional heating system.

ACKNOWLEDGEMENTS

I would like to express my sincere gratitude to my thesis supervisor, Dr. Radu Zmeureanu, for his guidance throughout my post-graduate studies at Concordia University and, in particular, during the preparation of this thesis.

I am indebted to my supervisor at Natural Resources Canada, Dr. Ian Beausoleil-Morrison, for his support and invaluable advice during the course of my studies. I would also like to thank Ian for understanding my distracted state of mind at the office on many occasions. I would like to thank Mark Riley, Frank Campbell and Bryan Cook at Natural Resources Canada for supporting my decision to continue my studies and for making it possible to do so with financial support. Many thanks to all of my colleagues at Natural Resources Canada for their encouragement, with special thanks to Alex Ferguson and Phylroy Lopez for answering many of my ESP-r- and Linux- related questions.

I am extremely grateful to my family and friends for their love and understanding these past three years.

The completion of this thesis would not have been possible without the love, patience and support of my husband, Stephen Day. Stephen supported me in many ways; from picking me up at the bus station late at night to listening to me ramble on about my work, no matter what mood I was in, always unselfishly.

In the memory of Nonna Serafina and Nonno Michele

TABLE OF CONTENTS

LIST OF FIGURES

LIST OF TABLES

LIST OF SYMBOLS

As	Surface area	$[m^2]$
COA	Coefficient of amplification	
COP	Coefficient of performance	
Cp	Specific heat	$[J/kg°C]$
D	Coefficient of Dubinin-Astakhov equation	
E	Internal energy	$[J]$
h_{amb}	Overall heat transfer coefficient to ambient	$[W/m^2°C]$
h_{fg}	Latent heat of vaporization	$[J/kg]$
k	Thermal conductivity	$[W/m°C]$
L	Length	$[m]$
m	Mass	$[kg]$
$\dot{m}$	Mass flow rate	$[kg/s]$
n	Coefficient of Dubinin-Astakhov equation	
P	Pressure	$[Pa]$
Q	Heat	$[J]$
$\dot{Q}$	Heat flow rate	$[W]$
r	Heat-recovery ratio	
R	Thermal resistance	$[m^2°C/W]$
SCP	Specific cooling power	$[W/kg]$
SHP	Specific heating power	$[W/kg]$
t	Time	$[seconds]$
T	Temperature	$[°C]$
W	Work	$[J]$
$\dot{W}$	Rate of work	$[W]$
W_o	Volume of adsorption space	$[m^3/kg\ adsorbent]$
X	Ratio of adsorbate mass to adsorbent mass	$[kg/kg\ adsorbent]$

Greek symbols

ΔH	Enthalpy of adsorption	*[J/kg]*
ΔT^*	Temperature interval used to evaluate $\frac{\partial X}{\partial T}$	*[°C]*
ε	Effectiveness	
η	Efficiency	
ρ	Density	*[kg/m^3]*

Subscripts

a	Adsorption/Adsorber
air	Outdoor air
amb	Ambient
aux-burner	Auxiliary burner
c	Condensation/Condenser
c-e	Condenser/Evaporator
charge	Charging cycle
cond-fan	Condenser fan
cycle	Charging/discharging cycle
d	Desorption
discharge	Discharge cycle
e	Evaporation/Evaporator
evap	Evaporator
f	Heat transfer fluid
fc	Fuel cell
h/x	Heat exchanger
i	Adsorber insulation layer
liq	Liquid
loss	Losses to ambient
min	Minimum
max	Maximum
r	Reservoir

ref	Reference
reg	Regeneration
sat	Saturation
tank	Water storage tank
vap	Vapour
vap,flow	Vapour flow between adsorber and condenser/evaporator
vessel	Adsorber vessel
w	Water
z	Zeolite (adsorbent)

Superscripts

t	Value at the beginning of a simulation time-step
$t+\Delta t$	Value at the end of a simulation time-step

1 INTRODUCTION

The expected negative effects of global warming include increased levels of smog in urban areas as well as extreme weather conditions such as droughts, ice storms and floods. In order to address climate change and protect our environment, Canada ratified the Kyoto Protocol in 2003. The Kyoto Protocol, an international response to climate change developed within the United Nations framework, establishes legally binding targets for the reduction of greenhouse gas emissions and sets timeframes for these targets to be met, under the assumption that the increase in concentration of greenhouse gases leads to climate change. Canada's target is to lower its greenhouse gas emissions to six percent below 1990 levels during the first commitment period of 2008 - 2012. At present, greenhouse gas emissions in Canada have increased 18% since 1990 (Environment Canada, 2005).

The reduction of greenhouse gas emissions requires the implementation of energy efficient practices in buildings, industry and transportation. Approximately thirty percent of the greenhouse gases that are produced by human activity are due to the energy consumption in buildings – energy consumed for heating and cooling, appliances, equipment and lighting (NRCan, 2001). The research and development of new technologies that can reduce the energy consumption of these end-uses are important for the environment and to help Canada meet its international commitment.

The objective of this work is to investigate the feasibility of a technology that has the potential to reduce the energy consumed to heat residential buildings, namely a seasonal storage system coupled to a fuel cell cogeneration system.

1.1 Fuel Cells

The British physicist Sir William Robert Grove invented the fuel cell in 1839. Although the initial application of fuel cell technology in the 1950s was restricted to space applications, the interest to develop fuel cells for both vehicles and buildings has increased in the past few decades with the need for environmentally-friendly technologies in these areas. Fuel cells for residential applications are attractive because it is claimed that they can provide all the heat and power requirements of private households at a higher efficiency and lower emissions than conventional power plants (Wolk, 1999). As well, they can be used in areas not served by an electric power grid, or where the power grid is unreliable. It is expected that residential fuel cells will become available to the public in the near future. The types of fuel cells targeted for small-scale stationary applications (< 10 kW electric power output) are: (1) the proton exchange membrane (PEM) fuel cell and (2) the solid oxide fuel cell (SOFC). In North America, Fuel Cell Technologies Ltd. is developing a modular 5 kW SOFC system (FCT, 2004), while Ballard Power Systems and EBARA Corporation of Japan are developing a 1 kW PEM fuel cell to operate in conjunction with the existing utility grid (Ballard, 2004). The SOFC and PEM fuel cells are discussed later in this section.

Fuel cells use an electrochemical process to convert chemical energy into electrical energy. Like a battery, a fuel cell consists of two electrodes, an anode and a cathode, separated by an electrolyte, which may be a solid or a liquid layer. Fuel cells are commonly categorized by their type of electrolyte. Table 1.1 lists several types of fuel cells and the electrolyte material for each type (Wolk, 1999), (U.S. DOE, 2000).

Table 1.1 Fuel cell types

Type	Electrolyte Material	Operating Temperature
Alkaline	Liquid potassium hydroxide	65 °C – 220 °C
Proton Exchange Membrane (PEM)	Solid polymer such as perfluorinated-sulfonic acid	80 °C
Phosphoric Acid Fuel Cell (PAFC)	Liquid phosphoric acid	205 °C
Molten Carbonate Fuel Cell (MCFC)	Liquid molten alkali such as potassium or sodium carbonate	650 °C
Solid Oxide Fuel Cell (SOFC)	Solid ceramic such as yttria-stabilized zirconia	600 °C – 1000 °C

Unlike a battery that stores the chemical reactant, a fuel cell operates continuously as hydrogen is fed to the anode and an oxidant (oxygen or air) is fed to the cathode. The chemical reaction that takes place at the anode results in electrons being released to an external circuit. These electrons travel via the external circuit to the cathode where they react with the oxidant. The formation of ions will occur at one of the electrodes (anode or cathode), depending on the type of fuel cell, and the ions will be conducted through the electrolyte layer to the other electrode, taking part in the reaction that occurs there. The nature of the reactions that take place at the electrodes, the ions that are formed and the direction the ions travel will depend on the type of fuel cell, fuel type and oxidant that are

used (U.S. DOE, 2000). Figure 1.1 presents the reactions for a solid oxide fuel cell with pure oxygen as the oxidant and pure hydrogen as the fuel. In this case, oxide ions are formed at the cathode and are conducted through the electrolyte to the anode. At the anode, hydrogen reacts with the oxide ions releasing water vapour and electrons. The water vapour is exhausted while the electrons travel via the external circuit to the cathode and react with oxygen, forming the oxide ions and thereby completing the process.

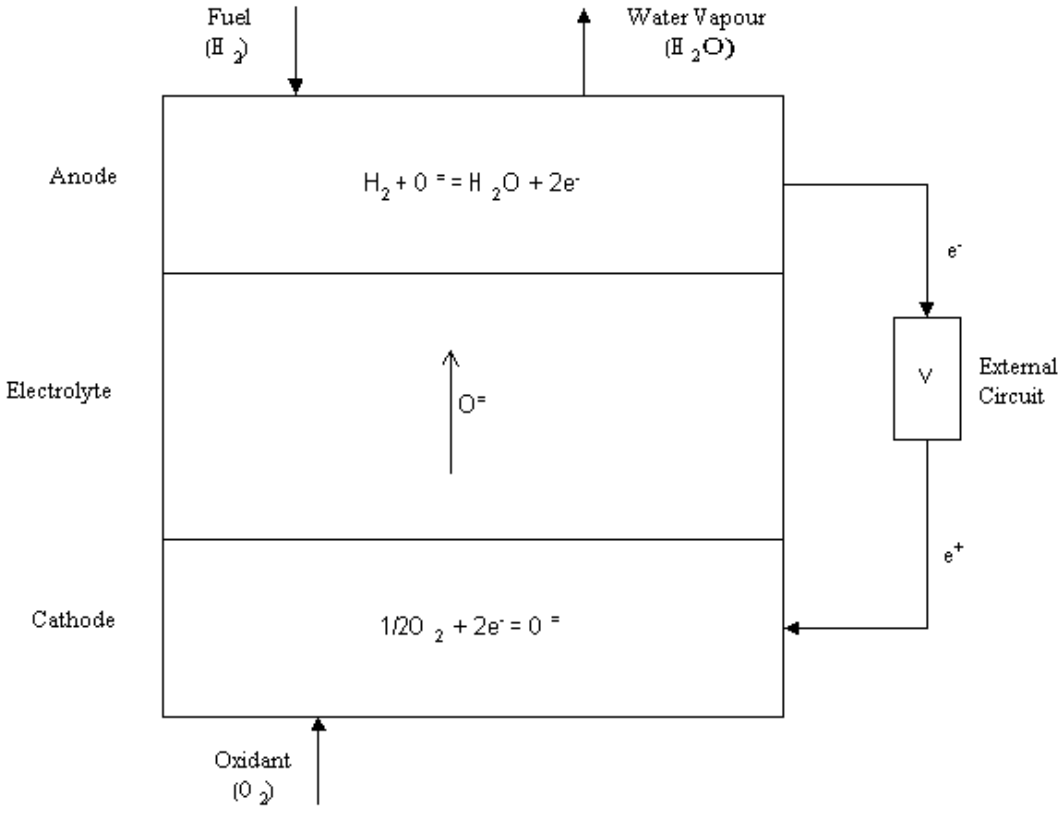

Figure 1.1 Reactions in a solid oxide fuel cell

Most of the small stationary fuel cells that have been developed at the present time have been fuelled by natural gas, a practical source of hydrogen as pure hydrogen is not readily available and can be hazardous. When natural gas is the fuel source, hydrogen must be extracted by processing the natural gas, most commonly with steam (this process, referred to as reforming, is endothermic). Fuel cells with low operating temperatures (90 °C) or intermediate operating temperatures (200 °C) require that natural gas be reformed to hydrogen externally, whereas fuel cells with high operating temperatures (> 600 °C) can internally reform natural gas to hydrogen (U.S. DOE, 2000). The operating temperatures of different fuel cell types are provided in Table 1.1. The reforming process will result in the production of hydrogen and carbon monoxide. External reforming fuel cells will require another reaction (referred to as a water shift reaction) to convert the carbon monoxide to hydrogen and carbon dioxide, whereas internally reforming fuel cells will not – both the hydrogen and carbon monoxide are fed to the anode where they will react with the ions internally to form water vapour and carbon dioxide. For example, the reforming reactions for methane (CH_4) are:

Externally reforming fuel cells:

$$CH_4 + H_2O = CO + 3H_2$$
$$H_2O + CO = H_2 + CO_2$$
$$H_2 + O^{=} = H_2O + 2e^{-} \quad (1.1)$$

Internally reforming fuel cells:

$$CH_4 + H_2O = CO + 3H_2$$
$$H_2 + O^{=} = H_2O + 2e^{-}$$
$$CO + O^{=} = CO_2 \quad (1.2)$$

For both internally and externally reforming fuel cells, the use of natural gas as the fuel source will result in the formation and exhaust of carbon dioxide. For internally reforming fuel cells, the carbon dioxide is a product of the fuel cell reactions whereas for

externally reforming fuel cells, carbon dioxide is a product of the reforming process. The exhaust gases, namely water vapour, carbon dioxide, any excess hydrogen and/or carbon monoxide, produced by the reactions within the fuel cell are at a high temperature, thus providing an opportunity for the cogeneration of heat and power. The temperature of the heat available for recovery is approximately equal to the fuel cell's operating temperature.

A fuel cell system can be described by its electrical efficiency and/or its cogeneration efficiency. The electrical efficiency of a fuel cell is defined as the cell's net electrical output in relation to the chemical energy contained within the fuel that is input to the cell. The net electrical output of the fuel cell takes into account the parasitic losses of the system (for example, power consumed to operate fans, pumps, the control unit), any losses during the reforming process (for externally reforming fuel cells) and any losses due to the conversion of electricity from DC to AC (Thorstensen, 2001). The cogeneration efficiency of a fuel cell is defined as the ratio of useful energy delivered by the fuel cell (electric power and heat) to the fuel's chemical energy input, taking into account the performance of heat recovery devices. A fuel cell system's cogeneration efficiency is thus a better performance indicator for cogeneration applications. Efficiency ratings are generally provided based on the lower heating value of the fuel. Generally, the electrical efficiency of a fuel cell system is in the range of 40-60%, while the cogeneration efficiency can reach 80% (Wolk, 1999).

An analysis based on the model of an internally reforming SOFC cogeneration system found that this technology has the potential for delivering high system efficiencies in residential buildings (Beausoleil-Morrison et al., 2002a). In the study, a 5kW SOFC system serves a modern, energy-efficient house of typical dimensions located in Montréal. The model assumes that the fuel cell has three different modes of operation: (1) it can respond to the house's electrical demand so that heat from the unit is only available when such a demand exists, (2) the fuel cell can operate at a constant electrical and thermal output, or (3) it can operate to meet the thermal load of the house. In the study, the fuel cell is controlled to respond to the house's electrical demand while the thermal output of the SOFC is transferred to a water storage tank that supplies the house's domestic hot water (DHW) and space heating loads. When the SOFC's thermal output exceeds the space heating and DHW load, a safety device rejects the excess thermal output from the water storage tank. When the SOFC's thermal output is insufficient to meet the DHW and space heating requirements, the water storage tank's backup natural gas burner cycles on. The study found that the total efficiency (electrical plus thermal) of the SOFC cogeneration system is 68% in terms of the fuel's lower heating value.

Natural Resources Canada estimates residential end-use energy consumption by using a residential end-use model to aggregate data collected from Statistics Canada (NRCan, 2001). Figure 1.2 presents the breakdown of the yearly energy consumption of a typical Canadian house by end-use, determined using the data from (NRCan, 2001). The values presented in Figure 1.2 are determined by dividing the total energy consumption of each end-use (considering all energy sources) by the total number of households. The heating

energy accounts for 65218 MJ/yr, or 58% of the total yearly energy consumption of the house, while domestic hot water heating accounts for 24880 MJ/yr, or 22%. Therefore, the thermal requirements of a typical Canadian house accounts for a total of 90098 MJ/yr, or 80% of the house's total energy consumption. Ideally, a fuel cell system will be able to meet both the electrical and thermal requirements of a house.

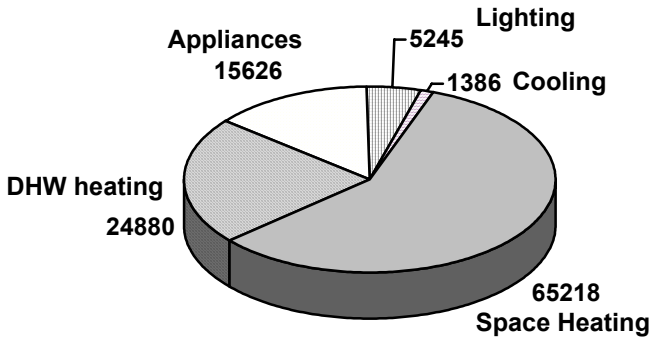

Figure 1.2 Yearly energy consumption of a typical Canadian house by end-use in MJ/year (data for 2001) (NRCan, 2001)

(Beausoleil-Morrison et al., 2002a) found that during the summer when the heating system is shut off (May through September), and in the swing months of April and October, when the space heating requirements are minimal, the thermal output of the fuel cell was greater than the house's thermal load and therefore the safety device operates frequently. Over the year, 25% of the SOFC's thermal output is rejected in order to prevent over-heating of the water storage tank. However, the yearly thermal load of the house (including space heating and domestic hot water heating) could not be satisfied

when the fuel cell was operated to respond to the house's electrical load. During the entire year, the SOFC was able to meet only 36% of the house's thermal load, with the tank's natural gas burner having to supply the remaining heating energy during the winter season.

The overall efficiency of the fuel cell system would be increased if the heat that is rejected primarily in the summer months can be stored and used during the winter months when the fuel cell cannot meet the house's thermal requirements. The mismatch in heat supply and demand can possibly be corrected with the use of a seasonal heat storage system in an effort to decrease the amount of heat that is wasted and increase the efficiency of the entire system.

It should be noted that, alternatively, the fuel cell system can operate continuously at a constant electrical and thermal output or the fuel cell system can operate to meet the thermal requirements of the house primarily. In the former case, the efficiency of the system will likely decrease as there will be a surplus of both electrical and thermal energy at different periods of the day and year. In the latter case, power may not be available when required (for example, during periods where there is no thermal demand) or may be available when not required (for example, at night when there is a thermal load but no electrical load), thereby reducing the efficiency of the system or requiring an electrical storage system.

This work addresses the question of whether a seasonal heat storage system can increase the overall efficiency of a residential fuel cell system that operates to respond to a house's electrical load.

1.2 Adsorption Storage

Thermal energy storage (TES) systems can be classified into three categories: sensible heat storage, latent heat storage and thermo-chemical storage. Sensible heat storage systems store thermal energy by an increase in the internal energy of the system, identified by a change in temperature of the storage medium. Possible storage mediums of sensible heat include water, air, rock beds, bricks and soil. Latent heat storage systems use the latent heat available when materials undergo a phase change, for instance from solid to liquid or from liquid to vapour. Possible phase change materials (PCM) include water/ice, salt hydrates and organic compounds. Thermo-chemical storage systems use the heat available from reversible chemical reactions. Adsorption storage systems fit into this latter category since the adsorption process, a reversible physico-chemical reaction, is used to store heat.

Sensible heat storage systems and thermo-chemical storage systems are being investigated for the seasonal storage of heat (Dinçer et al., 2002), (Visscher et al., 2005). Latent heat storage systems are being investigated for short-term (daily) storage applications where the phase change materials are either incorporated in the building materials to increase thermal mass, within solar thermal walls for storing excess solar

energy during the day for heating at night, or are combined with radiant floor systems for load-shifting to off-peak hours (Stritih, 2003), (Métivaud et al., 2005).

The low storage density of sensible heat storage materials, such as water or rock, in comparison to thermo-chemical storage materials favour the latter when the storage volume available is limited. The storage densities for water, rock and two different thermo-chemical systems are provided in Table 1.2. Energy densities of thermo-chemical storage systems are up to ten times greater than those of water storage systems.

Table 1.2 Storage densities of different media (MJ/m^3)

Sensible heat storage media	Water	83[1]
	Rock	43[2]
Thermo-chemical storage media	Zeolite/Water	432-720[3]
	Silica Gel/Water	900 [4]

[1] Based on density of 1000 kg/m3, specific heat of 4.19 kJ/kgK and temperature difference of 20K.
[2] Based on density of 2500 kg/m3, specific heat of 0.88 kJ/kgK and temperature difference of 20K.
[3] Range provided in (Fischer and Hauer, 1998).
[4] Maximum value provided in (Mittelbach and Henning, 1997).

Adsorption storage systems are briefly described in this chapter. The principles of adsorption, a review of the status of adsorption storage technology and a description of existing models of adsorption storage systems are described in chapter 2.

Adsorption is a thermo-chemical process. The adsorption process is represented by the reaction:

$$C(s) \leftrightarrow A(s) + B(g) \qquad (1.3)$$

where C represents the wet adsorbent, A represents the dry adsorbent, B represents the adsorbate in vapour form and (s) and (g) denote the solids phase and vapour phase, respectively. The forward reaction is endothermic, so that heat is required to separate C into the products A and B. The heat of adsorption is the energy that will be stored in the system. As long as the products of the forward reaction (A and B) are kept separate, the energy of the adsorption process is stored. The backward reaction is exothermic, so that heat is released when the products A and B are allowed to react to form the product C. The products A and B are defined as the working pairs of the adsorption storage system.

The conditions for a chemical reaction to be suitable for storage purposes are: (1) the reactants and products must be safe (non-toxic, non-corrosive and non-flammable), (2) the reactants and products should have good thermal conductivities, (3) there should not be any side reactions that occur which may affect the reversibility of the reaction (the chemical reaction must be reversible in order to repeatedly store and then release the stored heat) and (4) there should be no degradation in performance as the reaction is repeated. In addition to these factors, the temperature that is required for the forward endothermic reaction to occur must be the minimum temperature of the heat source, and the temperature that results from the backward exothermic reaction must be suitable for the intended use of the stored heat (De Maria et al., 1985), (Wentworth and Chen, 1976).

The turning temperature of a reversible chemical reaction is defined as the temperature at which the reactants and products of the reaction are at equilibrium, so that neither the forward reaction nor the backward reaction occurs. At temperatures greater than or equal

to the turning temperature, the forward endothermic reaction is favoured while at temperatures less than the turning temperature, the backward exothermic reaction is favoured. Therefore, temperatures greater than or equal to the turning temperature are required to charge the system while temperatures less than the turning temperature will be available from the storage system during the discharge phase. The turning temperature is therefore a good indicator of the chemical reactions that are suitable for a particular application.

The turning temperature is defined as the ratio of the change of enthalpy for the reaction to the change in entropy for the reaction. For an efficient storage of energy, the enthalpy change of the reaction must be large so that a large quantity of heat can be stored as the reaction moves forward. In order to keep the turning temperature within a practical range of operating temperatures, the entropy change of the reaction must also be large. Reactions with large entropy changes are observed in decomposition reactions in which the reactants are in a condensed phase and at least one of the products is in the gas phase (Casarin and Ibanez, 1993). The adsorption process where an adsorbent-adsorbate pair decomposes as heat is added into a solid dry adsorbent and a vapour adsorbate falls into this category.

Table 1.3 presents several chemical reactions that have been identified as suitable for heat storage purposes. Turning temperatures are provided for several reactions whereas the range of operating temperatures is provided for others if the former was not available from the literature.

Table 1.3 Chemical reactions investigated for storage applications

Reaction	Adsorbent	Adsorbate	Turning temperature/Operating temperature range (ºC)
	Zeolite[1]	Water	20-350[2]
	Charcoal	Water	30-250[2]
$Al_2O_3 \cdot 3H_2O \Leftrightarrow Al_2O_3 + 3H_2O$	Active alumina	Water	30-250[2]
$SiO_2 \cdot nH_2O \Leftrightarrow SiO_2 + nH_2O$	Silica gel	Water	20-150[2]
$MgCl_2 \cdot 4H_2O \Leftrightarrow MgCl_2 \cdot 2H_2O + 2H_2O$	Magnesium chloride dihydrate	Water	107[3]
$Na_2S \cdot 5H_2O \Leftrightarrow Na_2S \cdot 0.5H_2O + 4.5H_2O$	Sodium sulfide	Water	80[4]
$Mg(OH)_2 \Leftrightarrow MgO + H_2O$	Magnesium oxide	Water	325[3]
$Ca(OH)_2 \Leftrightarrow CaO + H_2O$	Calcium hyroxide	Water	525[3]
	Zeolite[1]	Methanol	- [2]
	Activated carbon	Methanol	20-140[2]

[1]Different types of zeolite have been investigated: 13X, 4A, 5A, 10A, MgA.
[2](Ülkü and Mobedï, 1989).
[3](Ervin, 1977).
[4](Bach and Haije, 1999).

An adsorption storage unit essentially contains the following components: a container which contains the adsorbent, commonly referred to as the adsorber, a container that acts as a condenser or an evaporator, a valve and a pipe that connects the adsorber and the condenser/evaporator. The working principle of an adsorption storage unit can best be described by its three stages: charging, storage and discharge. Figure 1.3 illustrates the charging and discharge stages.

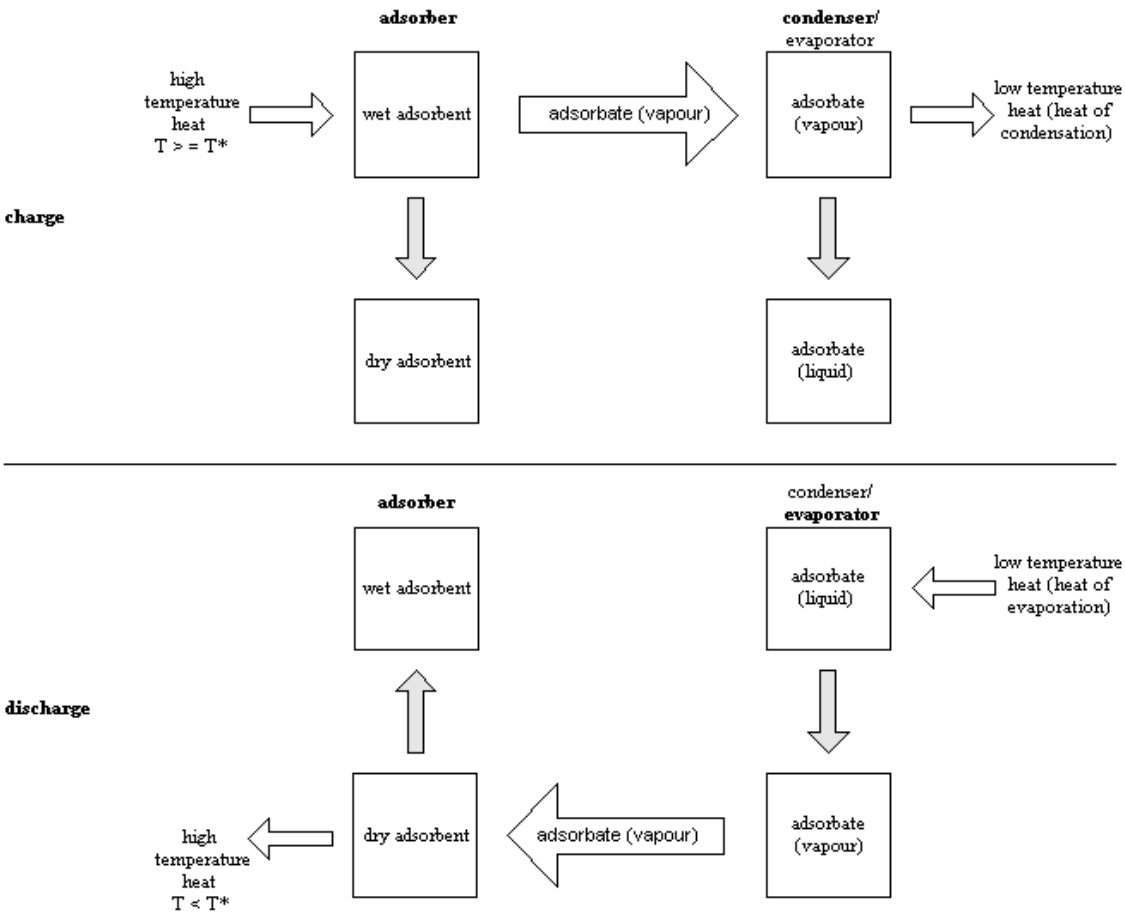

Figure 1.3 Stages of an adsorption storage unit (T* denotes turning temperature)

At the start of the charging process, the valve between the adsorber and the condenser/evaporator is closed. In order for the endothermic forward reaction to occur, heat at a temperature greater than the turning temperature must be supplied to the adsorber. Such heat flow can be obtained from a fuel cell, for example. Heat is supplied to the adsorber by a fluid that flows through a heat exchanger within the adsorber. As high temperature heat is supplied to the adsorber, the pressure in the adsorber increases, as the adsorbate leaves the adsorbent. When the pressure reaches the condenser pressure the valve between the adsorber and the condenser is opened. Desorption of the adsorbent

occurs and the vapour that is desorbed, referred to as the adsorbate, travels to the condenser, where it is converted to liquid form. This process continues until the adsorber reaches the charging temperature. The valve is now closed. At this point, the adsorber is dry as the maximum amount of adsorbate, a function of the operating temperatures and working pair of the unit, has been desorbed from the adsorbent. The heat of condensation that is released as the adsorbate is condensed can be rejected or used. During the storage stage, the liquid adsorbate in the condenser/evaporator is kept separate from the adsorbent in the adsorber, by keeping the valve connecting the two components closed.

During the discharge stage, the backward exothermic reaction occurs. Fluid at a lower temperature flows through the adsorber's heat exchanger, recovering the adsorber's heat and causing a pressure drop in the adsorber. When the pressure in the adsorber reaches the evaporator pressure, the valve connecting the adsorber to the evaporator is opened. The adsorbate in liquid form is evaporated with low temperature heat supplied to the evaporator. As it evaporates, the adsorbate in vapour form goes to the adsorber where it is adsorbed by the adsorbent. This results in the release of the heat of adsorption that was stored in the unit. This released heat will be at a temperature less than the turning temperature and will be available until the adsorbent bed has adsorbed all of the adsorbate that it can contain at the particular operating conditions of the unit. At this point the adsorbent is wet and the valve is closed. In addition to their high storage density, adsorption storage systems appear suitable for seasonal heat storage because of their potential to store heat for a long period of time with minimal heat losses. Although sensible heat losses will occur as the adsorption storage unit loses heat to its

surroundings, the greater portion of the heat that is stored within the unit is stored within a chemical reaction. The backward chemical reaction, which is exothermic, is only allowed to occur when the products of the forward reaction are allowed in contact with one another so that the heat of the chemical reaction can be stored indefinitely as long as the products are kept separate. In their study of an adsorption storage system for the seasonal storage of solar heat, (Mittelbach and Henning, 1997) found that more than 80% of the energy input to the storage unit is stored as chemical energy while the remaining 20% is stored as sensible energy.

At present, adsorption storage technology is at the research and development stage. A review of the present state of the technology is provided in chapter 2.

1.3 Building Energy Simulation

A building model is a mathematical representation of the various components within a particular building: the building envelope, heating, ventilating and air conditioning (HVAC) system, lighting system, electrical system and occupants; and their interactions, exposed to climatic conditions. A computer model of a building is the description of the building model in a software-based environment. Building energy simulation is the use of the building and computer models to predict the energy performance of the building. Computer modelling and simulation is increasingly being used as a tool to evaluate different design options during the building design process, to determine compliance to energy standards and programs and to predict the impact of energy saving retrofits.

Computer modelling and simulation can also be used to analyze a system that does not currently exist in order to investigate its feasibility and to improve its design. In this context, the advantage of using computer modelling and simulation versus doing experimental work is that it is generally faster and less expensive, and models can be adapted easily to consider different operating conditions or system configurations (Hensen, 1991). However, computer modelling and simulation and experimental work are complimentary, as the latter is necessary to uncover unknown phenomena, to provide experimental data for the theoretical parameters and for model validation.

The building energy simulation programs that are available and used in practice are either based on a weighting factor method, a heat balance method or a thermal network method (ASHRAE, 2001) for the calculation of the space thermal loads. All of these methods provide a solution to the differential equations that govern the heat transfer processes that occur within buildings.

The DOE-2 energy simulation program uses the weighting factor method (U.S. DOE, 1982), while TRNSYS (SEL, 1994) and EnergyPlus (U.S. DOE, 2001) are based on the heat balance method of solution. The weighting factor method used by DOE-2 and the heat balance method used by TRNSYS and EnergyPlus use conduction transfer functions to relate the heat transfer through walls at a certain time-step to the current and past wall surface temperatures and the past heat fluxes through the wall. The weighting factor method used by DOE-2 then uses another set of transfer functions, or response factors, to relate the zone air temperature to the net energy load of the zone, while the heat balance

method used by TRNSYS and EnergyPlus determines the zone air temperature by solving the energy conservation equations for each zone, interior surfaces and exterior surfaces simultaneously.

The weighting factor method assumes that the heat transfer processes can be represented by linear differential equations. Any non-linear processes, such as natural convection or radiation, are approximated linearly (U.S. DOE, 1982). The weighting factor method also assumes that properties of the system are independent of time or temperature. This method uses the superimposition principle: each component's response is determined independently of the other components within the system and the response of the overall system is determined by summing the responses of the individual components. This method will lead to inaccurate results when the components of the system strongly interact.

The thermal network method involves the discretization of the building into a network of nodes. One or more nodes represent each building component, and each node is assigned a set of governing conservation equations (mass, momentum and energy). The result is a set of partial differential equations that are solved simultaneously using numerical techniques. In this case, the governing equations are not decoupled and the assumptions of the weighting factor method (linear differential equations and constant system properties) are not required.

Although both the heat balance method and thermal network method use numerical methods of solution, generally fewer nodes are considered in the heat balance method to represent the building. For example, the heat balance method may use conduction transfer functions to calculate the transient heat conduction through walls, which results in each wall component being represented by two nodes (interior surface node and exterior surface node). The thermal network model can accommodate additional nodes to represent each wall component.

The advantages of the numerical method of solution versus the weighting factor method are (Clarke, 2001):

- Accuracy is ensured because the entire system of partial differential equations is solved simultaneously at each computational time-step;
- Complex interactions between flow paths can be handled;
- System parameters can be dependent on time or temperature;
- Time constants can vary for different parts of the problem.

The ESP-r simulation environment, described in the next section, uses a thermal network method of representation.

1.4 ESP-r Simulation Environment

The ESP-r simulation program, developed by the University of Strathclyde, is an energy simulation program that is capable of modelling the energy and mass flows within building and plant systems that are combined and subjected to control laws (ESRU, 2002). First developed in 1974, at present a number of organisations actively participate

in developing the system further. ESP-r is being used for education and research at universities and research centres in over 20 countries worldwide (Aasem et al., 1994). ESP-r has been extensively validated with other time-step energy simulation programs, empirical data and analytical solutions (ESRU, 2002).

The structure of ESP-r is presented in Figure 1.4. The *Project Manager* module is used to create the input model that describes the building and plant configuration, and provides access to ESP-r's standard databases of construction materials, plant components, event profiles, optical properties, pressure coefficients and climate. The Project Manager also accesses the *Simulator*, which performs the time-step simulation of heat, mass, moisture and electric flows, and the *Results Analyzer*, which permits users to view the simulation results.

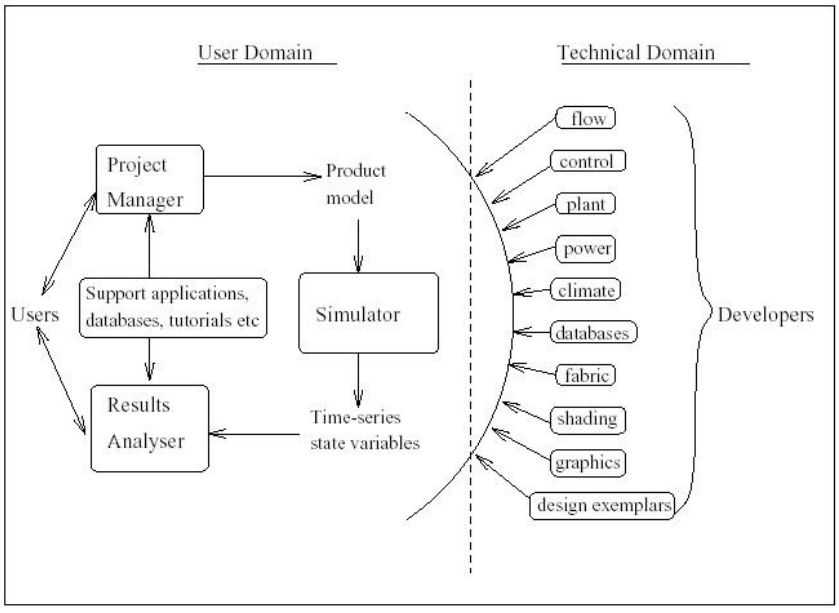

Figure 1.4 ESP-r structure (ESRU, 2002)

ESP-r's source code, written in FORTRAN 77, is organized into numerous technical domains that are integrated with the Simulator. Thus, developers who are interested in adding modelling capabilities to the program need only work with the source code that pertains to their domain of interest, without having to know and understand all aspects of the other technical domains that are part of the simulation environment. For instance, if a model to describe a plant element is being developed, the developer only needs to work with the source code in the plant technical domain without having to understand the details of the source code pertaining to other models such as the shading models, for example.

As mentioned in the previous section, ESP-r uses numerical methods to solve the partial differential equations that represent the energy, mass and momentum conservation equations governing the integrated building and plant system. The following three steps describe the process used by ESP-r to determine the thermal state of the building (Clarke, 2001):

1. The system is discretized using nodes that represent the physical volumes corresponding to room air, opaque and transparent boundary surfaces, envelope construction elements and plant components.

2. For each node, the partial differential equations that govern the conservation laws are written using finite difference methods, resulting in algebraic equations, which represent

the conservation of mass, momentum and energy at each node, by considering the interaction with its neighbouring nodes.

3. The set of algebraic equations from step 2, along with data at the current time step t, and climatic data at the future time step (t+1), is solved simultaneously to obtain the state variable at each node at the future time-step (t+1). Steps 2 and 3 are repeated for each time-step of the simulation.

The CANMET Energy Technology Centre (CETC) has added algorithms to the ESP-r simulation program to support the modelling of Canadian and international housing. The algorithms incorporated by CETC in the ESP-r program include a:

- model to calculate the total outdoor air flow to a residential building resulting from the combined effect of natural infiltration and mechanical ventilation;
- model to calculate heat losses from basements and slab-on-grade foundations in residential buildings based on a frequency-domain response factor method;
- model to predict the energy consumption of a furnace based on time-step calculations;
- model to simulate an air source heat pump for heating and/or cooling of residential buildings;
- model to simulate a heat recovery ventilator;
- plant component model to describe the performance of a fuel cell cogeneration system;

- model to describe the performance of a domestic hot water tank;
- model to describe the performance of a ground source heat pump system.

1.5 Research Objectives and Thesis Outline

Residential fuel cell systems are an emerging technology and are considered as energy efficient alternatives to power and heat our homes. Ideally, fuel cell systems can provide all of the yearly power and heat requirements of a house, thereby increasing their thermal efficiency. However, it has been shown that such systems generate excess heat in the summer and do not generate sufficient heat in the winter if they are controlled to respond to a house's electrical demand primarily. The mismatch in heat supply and demand can possibly be solved by the seasonal storage of heat. Adsorption storage systems seem advantageous when considering that these systems can store a greater amount of energy per unit volume than sensible heat storage systems.

The objective of this research is to investigate the technical feasibility of an adsorption system for the seasonal storage of heat supplied by a residential fuel cell cogeneration system. This will be done by developing a mathematical model of an adsorption storage unit and incorporating the model into a building simulation program, namely the ESP-r simulation environment. The existing model of a fuel cell cogeneration system, developed by (Beausoleil-Morrison, 2001), will also be used. The model will be validated with experimental data, when such data are available from the literature, and from sensitivity analysis techniques. Finally, the model will be applied to determine the performance of the system under a certain set of operating conditions.

Although an adsorption storage unit can be used to store waste heat from different types of cogeneration systems and/or for the storage of solar heat, the focus of this research will be limited to heat from a residential fuel cell system in order to expand on the work done in this area, as discussed in section 1.1. As the exhaust temperatures of solid oxide fuel cell (SOFC) systems are higher than PEM fuel cell systems, and therefore more suitable for charging adsorption storage systems, this research will focus on SOFC systems in particular.

In addition to its features described in section 1.4, the ESP-r simulation environment is chosen as the component-based program in which to incorporate the model of the adsorption storage unit because of the existing plant component models that are available within the program, namely the component models of the fuel cell cogeneration unit, water storage tanks, pumps and fans. The author's experience with ESP-r's programming modules and simulation environment is also a factor taken into consideration.

The model of the adsorption storage unit will be added to ESP-r's *Plant Components Database Management* module. This module manages a plant component database that contains a summary description and the data required by the Simulator to generate the coefficients of the differential equations that represent the conservation of energy and mass laws for each plant component.

The mathematical model that will describe the adsorption storage unit will take into account the computational time steps that will be used for the energy performance simulations, as this will impact the assumptions that can be made and the level of detail that will be required. Building-side time steps can be between ten and fifteen minutes while plant-side time steps will need to be five minutes or less for convergence and accuracy.

In Chapter 2, the fundamental principles of adsorption are presented and a literature review of adsorption systems and mathematical models of adsorption systems that have been developed is done. The mathematical model of an adsorption storage system developed for this work and its implementation in ESP-r is presented in Chapter 3. The mathematical model, and its implementation in ESP-r, is validated in Chapter 4 by comparing simulation results to published data and performing a sensitivity analysis of certain model input parameters. In Chapter 5, the ESP-r component model of the adsorption storage unit is combined with existing component models within ESP-r to form a complete plant network representing a residential cogeneration system coupled to an adsorption storage system. The energy performance of the overall system is determined and compared to two alternate systems. Finally, Chapter 6 presents conclusions and recommendations for future work.

2 LITERATURE REVIEW

The purpose of this chapter is to complement the background information provided in chapter 1 on adsorption storage technology. In particular, this chapter presents the fundamental principles of adsorption, reviews the current state of adsorption storage technology and presents existing models of adsorption systems available in the literature.

2.1 Adsorption Principles

When a porous solid is exposed to a gas for which it has an affinity, forces of attraction act between the individual gas molecules and the atoms or ions composing the solid, at the interface of the two phases (Gregg and Sing, 1982). The unbalanced forces at the phase boundary result in the adsorption of the gas by the solid. The solid is referred to as the adsorbent while the gas is referred to as the adsorbate.

There are two main types of forces acting between the adsorbent and adsorbate: physical forces and chemical forces. Physical forces include van der Waals (attractive) forces, which are always present, and electrostatic forces, which are only significant for adsorbents with an ionic structure (for example, zeolite) (Ruthven, 1984). Unbalanced physical forces lead to physical adsorption, which is governed largely by surface properties such as surface area, micropores and macropores, and size of granules (Srivastava and Eames, 1998). Unbalanced chemical forces lead to chemical adsorption. In this case, the adsorbent and adsorbate react chemically at the interface of the two phases and a new compound is formed. Chemical forces between an adsorbent/adsorbate pair are much stronger than physical forces between the pair (Ülkü and Mobedï, 1989).

The adsorption of a gas on a solid surface, physical and/or chemical, is an exothermic process. This can be understood by considering the change in free energy when adsorption occurs:

$$\Delta G = \Delta H - T\Delta S \quad (2.1)$$

The term ΔG is the change in free energy of adsorption, ΔH is the enthalpy of adsorption (often referred to as the heat of adsorption) of the gas and ΔS is the change in entropy of the gas. When a gas molecule is adsorbed at the surface of the adsorbent, it has a maximum of two degrees of translation whereas prior to adsorption, it its free state, it had three. Moreover, the rotational freedom of the adsorbed gas molecule is less than that of the molecule in its free state. Therefore, the entropy (degree of disorder) of the adsorbed gas molecule is less than the entropy of the free gas molecule and ΔS ($S_{g,adsorbed} - S_{g,free}$) is negative. In order for significant adsorption to occur, ΔG must be negative which implies that the enthalpy of adsorption (ΔH) is negative, a characteristic of an exothermic process (Ruthven, 1984). The reverse process, i.e. desorption of a gas from a solid surface, is endothermic.

The enthalpy of adsorption ΔH depends on the magnitude of the van der Waals forces, electrostatic forces, phase change and the presence of any chemical bonds (Srivastava and Eames, 1998). The enthalpy of adsorption is usually small in physical adsorption and large in chemical adsorption since physical forces are weaker than chemical forces.

Physical adsorption is a reversible process whereas chemical adsorption may be irreversible due to the possible chemical changes of the adsorbent and/or the high temperatures that are required for the forward or backward reaction to occur. This research deals with the physical adsorption process.

The amount of adsorbate that can be taken up by an adsorbent depends on the nature of the adsorbent and the nature of the adsorbate, and is a function of the adsorbate's pressure and temperature. For a given temperature, the function that relates the amount adsorbed by the adsorbent to the adsorbate's pressure is defined as an adsorption isotherm. Adsorption isotherms that result from physical adsorption can be classified into five different groups, according to the Braunauer classification (Gregg and Sing, 1982).

Different theoretical models have been developed to describe the relationship between the mass of adsorbate adsorbed by an adsorbent and the adsorbate's pressure and temperature, with each model suited to a particular group, or several groups, classified by Braunauer. For instance, the Langmuir model for monolayer adsorption is best suited for Type I isotherms. This model assumes that the gas molecules are adsorbed at a fixed number of sites, that each site can hold one gas molecule, that all sites are energetically equivalent and that there is no interaction between gas molecules that are adsorbed at neighbouring sites (Ruthven, 1984). The Langmuir model provides the following relationship between the fractional coverage of adsorbate to adsorbent, θ, (defined as the number of molecules in the adsorbed phase to the total number of adsorption sites within the adsorbent) and the adsorbate's pressure p:

$$\theta = \frac{bp}{1+bp} \tag{2.2}$$

The term b is the adsorption equilibrium constant for the adsorbent/adsorbate pair, and is a function of the adsorbate temperature. The Langmuir model is not frequently applicable to physical adsorption, as the latter most often involves multilayer, versus monolayer, adsorption.

The Brunauer, Emmett and Teller (BET) model of adsorption is an extension of the Langmuir model of adsorption and takes into account the multilayer characteristic of physical adsorption. The BET model, suitable for Type II isotherms, provides the following relationship between the fractional coverage of adsorbate to adsorbent, θ, the adsorbate pressure, p, and the saturated vapour pressure, p_s, of the adsorbate at the relevant temperature:

$$\theta = \frac{b(p/p_s)}{(1-p/p_s)(1-p/p_s+bp/p_s)} \tag{2.3}$$

The BET model is applicable when the reduced pressure p/p_s is in the range 0.5-0.35 (Ruthven, 1984).

It is helpful to identify a third theoretical model that provides adsorption equilibria for microporous adsorbents, at this time. Microporous adsorbents are defined as adsorbents with pore sizes less than 20 Å (1 Å = 10 nm), such as activated carbon, zeolites and very

fine porous silica gels. The Dubinin theory of adsorption was developed to take into account the fact that there are important differences between adsorption taking place in microporous adsorbents and adsorption taking place on the surface of adsorbents with larger-sized pores or non-porous adsorbents (Dubinin, 1967). Both the Langmuir and BET models of adsorption, described above, assume that adsorption occurs at the surface with the formation of one or more successive layers. The Dubinin theory on the other hand, characterizes adsorption in microporous adsorbents as a volume filling of the adsorption space. The following equation, known as the Dubinin-Astakhov (D-A) equation, relates the ratio of mass of the adsorbate to the mass of adsorbent in a bed, X, to the adsorbate pressure, P, and temperature, T (Lachance, 2003):

$$X(P,T) = W_o \rho(T) \exp(-D[T \ln(\frac{P_{sat}}{P})]^n) \tag{2.4}$$

The variables D and n are adsorption characteristics of the adsorbent/adsorbate pair while W_o represents the volume of the adsorption space, i.e. the micropore volume, which is a characteristic of the adsorbent. The variable ρ(T) is the density of the adsorbate in its bulk liquid form, which is a function of the adsorbate temperature. Although different equations pertaining to Dubinin's theory exist, they are all of the same form as the D-A equation provided above.

Physical adsorption of water on dessicants is used extensively for dehumidification and/or drying in air processing applications. The use of adsorption processes for storage,

heat pump and refrigeration applications is currently at the laboratory testing stage with promising developments in Europe, Japan and the U.S.A. (Srivastava and Eames, 1998).

2.2 Adsorption Systems

Adsorption systems can be open or closed systems. The most common example of an open adsorption system is a dessicant dehumidification/drying system. In this type of system, the adsorbate is water vapour and the adsorbent a dessicant bed or wheel. Water vapour within a humid air stream is physically adsorbed as the latter passes over the dessicant, causing heat to be released to the air stream in the process (adsorption is an exothermic process). The air stream leaving the adsorbent bed is thus dried and heated. For air-conditioning applications, the dessicant cooling system removes the latent load of the space while a separate system sensibly cools the hot dry air leaving the dessicant before it is introduced to the space. Applying heat to the dessicant regenerates the system by causing desorption of the water vapour from the dessicant (desorption is an endothermic process), after which it is dry and ready to adsorb water vapour once again.

The components of a closed adsorption system will consist of vessel A containing the adsorbent, vessel B that acts as a condenser or evaporator and contains the adsorbate, a valve and a pipe connecting the two vessels. The operating cycle of a closed adsorption system is described here as this type of system is being investigated in this work. One operating cycle of the system will consist of four distinct steps, described below and presented graphically in the Clapeyron-Clausius diagram of Figure 2.1.

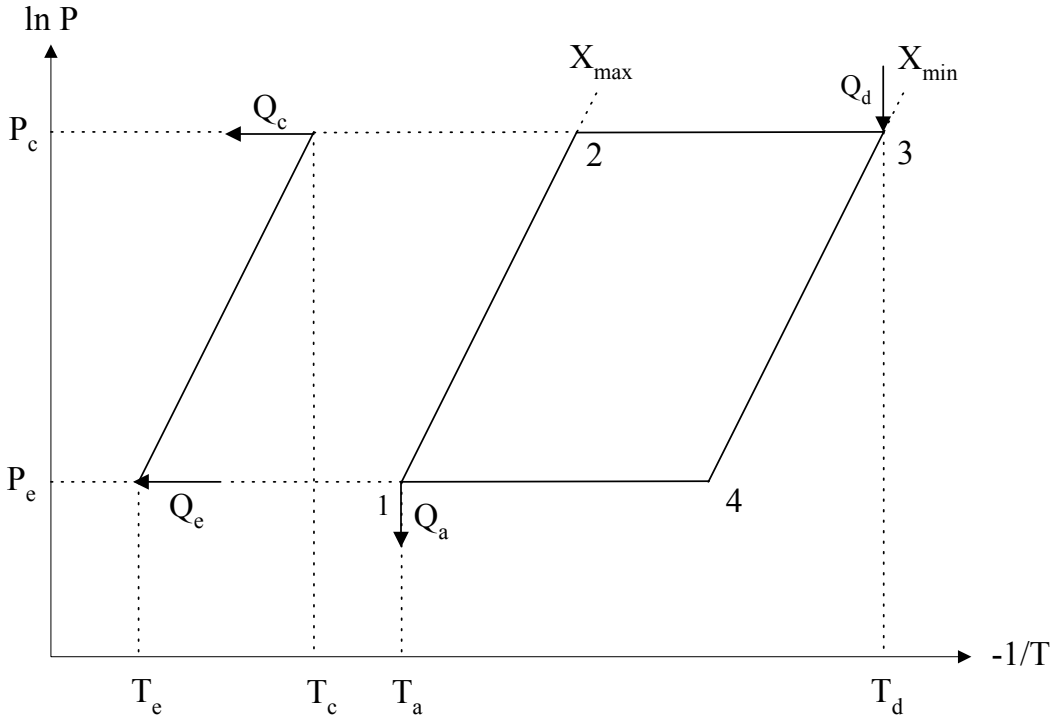

Figure 2.1 An adsorption cycle represented in a Clapeyron-Clausius diagram

Step 1: Isosteric heating of the wet adsorbent (charging stage)

At the beginning of the cycle, point 1 in Figure 2.1, the adsorbent of vessel A contains the maximum amount of adsorbate within its pores, i.e. the adsorbent is wet. The ratio X of adsorbate mass to the dry mass of adsorbent at this point is X_{max}. The valve between the adsorbent vessel A and the condenser/evaporator (vessel B) is initially closed. As heat Q_d at temperature T_d is applied to vessel A containing the wet adsorbent, the pressure of the adsorbate in vessel A will increase to the condenser pressure, P_c, with no change in X. Therefore, the ratio of mass of adsorbate to mass of adsorbent is X_{max} (point 2 in Figure 2.1). The process between points 1 and 2 is referred to as the isosteric (constant mass) heating of the wet adsorbent.

Step 2: Desorption and condensation of adsorbate (charging stage)

At point 2 (Figure 2.1), the valve connecting the adsorbent vessel A to the condenser (vessel B) is opened. Heat Q_d continues to be supplied to the adsorbent in vessel A and desorption of the adsorbate from the adsorbent occurs until the adsorbent vessel A and the condenser (vessel B) reach the equilibrium pressure. The adsorbate gas from vessel A flows to the condenser (vessel B), where it is condensed to its liquid state. Heat of condensation Q_c is rejected at temperature T_c. The desorption of the adsorbent in vessel A at a constant pressure P_c continues until the adsorbent reaches the temperature T_d and the ratio of mass of the adsorbate to mass of adsorbent is at the minimum value X_{min}, i.e. the adsorbent is dry (point 3 in Figure 2.1). The valve connecting the adsorbent vessel A to the condenser/evaporator (vessel B) is now closed.

Step 3: Isosteric cooling of the dry adsorbent (discharge stage)

At point 3 (Figure 2.1), the adsorbent within the adsorbent vessel A has a minimum amount of adsorbate within its pores, X_{min}. The adsorbent is at a temperature T_d, and is separated from the adsorbate in liquid form that is contained within the condenser/evaporator (vessel B). The valve is kept closed. As the adsorbent vessel A cools, the pressure of the adsorbate contained within the pores of the adsorbent decreases to the evaporator pressure P_e with no change in the ratio of mass of the adsorbate to mass of the adsorbent, X_{min} (point 4 in Figure 2.1). The process between point 3 and 4 is referred to as the isosteric (constant mass) cooling of the adsorbent.

Step 4: Evaporation of the adsorbate and adsorption (discharge stage)

At point 4 (Figure 2.1), the valve connecting the adsorbent vessel A to the evaporator (vessel B) is now opened. Heat Q_e is supplied to the evaporator so that the liquid adsorbate within the evaporator returns to its gaseous state. Heat continues to be supplied to the evaporator B and the equilibrium pressure is achieved as the adsorbate gas flows from vessel B to the adsorbent vessel A. Adsorption at a constant pressure P_e continues until the adsorbent in vessel A reaches the temperature T_a. At this point, the ratio of mass of adsorbate to mass of adsorbent that can be contained within the pores of the adsorbent is at the maximum value X_{max}(point 1 in Figure 2.1). Heat of adsorption Q_a is released during this process. This last process completes one operating cycle.

If the adsorption system is used for storage applications, the operating cycle described above is discontinuous. Assuming an ideal cycle, the charging phase consists of steps 1 and 2, where the temperature required to charge the system is T_d and the heat to be stored is Q_d. Heat can be stored indefinitely as long as the valve connecting the adsorbent vessel A and the condenser/evaporator (vessel B which contains the liquid adsorbate) remains closed at the end of step 2. If no sensible heat losses are assumed during the storage cycle, then an amount of heat Q_a (equal to the stored heat Q_d) is available during the discharge phase, which consists of steps 3 and 4.

If the adsorption system is used for refrigeration or heat pump applications, then the operating cycle is continuous. The cooling effect that can by provided by the system is Q_e, i.e. the heat required to evaporate the liquid adsorbate in vessel B. The heating effect that can by provided by heat pump systems is Q_c and Q_a, the condensation heat and

adsorption heat, respectively. The thermal energy required to operate the adsorption system (Q_d) can be supplied by waste heat from co-generation equipment, solar energy, etc. This thermal energy replaces the power requirements of vapour compression systems used for refrigeration and heat pump applications.

2.3 Adsorption Storage Technology

One of the earliest attempts to develop a seasonal heat storage system based on the adsorption process was the TEPIDUS system, developed in Sweden in the late 1970s (Brunberg, 1980). The TEPIDUS system was based on a sodium sulphide (Na_2S)/water adsorption pair and the system's heat source was solar energy. The system was able to release 1 kWh of heat per kilogram of dry adsorbent during the discharge phase. The TEPIDUS project was disbanded in the early 1980s due to technical problems (Lund, 1996), however interest in an adsorption system based on Na_2S and water for air conditioning purposes has resurfaced with the development of the Salt-Water Energy Accumulation and Transformation (SWEAT) system (Bach and Haije, 1999). The SWEAT system is designed to use waste heat at 80 °C and its development is directed to cooling applications in industry, commercial buildings and the automotive sector.

The development of an adsorption storage system for the seasonal storage of solar energy for heating applications in low-energy residential buildings is currently underway in Germany (Mittelbach and Henning, 1997), (Mittelbach et al., 2000). The project falls within the scope of the European Union programme NNE-JOULE C (Non-nuclear Energy- Joint Opportunities for Unconventional or Long Term Energy Supply). The

proposed system is charged with heat from solar collectors during the summer, and the heat discharged during the winter is directed to the house's hot water heating system. The system under investigation is a closed system based on water as the adsorbate. Research done to identify the most suitable adsorbents to be paired with water, for heat storage applications, found that for low temperature applications (charging temperatures up to 100 °C and discharge temperatures less than 50 °C), selective water sorbents (modified silica gels) and commercial silica gels were the most suitable adsorbents, while for medium temperature applications (charging temperatures of 200 °C and discharge temperatures in the range 80°C-130°C), zeolite was the most effective adsorbent (Nùñez et al., 1999). Current work on the development of the system is focused on optimizing and selecting effective adsorbents, improving the heat exchange between the adsorbent bed and the heat source or sink (a greater thermal conductivity of the adsorbent bed is associated with a reduction in mass transfer and therefore a compromise between heat transfer and mass transfer effects is required), and the construction and vacuum tightness of the vessels containing the adsorbent and adsorbate (Mittelbach et al., 2000). The testing of adsorption storage units that were installed in a real size test facility showed that the adsorbents used in the experiment, modified silica gels, lost their adsorption capacity as cycles were repeated. In addition, the condenser and evaporator efficiencies were far below expected values due to gas formation problems originating from internal coatings within the condenser/evaporator (Mittelbach et al., 2000).

A short-term storage system based on a zeolite/water adsorption pair has been investigated to reduce the peak power demand from a district heating network (Fischer

and Hauer, 1998). The storage system, installed in a school in Germany, is charged during off-peak hours, mostly evenings and weekends, and discharged during peak hours, mostly weekdays. The system is an open system and functions much like a dessicant dehumidification system, described in section 2.2. Ideally, open adsorption storage systems can be used for heating as well as air-conditioning and drying applications. The adsorption storage system installed in the school was expanded to a dessicant cooling system connected to the air conditioning system of a nearby jazz club, also connected to the district heating network (Hauer, 2002).

Much of the current research on adsorption technology is focused on the design and optimization of adsorption systems for heat pump and refrigeration applications. A magnesium oxide/water chemical heat pump driven by surplus heat from cogeneration equipment is investigated by (Kato et al., 2001), while (Ogura et al., 2003) research the application of a calcium oxide/water chemical heat pump for high-density heat storage, heating and cooling applications. Zeolite-water heat pumps for domestic heating are investigated by (Restuccia et al., 1988) and (Lang et al., 1999).

Although not an exhaustive list, the following list identifies the research that has been carried out on the use of adsorption technology for refrigeration and air conditioning applications:

- A prototype of a gas-fired adsorption air-conditioning system based on a zeolite-water working pair, for residential and small commercial buildings, was tested by (Poyelle et al., 1997).

- A zeolite-water adsorption heat pump for refrigeration purposes was experimentally studied and modelled by (Lachance, 2003).
- A coupled adsorption-absorption system wherein the thermal energy released by the adsorption system is supplied to a water-lithium bromide absorption system was suggested for a greater overall system efficiency by (Lachance et al., 2002).
- A two-stage adsorption chiller based on a silica-gel water working pair and driven by solar or waste heat was proposed by (Saha et al., 2001).

2.4 Mathematical Models of Adsorption Systems

In this section, mathematical models of adsorption storage systems as well as adsorption heat pumps are described. Adsorption heat pumps differ from adsorption storage systems in that the operating cycle of the former is continuous while the operating cycle of the latter is not; steps 1-2 and 3-4, described in section 2.2, are interrupted by the storage period. However, the models created for the two applications are similar in that the same phenomena are described.

Two models of adsorption systems used for heat storage applications were found in the literature: one developed by (Seewald et al., 1999) and the other by (Mittelbach and Henning, 1997). Both of these models, described in the subsequent two paragraphs, were developed within the framework of the NNE-JOULE C programme to develop an adsorption storage system for the seasonal storage of solar heat in low-energy residential buildings.

A model of the heat and mass transfer processes within an adsorption storage system was developed and implemented in a finite element numerical simulation program by (Seewald et al., 1999) in order to support the design and optimization of the system. The storage unit that is considered consists of a cylindrical vessel containing a silica gel adsorbent and heat exchanger pipes. The vessel is connected to a condenser/evaporator with water as the adsorbate. The discharge phase was identified as the most important in the operation of the unit and therefore only this phase was considered in the preliminary model. A heat balance is done for the adsorption bed during the discharge phase taking into account the transient discharge of sensible heat in the solid adsorbent bed, the heat of adsorption as a source of heat during the discharge process and the conduction of heat within the solid adsorbent bed. The problem is described in cylindrical co-ordinates and approximated as one-dimensional in the radial direction. The heat balance equation and appropriate boundary conditions are solved numerically with KARDOS, a finite element code that can solve transient differential equations coupled with algebraic equations and boundary conditions in one to three spatial dimensions. KARDOS automatically adapts the spatial grid and timestep to obtain a good numerical resolution with a reasonable computing time and memory. The results of the simulation provide the temperature of the solid adsorbent bed as a function of time during the discharge phase and the impact of input parameters (for example, density of the dry adsorbent, heat capacity of the dry adsorbent, heat capacity of the adsorbate, thermal conductivity of the adsorbent bed) on the operational behaviour of the adsorption storage system.

A second model to support the development of an adsorption storage system to store solar heat was developed and implemented in TRNSYS by (Mittelbach and Henning, 1997). The model describes an adsorption storage unit with a silica gel/water working pair connected to a field of solar collectors (heat source) and a residential low-temperature heating system (heat sink). Experimental data describing the adsorption characteristics of the silica gel/water working pair are incorporated in the model. The objective of the work was to determine the relation between the size of the solar collector fields and the storage volume that would be required for a given low-energy residential building (defined as a house with an annual thermal energy load of 30-50 kWh/m^2), and to evaluate the impact of system parameters, such as the solar collector efficiency and the temperature requirements of the heating system, on the capacity of the storage system. The residential building considered in the study was represented by a constant heating load and a constant indoor room temperature.

Several dynamic models of adsorption heat pumps were found in the literature and are briefly described here. (Yong and Sumathy, 2002) provide a good overview of the numerous mathematical models of adsorption heat pumps.

(Lachance, 2003) developed a dynamic mathematical model of a zeolite-water adsorption heat pump and validated the model using experimental data. Energy balance equations are written for: (1) the adsorber container, (2) the heat exchanger surface within the adsorber, (3) the fluid flowing through the adsorber heat exchanger, (4) the adsorbent bed within the adsorber, (5) the heat source (a boiler), (6) the condenser and (7) the

evaporator. Mass balance equations are written for the adsorber, the condenser and the evaporator. Thermodynamic equilibrium between the adsorbent and vapour adsorbate is assumed. The D-A equation (2.4) is used to relate the amount of adsorbate adsorbed to the pressure and temperature of the adsorber, with the coefficients of equation (2.4) determined experimentally. The governing first-order differential equations, a total of thirty, are solved numerically using the Euler explicit method. The simulation results agree well with the experimental results for the three different test conditions considered by (Lachance, 2003). Each test condition corresponds to a particular set of operating temperatures for the adsorption heat pump.

(Cacciola et al., 1993) developed a dynamic model to evaluate the performance of a regenerative adsorption system for heat pump and cooling applications. Regenerative systems use multiple reactors and operate such that the heat released in one adsorber during the adsorption process can be recovered and used to heat a second adsorber during the desorption process. (Cacciola et al., 1993) derive the governing equations of the mathematical model by considering the energy and mass balances for the system components for each of the cycle steps (isosteric heating and cooling, isobaric adsorption and desorption) and thermodynamic equilibrium relationships. The governing equations were cast in a dimensionless form and solved numerically using an explicit scheme. Results of the model showed that the adsorption and desorption steps are not isobaric due to the finite performances of the condenser and evaporator, which are expressed in terms of an effectiveness value in the model. (Cacciola et al., 1993) found good agreement

between results obtained from the simulation of a double-reactor, zeolite-water, adsorption heat pump using their model and data available in the literature.

(Sami and Tribes, 1996) developed a dynamic, one-dimensional, lumped parameter model to predict the performance of adsorption cycles. The adsorption system is described with different discrete control volumes and conservation equations are applied to each control volume. Of particular interest to note is that the energy conservation equation that is applied to the adsorber during the cooling phase contains a term to account for the thermal effects due to the flow of adsorbate, in vapour form, from the evaporator to the adsorber. (Sami and Tribes, 1996) consider this term to be significant because the vapour adsorbate enters the adsorber at temperatures lower than that of the adsorber. The governing partial differential equations are discretized using the finite-difference method and solved numerically. The model was validated with experimental data for a single, active carbon-methanol, adsorber system and for a double, zeolite-water, adsorber system. The numerical results obtained from the model compared well with the experimental data.

The dynamic model of an adsorption heat pump developed by (Wu et al., 2000) is similar to the model developed by (Sami and Tribes, 1996). The energy balance on the adsorbent includes a term to account for the thermal effects due to the flow of adsorbate, in vapour form, from the evaporator to the adsorber. To validate their model, (Wu et al., 2000) compare the results obtained from their model to experimental data and report differences between the performance indices that are calculated and those determined

experimentally. The authors attribute the differences found to the system heat losses that are neglected in the simulation and to the assumption of the model that the operation of the adsorption system follows an ideal cycle.

In their two-dimensional dynamic model of an adsorption heat pump, (Chahbani et al., 2004) consider both the heat and mass transfer effects in the adsorber. In particular, energy balances are considered for the heat transfer fluid flowing through the heat exchanger, the heat exchanger tube and the adsorber. Two different models are used to describe the mass transfer between the vapour adsorbate and the solid adsorbent bed: (1) the equilibrium model, which assumes that the vapour and solid phases are in thermodynamic equilibrium and (2) the linear driving force model derived from the solid diffusion model which is based on Fick's law. The set of governing equations are discretized using the finite difference method and solved numerically. (Chahbani et al., 2004) considered the ammonia-carbon pair in their study and found that the numerical results of the two different mass transfer models are similar for long cycle times but important for short cycle times. Also, the authors conclude that for the case where the adsorbate is slow-diffusing, the performance of the adsorption heat pump will be overestimated if the equilibrium model is used.

(Leong and Liu, 2004a) developed a two-dimensional numerical model to describe the combined heat and mass transfer in an adsorbent bed. The model is used to assess the impact of the adsorbent bed configuration and of operating conditions on the performance of a zeolite-water adsorption cooling system. In their model, (Leong and Liu, 2004a)

determine an equivalent thermal conductivity for the adsorbent bed that takes into account the porosity of the adsorbent bed, the thermal conductivity of the heat transfer fluid and the thermal conductivity of the adsorbent. The mass transfer resistance within the adsorbent particles is accounted for by using the linear driving force model. As in the model by (Chahbani et al., 2004), energy balances are considered for the heat transfer fluid, the heat exchanger tube and the adorbent bed and a mass balance is considered for the adsorbent bed. The governing equations are discretized using a finite difference method within the computational domain, a two-dimensional, non-uniform, staggered grid. The discretized equations are solved numerically using a line-by-line procedure that combines the tri-diagonal matrix algorithm and the Gauss-Seidel iteration technique. The numerical results of the model developed by (Leong and Liu, 2004a) show that by considering the mass transfer resistance within the adsorbent bed, the process paths of the thermodynamic cycle differ significantly from the process paths of an ideal cycle, especially in the isosteric heating (process 1-2 in Figure 2.1) and isobaric adsorption (process 4-1 in Figure 2.1) phases.

3 MODEL DEVELOPMENT

3.1 Choice of Mathematical Model

Yong and Sumathy (2002) classify the various mathematical models of adsorption heat pumps that have been developed into three main groups: thermodynamic models, lumped parameter models and heat and mass transfer models. Heat and mass transfer processes are not considered in thermodynamic models and the adsorption system's heat source and heat sink are assumed to operate at constant temperatures. These simple thermodynamic models are used to determine the performance limits of an adsorption system.

Lumped parameter models consider the heat transfer processes that occur in an adsorption system, however, they assume that the temperature of the adsorbent layer is uniform, that the adsorbate is adsorbed uniformly by the adsorbent and that the solid and gas phases in the adsorber exist in thermodynamic equilibrium (this implies that any resistance to heat and mass transfer between the solid and gas phases is neglected). The temperature and the mass of adsorbate within the adsorbent layer vary with time but they do not vary with space.

Finally, as implied by their name, heat and mass transfer models consider both heat and mass transfer processes. Thus, the temperature and the mass of adsorbate within the adsorbent layer vary both with time and with space. These types of models can be one-, two-, or three-dimensional and are important tools to investigate the optimal design of an adsorption system.

A lumped parameter type model (versus a heat and mass transfer model) is the most appropriate as this research is concerned with developing a model of an adsorption storage system to investigate the technical feasibility of employing such a system to store exhaust heat from a fuel cell cogeneration unit and not to design or optimize the individual components of an adsorption storage system. Also, a lumped parameter type model is better suited for this work due to the lack of detailed experimental data available in the literature.

There are two different approaches that can be taken in the development of a mathematical model of an adsorption storage unit: the unit can be described empirically by defining a control volume such that it surrounds the entire system, or the unit can be described in more detail by considering the individual components that make up the system. In the latter case, the system is comprised of several control volumes with each control volume surrounding a system component. Energy and mass balances are considered for each control volume.

In order to develop a single control volume empirical model (also commonly described as a black box model), the relationship between the energy output from the unit to the energy input to the unit (heat is input to the adsorber and output from the condenser during the charging phase while heat is input to the evaporator and discharged from the adsorber during the discharge phase) must be known. At the present time, as adsorption storage technology is at the research phase, the experimental data that would be necessary

to develop a single control volume empirical model that can take into account different operating conditions are not available in the literature. Although the energy densities of an adsorption storage unit for several adsorbents with water as the adsorbate are available in (Mittelbach et al., 2000), these values only apply for a certain set of fixed operating conditions (i.e. fixed charging (desorption) temperature, condenser temperature, evaporator temperature and discharge (adsorption) temperature). Thus, a single control volume empirical model based on the energy density data available in the literature has a limited applicability - the model would not be able to take into account varying operating temperatures and the ability of the unit to meet the house's heating load during the discharge phase could not be properly investigated. If sufficient experimental data were available for the development of a single control volume empirical model that could take into account varying operating temperatures, the advantage of such a model would be its simplicity to develop and to use.

An example of a single control volume empirical model used in a building energy simulation program is that of a furnace. An empirically based model may consider one energy balance for the entire furnace. Parameters such as the heat loss through the furnace jacket, the heat flow through the chimney and the useful heat flow rate are expressed in terms of the heat flow rate input to the furnace due to combustion, in the form of a parametric equation, the coefficients of which are determined experimentally. In contrast, a fundamental detailed model of a furnace would consider both the combustion and heat transfer processes that occur in the furnace and would require detailed data on the shape and size of the furnace (Bourdouxhe et al., 1998). Such a

model might consider the energy balances on the flue gases, the heat exchanger surface, circulating air and furnace jacket.

A mathematical model that considers the individual components of an adsorption storage system and the links between the components results in a set of governing equations (conservation of mass and energy is applied to each component) that is complex and certain assumptions are needed to describe the problem. As the set of governing equations is difficult to solve analytically, a numerical solution of the mathematical model is often needed. The advantages of developing a detailed component model of an adsorption storage system include:

- the underlying thermodynamics of the problem are fully understood;
- the adsorption equilibrium data that are available from the literature for refrigeration applications can be used. Adsorption equilibrium data relates the amount of adsorbate contained within the adsorbent to the pressure and/or temperature of the adsorbate and takes into account the characteristics of the adsorbent/adsorbate working pair;
- the impact of operating conditions on the performance of the adsorption storage system can be investigated;
- the model can be developed to consider different adsorbent/adsorbate working pairs (provided that the characteristics of the working pair can be described using the particular equilibrium equation implemented in the model).

Taking into account the lack of experimental data to develop an empirical model and the advantages of developing a component-based mathematical model of an adsorption storage system, the latter option was chosen for this work.

3.2 Description of Mathematical Model

The mathematical model proposed in this research work considers the three components of an adsorption storage unit: the adsorber, condenser and evaporator. A control volume surrounds each component, as illustrated in Figure 3.1.

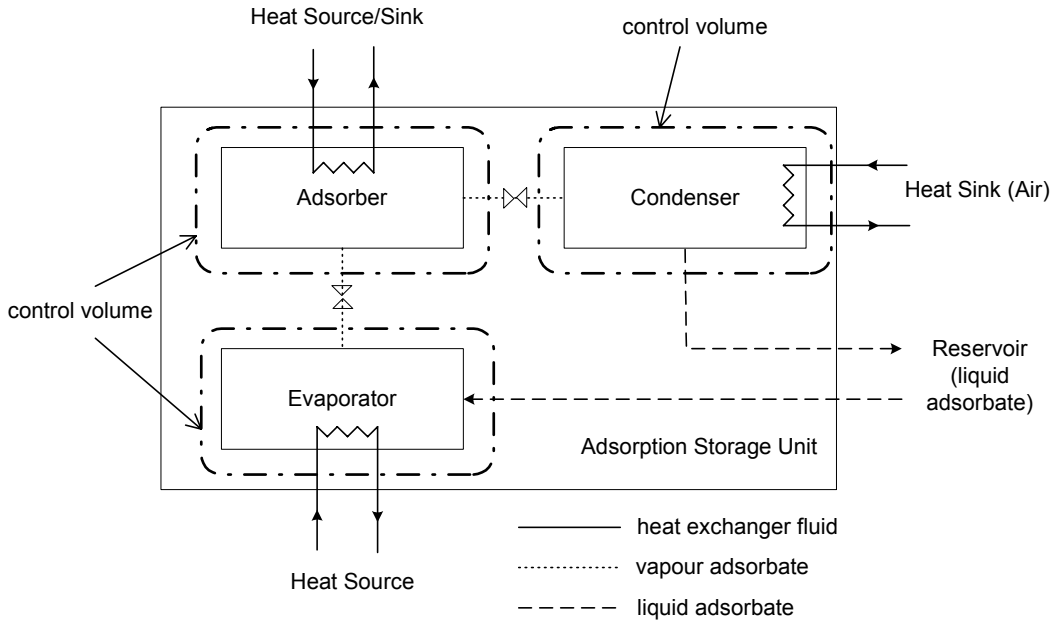

Figure 3.1 Adsorption storage unit control volumes

As discussed in section 2.2, the operating cycle of an adsorption system consists of four distinct steps. The Clapeyron-Clausius diagram, which shows the four steps graphically and is introduced in section 2.2, is repeated in Figure 3.2 to serve as a reference for the subsequent sections.

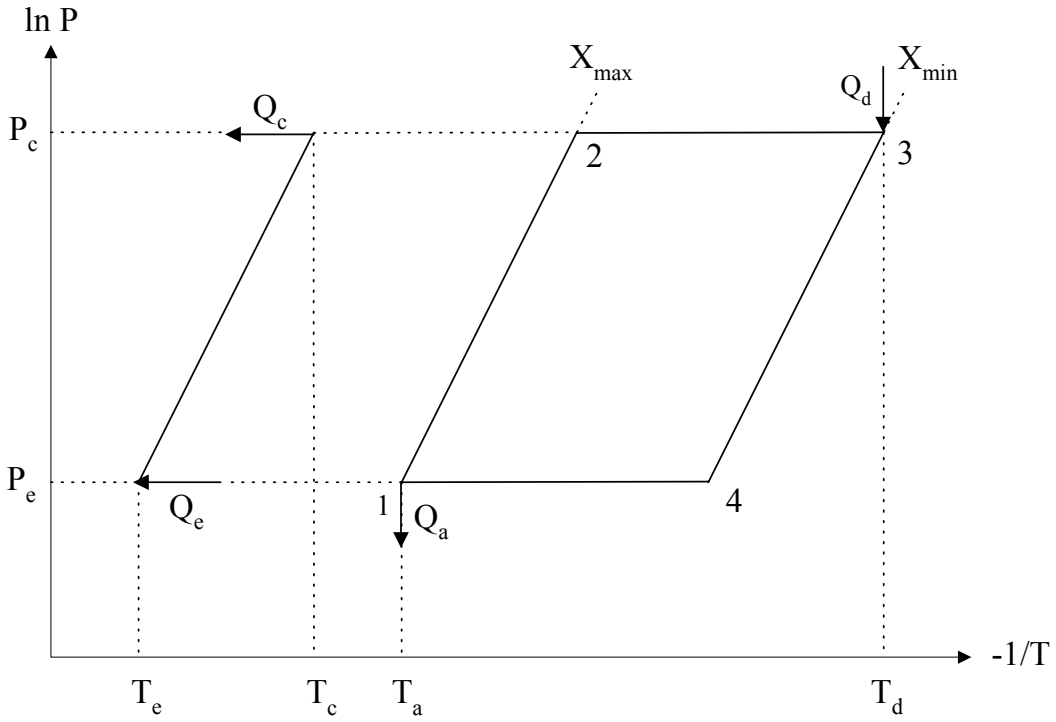

Figure 3.2 Clapeyron-Clausius diagram for adsorption cycle

3.2.1 Adsorber

A control volume surrounds the adsorber, including the adsorber vessel and the heat exchanger material within the adsorber. The heat source provides heat to the adsorber during charging while a heat sink accepts heat from the adsorber during discharge via the heat exchanger. The adsorber is connected to both the condenser and the evaporator.

During the charging phase, vapour flows from the adsorber to the condenser when the valve between the two components is open, while during the discharge phase, vapour flows from the evaporator to the adsorber when the valve between the two components is open. The typical configuration of an adsorber cited in the literature consists of a cylindrical container with a shell and tube heat exchanger layout. A schematic of the two configurations that seem to be the most common for adsorption heat pumps are shown in cross-section in Figure 3.3 (Lachance, 2003), (Chahbani et al., 2002). It should be noted that the adsorber vessel can contain several tubes. Since the control volume will surround the entire adsorber, the model developed for this work can represent both of the configurations presented in Figure 3.3.

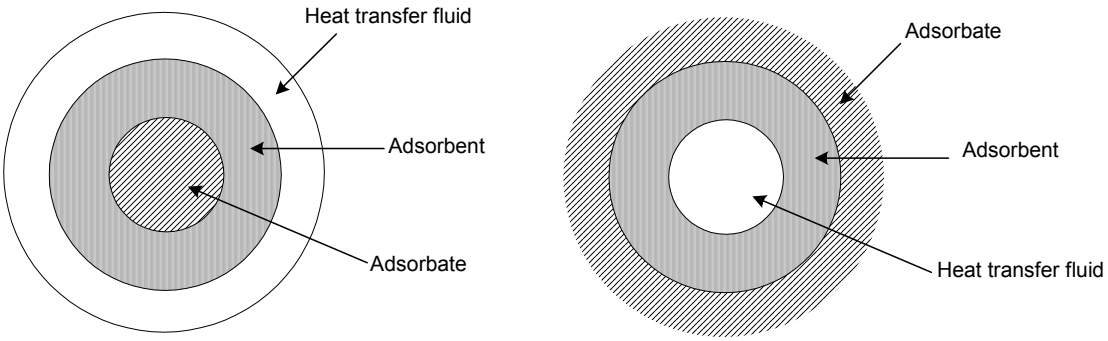

(a) (Chahbani et al., 2002) (b) (Lachance, 2003)

Figure 3.3 Adsorber configurations in cross-section

The heat transfer phenomena occurring within the adsorber control volume are presented schematically in Figure 3.4 and are described below.

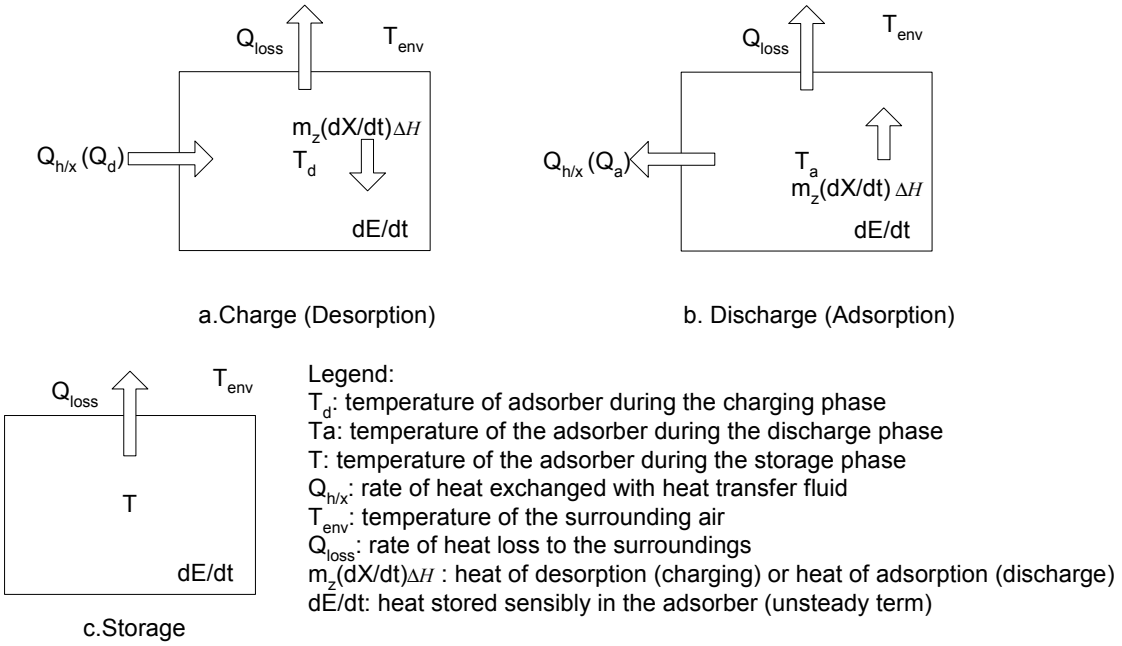

Figure 3.4 Heat transfer phenomena within the adsorber control volume

a. Heat exchange with heat transfer fluid ($\dot{Q}_{h/x}$): The adsorber gains heat from the fluid during the charging phase (Q_d in Figure 3.2) and loses heat to the fluid during the discharge phase (Q_a in Figure 3.2). During the storage phase, there is no fluid flowing through the heat exchanger contained within the unit's adsorber.

b. Heat loss to the environment ($\dot{Q}_{loss}$): Sensible heat losses via convection to the surrounding air and longwave radiation exchange with surfaces in the containing room occur during all three phases of the adsorption storage unit's operating cycle.

c. Adsorption or desorption of vapour ($m_z \frac{dX}{dt} \Delta H$): The adsorption or desorption of adsorbate vapour by and from the adsorbent, respectively, occurs when the valve between the adsorber and the condenser/evaporator is opened. During the charging phase, the adsorbate is desorbed from the adsorbent bed whereas during the discharge phase, the adsorbate is adsorbed by the adsorbent. The desorption of vapour is an endothermic process and the heat required for it to occur can be considered as a heat sink term. On the other hand, the adsorption of vapour is an exothermic process and the heat released can be considered as a heat source term. The magnitude of the heat source/sink term is equal to the product of: the mass of dry adsorbent, m_z; the change with respect to time of the ratio of mass of adsorbate per mass of dry adsorbent, dX/dt; the heat of adsorption, ΔH.

d. Sensible Heat Storage ($\frac{dE}{dt}$): Heat is stored sensibly by the adsorbent, the adsorbate and the heat exchanger material contained within the adsorber vessel, as well as by the adsorber vessel itself.

The temperature in the adsorber is assumed to be uniform in space. This assumption has been proven to be reasonable for a zeolite-water adsorption heat pump (Lachance, 2003).

3.2.2 Condenser and Evaporator

The condenser receives the adsorbate vapour from the adsorber during the charging phase and condenses the adsorbate to a liquid. The resulting heat of condensation is removed from the unit; it can be recovered or rejected. In this research, it will be supposed that the

adsorption storage unit contains an air-cooled condenser and that the heat of condensation is rejected to the outdoors. The adsorbate in liquid form is directed to a reservoir where it is stored until it is needed at the evaporator for the discharge of the storage unit. It should be noted that other configurations are possible; for example, the adsorbate in liquid form can remain in the condenser until it is needed at the evaporator at which time it is directed to the latter. In this research, it will be supposed that the adsorbate in liquid form is stored in a reservoir.

The evaporator receives the liquid adsorbate from the reservoir prior to the discharge of the storage unit. Heat is supplied to the evaporator to return the adsorbate to its vapour form and to start the discharge process. When the valve between the evaporator and the adsorber is opened, vapour flows from the evaporator to the adsorber.

Essentially, the condenser and the evaporator can be modelled as a single component that acts as an air-cooled condenser when the adsorption storage unit is in charging mode and an evaporator when the adsorption storage unit is in discharge mode. The heat transfer phenomena occurring in the condenser/evaporator control volume are presented schematically in Figure 3.5 and are described below.

a. Change of phase ($\dot{m}_{vap} h_{fg}$): In the charging mode, the adsorbate vapour is condensed to a liquid, an exothermic process. The heat released is a source term. In the discharge mode, the liquid adsorbate is evaporated to a vapour, an endothermic process. The heat

input is a heat sink term. The heat source/sink term is represented by $\dot{m}_{vap} h_{fg}$, the product of the mass flow rate of the vapour, $\dot{m}_{vap}$, and the latent heat of vaporization, h_{fg}.

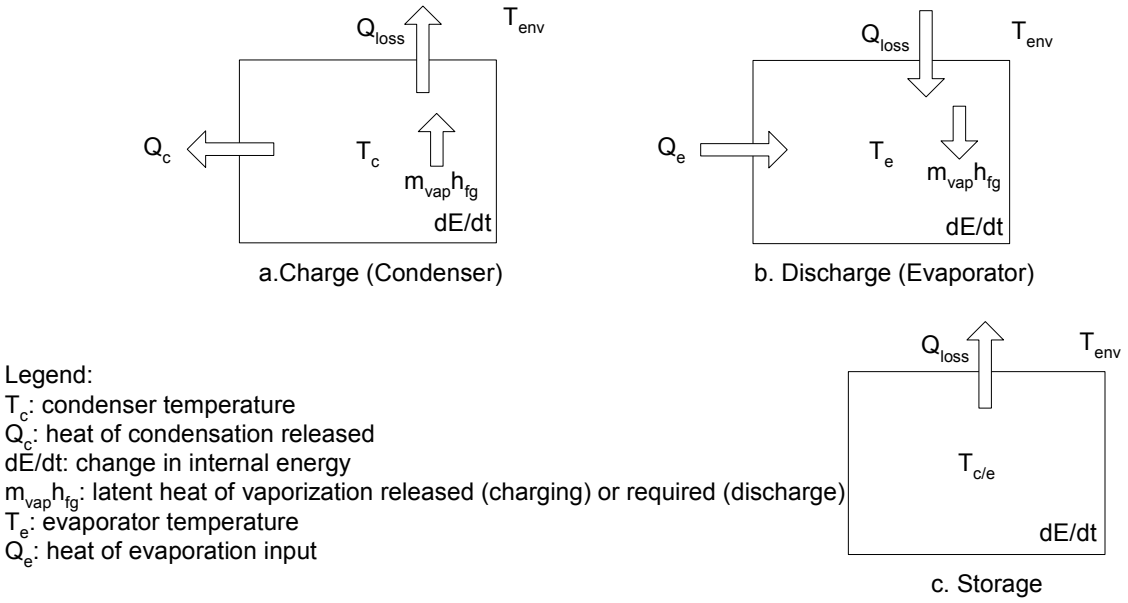

Figure 3.5 Heat transfer phenomena within the condenser/evaporator control volume

b. Heat transfer ($\dot{Q}_c, \dot{Q}_e$): During the charging phase, the heat released upon condensation ($\dot{Q}_c$) is transferred to the outside air. During the discharge phase, heat is input to the evaporator ($\dot{Q}_e$).

c. Heat loss to the ambient ($\dot{Q}_{loss}$): Sensible heat losses or gains via convection to the surrounding air and longwave radiation exchange with surfaces in the containing room can occur during all three phases of the adsorption storage unit's operating cycle.

d. Change in internal energy ($\frac{dE}{dt}$): The change in internal energy of the adsorbate contained within the condenser/evaporator as well as the solid material comprising the vessel.

3.3 Plant Configuration

The plant configuration envisioned is shown schematically in Figure 3.6. The plant consists of a solid oxide fuel cell (SOFC), a main water storage tank, an adsorption storage unit, a reservoir which contains the liquid adsorbate, an auxiliary water storage tank, an air-handling unit, circulating pumps and controls. The temperature and pressure ranges noted for some of the plant components in Figure 3.6 represent the approximate operating conditions of the components. A zeolite adsorbent and water adsorbate working pair is assumed for the adsorption storage unit.

The temperature range of the exhaust gases leaving the SOFC stack, when it is operating, is approximately 300 - 400 ºC (Beausoleil-Morrison et al., 2002a). Exhaust heat is directed either to the main water storage tank (loop A identified in Figure 3.6) or the adsorption storage unit (loop B), as will be discussed in the succeeding paragraphs. For those periods of the day when the fuel cell is not operating, the pumps associated with circulation loops A and B are off.

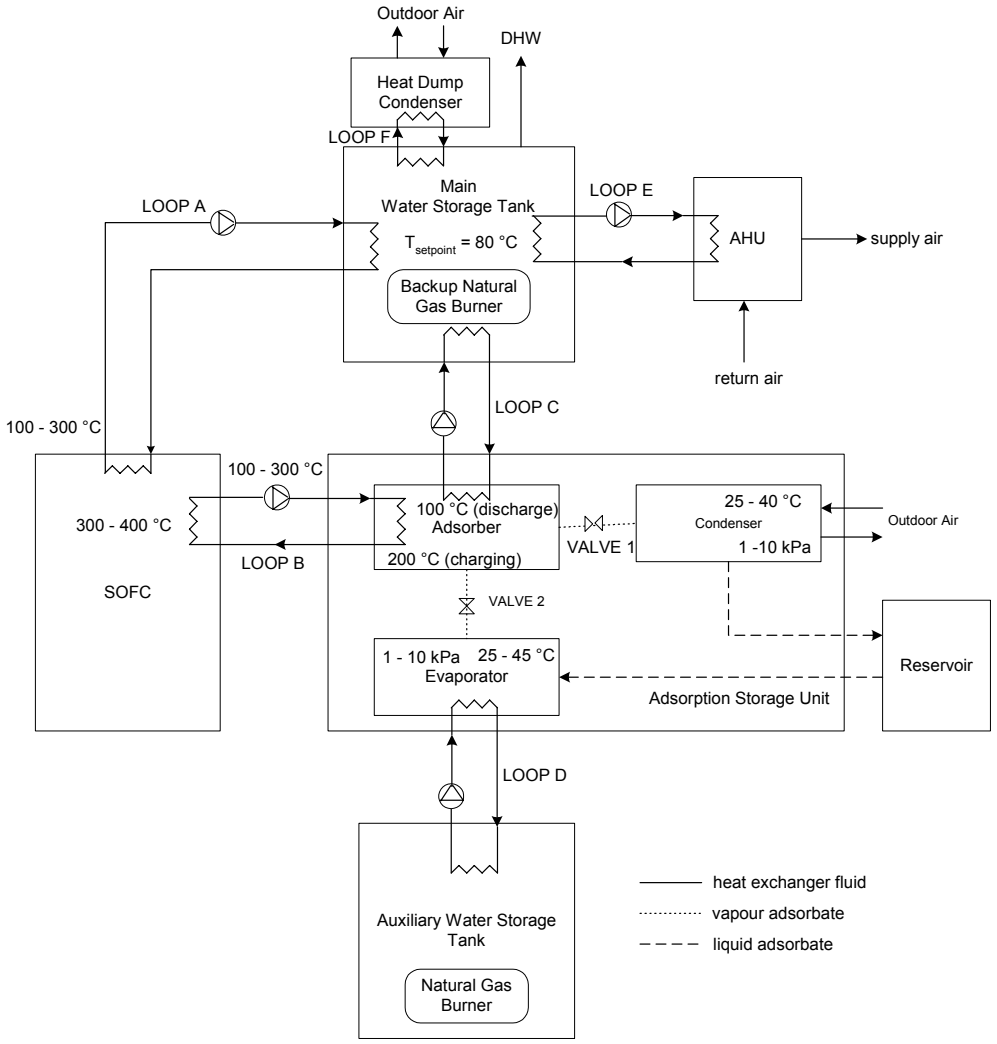

Figure 3.6 HVAC plant configuration

The main water storage tank meets the house's space heating load via an air-handling unit. The air-handling unit contains a heating coil served by the main water storage tank (loop E in Figure 3.6) and a fan that circulates air to and from the house. The circulating fan and the loop E pump operate only when the temperature in the house is below the thermostat setpoint temperature. A heat recovery ventilator (HRV) operates continuously to supply the required ventilation (not shown in Figure 3.6). The main water storage tank

also serves the house's domestic hot water requirement. The main water storage tank receives heat exhausted by the fuel cell (loop A) and/or heat recovered from the adsorption storage unit (loop C) to meet the heating loads imposed on it.

The adsorption storage unit stores heat on a seasonal basis. It is expected that most of the exhaust heat available from the SOFC will not be required in the summer as no space heating load exists during this period. Excess heat is stored in the adsorption storage unit during the cooling season and is recovered during the heating season when the SOFC is not able to meet the space heating and domestic hot water requirements of the house. The unit is only permitted to switch into the charging mode of operation during the cooling season and into the discharge mode of operating during the heating season.

During the cooling season, the adsorption storage unit switches into the charging mode if all of the following conditions are met:

- the temperature in the main water storage tank is above the upper (ON) set-point temperature for more than 25 minutes. A reset period of 25 minutes is chosen to avoid the cycling on and off of the adsorption storage unit;
- the temperature of the adsorber is less than the maximum value. The maximum temperature of the adsorber can be set to the temperature of the water leaving the SOFC's heat exchanger (this implies that no further heat can be transferred) or slightly lower so as to account for the temperature difference between the heat source and adsorber that is required for proper heat transfer (Restuccia and Cacciola, 1999);

- the temperature of the water leaving the SOFC's heat exchanger is greater than the minimum charging temperature required by the adsorber. The charging temperature required by the adsorption storage system depends on the adsorbent/adsorbate pair chosen for the system. For example, a minimum charging temperature in the range 150 ºC - 200 ºC is required for a zeolite adsorbent and water adsorbate working pair.
- the fuel cell is operating.

The SOFC's thermal output is directed to the adsorption storage unit so that the excess heat available can be stored (loop B in Figure 3.6) when the latter is in the charging mode of operation.

At the start of the charging mode, the valve between the storage unit's adsorber and condenser (valve 1 in Figure 3.6) is closed. Heat is supplied to the adsorber causing the vapour pressure within the adsorber to increase. The valve remains closed until the pressure in the adsorber reaches the pressure at the condenser. At this point, the valve is opened while heat continues to be supplied to the adsorber. Desorption of the adsorbate vapour continues and the desorbed vapour flows to the condenser where it is condensed to a liquid. The liquid adsorbate is directed to a reservoir. The heat of condensation is released to the outdoors. For a zeolite adsorbent and water adsorbate working pair, condensation temperatures are in the range 25 – 40 ºC. The charging of the adsorption storage unit ends when any of the following conditions is met:

- the temperature in the main water storage tank is less than the lower (OFF) setpoint temperature;
- the temperature of the adsorber is greater than or equal to the maximum temperature of the adsorber;
- the temperature of the heat source is below the minimum charging temperature required by the adsorbent/adsorbate pair;
- the fuel cell is switched off.

At the end of the charging phase, the valve between the unit's adsorber and condenser is closed.

For periods when the temperature in the main water storage tank is above a maximum setpoint temperature and excess heat cannot be stored, a safety device rejects heat from the water storage tank (loop F in Figure 3.6) to prevent scalding.

During the heating season, the adsorption storage unit switches into the discharge mode if both of the following conditions are met:

- the temperature in the main water storage tank is less than the lower (ON) set-point temperature for more than 25 minutes. A reset period of 25 minutes is chosen to avoid the cycling on and off of the adsorption storage unit;
- the temperature of the adsorber is greater than the minimum value. The minimum temperature of the adsorber can be set to the water tank's temperature (this implies that no further heat can be transferred) or slightly greater so as to account

for the temperature difference between the heat sink and adsorber that is required for proper heat transfer.

At the start of the discharge phase, the valve permitting vapour exchange between the storage unit's adsorber and evaporator is closed. The liquid adsorbate stored in the reservoir is directed to the evaporator. The vapour pressure in the adsorber must be reduced to the evaporator pressure. When the pressure in the adsorber is at the evaporator pressure, the valve between the two components is opened. Low temperature heat is supplied by the auxiliary water storage tank to the evaporator for the evaporation of the liquid adsorbate (loop D in Figure 3.6). For a zeolite adsorbent and water adsorbate working pair, evaporation temperatures are in the range 25 – 45 ºC. The adsorbate vapour that flows from the evaporator to the adsorber is adsorbed by the adsorbent and the heat of adsorption that is released at the adsorber is directed to the water storage tank via loop C. The discharge temperature of the adsorption storage unit will be less than the charging temperature. The discharge of the adsorption storage unit ends when any of the following conditions is met:

- the temperature in the main storage tank is above its upper (OFF) set-point temperature;
- the temperature in the adsorber is less than the minimum adsorber temperature;
- the adsorbent is wet and cannot contain any more adsorbate.

At the end of the discharge phase, the valve between the adsorber and evaporator is closed.

The adsorption system operating pressures are controlled with devices, such as electrical vacuum valves. For this work, the operating pressures cited in the literature are considered. (Leong and Liu, 2004a) consider an evaporator pressure of 1 kPa and a condenser pressure of 10 kPa in their work on adsorption heat pumps; both operating pressures are below atmospheric pressure.

The main water storage tank contains a backup natural gas burner that operates when the SOFC or the adsorption storage unit cannot meet the house's heating demands.

As mentioned above, the purpose of the auxiliary water tank during the discharge phase is to provide the low-temperature heat that is required at the evaporator. Approximately 244 MJ of energy is needed at the evaporator to fully discharge an adsorption storage unit based on a zeolite-water working pair, an adsorber volume of 800 litres, a charging temperature of 200 ºC, a condensing temperature of 35 ºC, a discharge temperature of 100 ºC and an evaporator temperature of 25 ºC[1]. In this work, it will be supposed that the auxiliary water tank is heated to the required temperature with a natural gas burner in order to ensure that a heat source is available to start the discharge of the storage unit. However, ideally, the heat required at the evaporator can be supplied by a renewable energy source such as solar, geothermal, etc. or the auxiliary water tank can be maintained at the required temperature by recovering heat from the fuel cell exhaust gases or from the house's exhaust air. These possibilities should be investigated in future research.

[1] Based on the heat of vaporization equal to 2.25 MJ/kg and the bulk density of zeolite equal to 896.3 kg/m^3 (Nùñez et al., 1999).

3.4 Efficiency

There are several approaches to define the efficiency of the adsorption storage system. If the performance of the adsorption storage unit is considered over a complete cycle including the charging and discharging phases, the efficiency η_1 can be defined as the ratio of useful energy retrieved from the adsorption storage unit, in J, to the energy required to operate the unit, in J:

$$\eta_1 = \frac{Q_{discharge}}{Q_{charge} + W_{aux-burner} + W_{pumps} + W_{cond-fan}} \tag{3.1}$$

where $Q_{discharge}$ is the amount of heat transferred from the unit's adsorber to the main water storage tank during the discharge phase [J], Q_{charge} is the amount of heat input to the adsorber during the charging phase [J], $W_{aux\text{-}burner}$ is the energy consumption of the auxiliary water tank's natural gas burner that is required during the discharge phase [J] (this represents the heat input to the evaporator and takes into account any heat losses), W_{pumps} is the energy consumption of the circulating pumps during the charging and discharge phases [J] and $W_{cond\text{-}fan}$ is the energy consumption of the adsorption unit's condenser fan during the charging phase [J]. The work of the following pumps are considered in the calculation of W_{pumps}:

- the pump that circulates the fluid between the SOFC and the adsorber (loop B in Figure 3.6).
- the pump that circulates the fluid between the evaporator and the auxiliary water tank (loop D in Figure 3.6).

- the pump that circulates the fluid between the adsorber and the main water storage tank (loop C in Figure 3.6).

It should be noted that the electric consumption of the pumps within the adsorption storage unit that circulate the liquid adsorbate from the condenser to the reservoir during the charging phase and from the reservoir to the evaporator during the discharge phase is not considered in the above definition. An optimal design of an adsorption storage unit may eliminate the need for such pumps and/or the need for a reservoir. As the design of an adsorption storage unit is not known, no information on the existence or size of the pumps that would be required is known and therefore their consumption is neglected. This assumption should be revisited in future work if design data on adsorption storage units is available.

The second definition of efficiency takes into account the amount of thermal energy that would be generated by the SOFC and wasted (Figure 3.6) over an entire year, in the absence of the adsorption storage unit. The efficiency of recovering the heat that would be lost in the absence of a storage system can be determined by considering the difference between (a) the amount of heat generated from the SOFC and rejected from the main water storage tank for the case where the plant does not contain a storage unit, and (b) the heat rejected from the tank for the case where a storage unit is present, with all other parameters such as the SOFC's thermal output and the thermal load of the house remaining constant. Therefore, the efficiency η_2 is defined as:

$$\eta_2 = \frac{Q_{heat-dump-no-storage} - Q_{heat-dump-with-storage}}{Q_{aux-burner} + W_{pumps} + W_{cond-fan}} \tag{3.2}$$

where $Q_{heat\text{-}dump\text{-}no\text{-}storage}$ is the annual energy rejected from the main water storage tank, in order to keep the temperature in the tank below the maximum heat dump set-point temperature, for the case where the plant does not contain an adsorption storage unit [J]. Similarly, $Q_{heat\text{-}dump\text{-}with\text{-}storage}$ is the annual energy rejected from the main water storage tank for the case where the plant does contain an adsorption storage unit [J]. The numerator in equation (3.2) represents the reduction in the amount of energy that is lost due to the presence of the adsorption storage unit while the denominator represents the amount of auxiliary energy required to store the energy. The parameters $Q_{aux\text{-}burner}$, W_{pumps} and $W_{cond\text{-}fan}$ in equation (3.2) are as defined for the equation (3.1). It should be noted that the efficiency η_2 is a function of the size and operating characteristics of the adsorption storage unit as well as the size and setpoint temperature of the main water storage tank. If the main water storage tank is sufficiently large and/or the tank's heat dump set-point temperature sufficiently high, no heat will be rejected from the tank even in the absence of an adsorption storage unit. For such a case, the value of η_2 will be zero.

The third definition of efficiency takes into account the difference in the consumption of the backup natural gas burner in the main water storage tank for the case where the plant does not contain a storage unit, and for the case where the plant does contain an adsorption storage unit, over a one-year period:

$$\eta_3 = \frac{Q_{main-burner-no-storage} - Q_{main-burner-with-storage}}{Q_{aux-burner} + W_{pumps} + W_{cond-fan}} \tag{3.3}$$

where $Q_{main\text{-}burner\text{-}no\text{-}storage}$ is the annual thermal output of the backup natural gas burner in the main water storage tank for the case where the plant does not contain an adsorption storage unit [J] and $Q_{main\text{-}burner\text{-}with\ storage}$ is the annual thermal output of the backup natural gas burner for the case where the plant does contain a storage unit [J]. It should be noted that in the calculation of $Q_{main\text{-}burner\text{-}no\text{-}storage}$ and $Q_{main\text{-}burner\text{-}with\ storage}$, all other plant parameters such as the fuel cell thermal output and the thermal load of the house remain constant.

(Beausoleil-Morrison et al., 2002a) defines the total (electrical plus thermal) efficiency of a SOFC cogeneration system, η_{cogen}, in terms of the lower heating value of natural gas, $LHV_{nat\text{-}gas}$ [GJ/m^3]:

$$\eta_{cogen} = \frac{SOFC_{elec-out} + SOFC_{thermal-out} - Tank_{rej-heat}}{SOFC_{nat-gas} \cdot LHV_{nat-gas}} \tag{3.4}$$

where

$SOFC_{elec\text{-}out}$ is the SOFC's annual electrical output (GJ);

$SOFC_{thermal\text{-}out}$ is the SOFC's annual thermal output (GJ);

$Tank_{rej\text{-}heat}$ is the annual energy rejected from the water storage tank by the safety device (GJ) and

$SOFC_{nat\text{-}gas}$ is the annual natural gas consumption of the SOFC (m^3).

The SOFC cogeneration system considered by (Beausoleil-Morrison et al., 2002a) is similar to the system depicted in Figure 3.6, except that there is no adsorption storage system for the seasonal storage of the SOFC's excess thermal output.

Additional performance characteristics of the adsorption storage unit can be defined. (Ogura et al., 2003) define a coefficient of performance (COP) for a chemical heat pump, focusing on the upgraded heat during the discharge phase:

$$COP_h' = \frac{Q_{H,R}}{Q_{L,R}} \tag{3.5}$$

The value $Q_{H,R}$ in equation (3.5) represents the amount of heat released by the adsorber during the discharge phase (the heat releasing step denoted by the subscript R), while $Q_{L,R}$ is the amount of low temperature heat (hence the subscript L) supplied to the evaporator during the discharge phase. The subscript H denotes the high temperature heat retrieved from the adsorber during the discharge phase.

(Ogura et al., 2003) also define a local efficiency of a chemical heat pump based on the used heat, in this case the heat released during the discharge phase:

$$\eta_h = \frac{Q_{H,R}}{Q_{L,R} + Q_{H,S}} \tag{3.6}$$

The value $Q_{H,S}$ in equation (3.6) represents the amount of heat supplied to the unit during the charging phase (the heat stored, denoted by the subscript S). The above expression is similar to the expression (3.1) except that the work of the circulating pumps and condenser fan is not considered.

(Lachance, 2003) and (Leong and Liu, 2004a) evaluate the performance of an adsorption heat pump using the COP and specific cooling power (SCP) parameters. They are defined, respectively, as:

$$COP = \frac{Q_{evap}}{Q_{reg}} \tag{3.7}$$

$$SCP = \frac{Q_{evap}}{t_{cycle} \cdot m_z} \tag{3.8}$$

where Q_{evap} is the amount of heat input to the evaporator during the discharge process [J], Q_{reg} is the amount of heat input to the adsorber during the charging process [J], t_{cycle} is the length of the complete cycle [s] and m_z is the mass of adsorbent [kg].

(Gui et al., 2002) define the coefficient of amplification (COA), the specific heating power (SHP) and the heat-recovery ratio (r) for an adsorptive reversible heat pump:

$$COA = \frac{Q_c + Q_{3-4} + Q_{4-1} - Q_r}{Q_{1-2} + Q_{2-3} - Q_r} \tag{3.9}$$

$$SHP = \frac{Q_c + Q_{3-4} + Q_{4-1} - Q_r}{m_z \cdot t} \tag{3.10}$$

$$r = \frac{Q_r}{Q_{1-2} + Q_{2-3}} \tag{3.11}$$

where

Q_c is the amount of heat released by the condenser during the charging phase [J];

Q_{3-4} is the amount of heat released during the isosteric cooling of the adsorber [J]. This is the step in which the pressure in the adsorber is reduced from the condenser to the evaporator pressure (point 3 to point 4 in Figure 3.2);

Q_{4-1} is the amount of heat released during the adsorption of the vapour by the adsorbent (point 4 to 1 in Figure 3.2) during the discharge phase [J];

Q_r is the amount of heat recovered from the adsorption storage unit [J];

Q_{1-2} is the amount of heat required for the isosteric heating of the adsorber [J]. This is the step in which the pressure in the adsorber is increased from the evaporator to the condenser pressure (point 1 to 2 in Figure 3.2);

Q_{2-3} is the amount of heat required for the desorption of vapour from the adsorbent (point 2 to point 3 in Figure 3.2) during the charging phase [J];

m_z is the mass of adsorbent [kg], and

t is the half cycle time, or the length of time of the discharge process [s].

The mathematical model of the adsorption storage unit described in the next section is conceived to allow different adsorbent-adsorbate working pairs to be investigated. The zeolite-water working pair will be investigated in this work because of the suitability of the pair to the application being considered for this research. The suitability of an adsorption storage unit's working pair depends significantly on the operating conditions of the application (Nùñez et al., 1999). For this application, temperatures in the range of 300 – 400 ºC are available for charging the storage unit (this is the range of temperatures available from the fuel cell exhaust gases), and temperatures in the range of 60 – 80 ºC are required upon discharge of the storage unit for space heating and domestic hot water. (Nùñez et al., 1999) found that for systems with desorption (or charging) temperatures greater than 200ºC and adsorption (or discharge) temperatures greater than 40ºC above evaporation temperatures, zeolite is the most appropriate adsorbent. Zeolite adsorbents can adsorb large amounts of water vapour and as water has a high latent heat of vaporization and a convenient boiling point, the zeolite-water pair is one of the most preferred adsorbent-adsorbate pairs (Tather et al., 1999). Specifically, zeolite type 13x has the highest adsorption capacity for water (Tather et al., 1999).

The mathematical model can be adapted to investigate the feasibility of other working pairs for the adsorption storage unit in future work.

3.5 Governing Equations

3.5.1 Assumptions

The following assumptions are made in the mathematical model:

- The solid and gas phases within the adsorber are in thermodynamic equilibrium. This assumption ignores the resistance to mass transfer between the vapour adsorbate and the adsorbent and assumes that equilibrium is reached instantly. As discussed in chapter 2, (Chahbani et. al, 2002) found that the performance of an adsorption heat pump could be properly predicted using the equilibrium model if the vapour adsorbate has a high diffusivity and if the cycle time is long.
- The pressure and temperature in each system component are uniform in space.
- The adsorbate is adsorbed and desorbed uniformly by the adsorbent during the discharge and charging phases, respectively.
- The adsorbate, when in vapour form, behaves as an ideal gas.
- The adsorption storage unit operates ideally. That is, during the isosteric heating and cooling phases, the ratio of adsorbate mass to adsorbent mass is constant and during the adsorption and desorption phases, the pressure is constant.
- Any heat losses through the pipes connecting the plant components are neglected.
- The electric consumption of the pump that transfers the liquid adsorbate from the condenser to the reservoir during the charging phase and from the reservoir to the evaporator during the discharge of the storage unit is neglected.
- The adsorption characteristics of the adsorbent and adsorbate pair can be described using the Dubunin-Astakhov relation.

3.5.2 Equations of State

The Dubunin-Astakhov (D-A) equation relates the ratio of mass of adsorbate within the adsorbent to the mass of dry adsorbent, X [kg adsorbate/kg adsorbent], to the adsorbate's pressure P [mbar], and temperature, T [Kelvin]:

$$X(P,T) = W_o \rho(T) \exp(-D[T \ln(\frac{P_{sat}}{P})]^n) \tag{3.12}$$

The variables D and n are adsorption characteristics of the adsorbent/adsorbate pair while W_o [m^3/kg adsorbent] represents the volume of the adsorption space, i.e. the micropore volume, which is a characteristic of the adsorbent. The variable ρ(T) [kg/m^3] is the density of the adsorbate in its bulk liquid form, which is a function of the adsorbate temperature. Equation (3.13) provided in (IAPWS, 1992) is used to determine ρ(T):

$$\frac{\rho}{\rho_{ref}} = 1 + b_1\tau^{1/3} + b_2\tau^{2/3} + b_3\tau^{5/3} + b_4\tau^{16/3} + b_5\tau^{43/3} + b_6\tau^{110/3} \tag{3.13}$$

where

$$\tau = 1 - \frac{T[K]}{T_{ref}} \tag{3.14}$$

T_{ref} = 647.096 K

ρ_{ref} = 322 kg/m^3

b_1 = 1.99274064

b_2 = 1.09965342

b_3 = -0.510839303

b_4 = -1.75493479

b_5 = -45.5170352

b_6 = -6.74694450E05

The saturation pressure P_{sat} [MPa][2] of the water adsorbate is determined using Equation (3.15) from (IAPWS,1992):

$$\ln\left(\frac{P_{sat}}{P_{ref}}\right) = \frac{T_{ref}}{T}[a_1\tau + a_2\tau^{1.5} + a_3\tau^3 + a_4\tau^{3.5} + a_5\tau^4 + a_6\tau^{7.5}] \quad (3.15)$$

where

P_{ref} = 22.064 MPa

a_1 = -7.85951783

a_2 = 1.84408259

a_3 = -11.7866497

a_4 = 22.6807411

a_5 = -15.9618719

a_6 = 1.80122502

An ideal cycle is assumed for the adsorption storage unit. That is, during the adsorption and desorption phases, the pressure is assumed constant and equal to the evaporator and condenser pressure, respectively. Thus, these values are used in equation (3.12) to determine the ratio of mass of adsorbate to mass of adsorbent, X, for a particular adsorber temperature T. During the isosteric heating and cooling phases, the ratio X is assumed constant and equation (3.12) is solved iteratively using a bi-section method (Press et al., 1986) to determine the pressure P at a particular adsorber temperature T. The pressure P is required to determine at which point the adsorber switches from the isosteric heating phase to the desorption phase during charging (this occurs when the adsorber pressure is equal to the condenser pressure), and from the isosteric cooling phase to the adsorption

[2] 1 MPa = 10000 mbar

phase during the discharge process (this occurs when the adsorber pressure is equal to the evaporator pressure).

Figure 3.7 presents schematically the variation of the ratio X with temperature T for different values of pressure P for a zeolite-water sorption pair. The coefficients Wo, D and n of equation (3.12) were obtained from (Lachance, 2003).

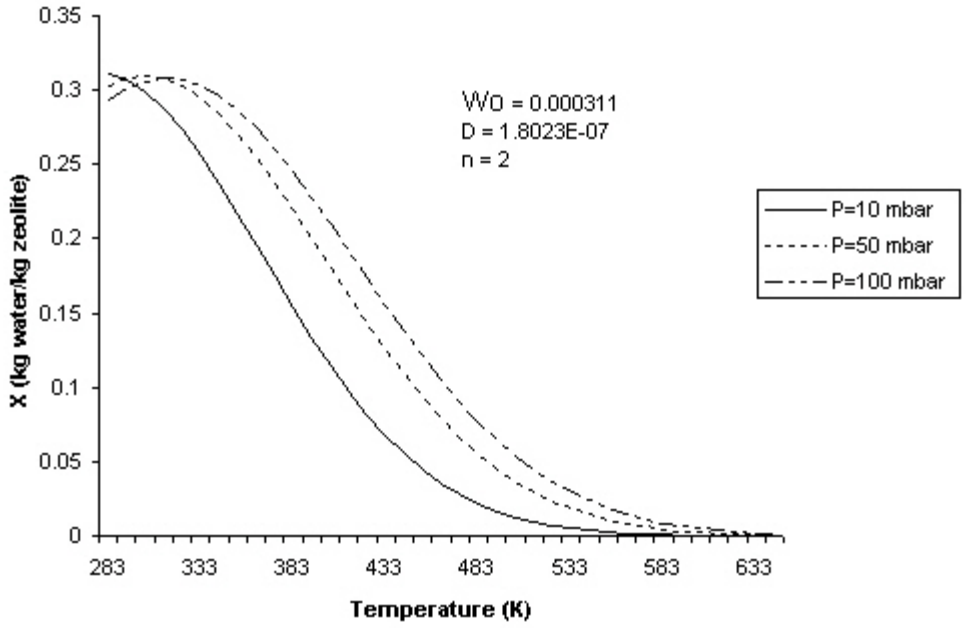

Figure 3.7 X (kg water/kg zeolite) as a function of T (K) and P (mbar) for a zeolite-water pair

3.5.3 Heat Balance Equations

3.5.3.1 Adsorber Heat Balance

An energy balance on the control volume surrounding the adsorber leads to:

Charging state: $$\frac{\partial E_{ads}}{\partial t} = -\dot{Q}_{loss} + \dot{Q}_{h/x} - \left| m_z \frac{\partial X}{\partial t} \Delta H \right| \quad (3.16)$$

Discharge state: $$\frac{\partial E_{ads}}{\partial t} = -\dot{Q}_{loss} - \dot{Q}_{h/x} + \left| m_z \frac{\partial X}{\partial t} \Delta H \right| \quad (3.17)$$

Storage state: $$\frac{\partial E_{ads}}{\partial t} = -\dot{Q}_{loss} \quad (3.18)$$

The term on the left hand side of equations (3.16), (3.17) and (3.18) is the variation of energy stored sensibly in the adsorber. It can be expressed as the sum of the energy variation in the dry adsorbent, in the vapour adsorbed within the adsorbent, in the adsorber vessel and in the heat exchanger contained within the adsorber:

$$\frac{\partial E_{ads}}{\partial t} = \{m_z Cp_z + m_z X \cdot Cp_w + m_{vessel} Cp_{vessel} + m_{h/x} Cp_{h/x}\} \frac{\partial T}{\partial t} \quad (3.19)$$

where:

m_z is the mass of the dry adsorbent in the adsorber (kg);

Cp_z is the specific heat of the dry adsorbent, which is assumed to be constant (J/kg°C);

X is the ratio of mass of adsorbate within the adsorbent per mass of dry adsorbent (kg/kg);

m_zX is the mass of adsorbate within the adsorbent (kg);

Cp_w is the specific heat of the adsorbate, which can be assumed to be equal to the specific heat of the adsorbate in liquid form (Cacciola and Restuccia, 1995) (J/kgºC); the Shomate equation (3.20), obtained from the National Institute of Standards and Technology Chemistry Webbook (NIST, 2003) is used to determine this value as a function of temperature:

$$Cp_w = \{A + B \cdot t_K + C \cdot t_K{}^2 + D \cdot t_K{}^3 + E / t_K{}^2\} / [\text{Mol weight}]_{H_2O} \quad (3.20)$$

where

Cp_w is the specific heat of water [J/kg°C];

A = -203.6060

B = 1523.290

C = -3196.413

D = 2474.455

E = 3.855326

t_K = T[Kelvin]/1000

$[\text{Mol weight}]_{H2O}$ = 0.0180155 kg/mol

m_{vessel} is the mass of the adsorber vessel (kg);

Cp_{vessel} is the specific heat of the vessel material, which is assumed to be constant (J/kgºC);

$m_{h/x}$ is the mass of the heat exchanger material contained within the adsorber (kg);

$Cp_{h/x}$ is the specific heat of the heat exchanger material, which is assumed to be constant (J/kgºC);

T is the temperature in the adsorber (ºC). It is assumed that the adsorbate, adsorbent, heat exchanger and adsorber vessel are all at temperature T.

The first term on the right hand side of the adsorber heat balance equations (3.16)-(3.18), $\dot{Q}_{loss}$, represents the heat loss to the surroundings. The term $\dot{Q}_{loss}$ can be estimated by considering the thickness and thermal conductivity of the insulation layer surrounding the adsorber vessel and an ambient heat transfer coefficient that takes into account convection to the surrounding air and longwave radiation exchange with surfaces in the containing room. These parameters are shown schematically in Figure 3.8.

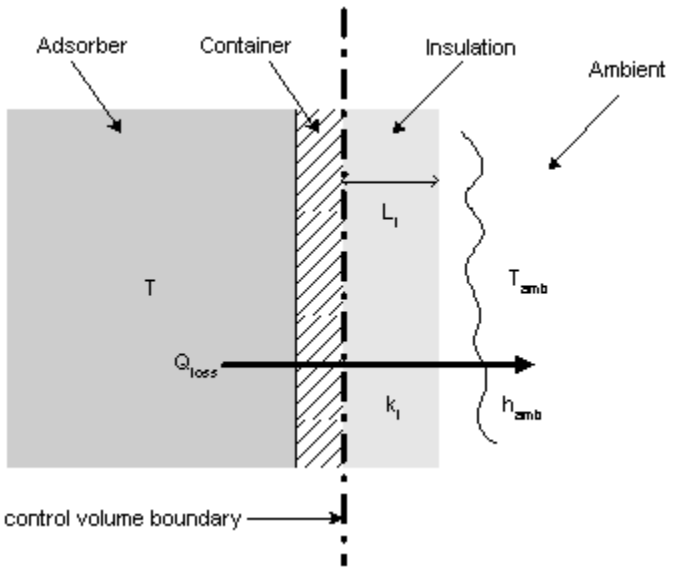

Figure 3.8 Schematic showing thermal resistances between adsorber control volume and surroundings

The total resistance, R_{total}, between the adsorber and the ambient can be calculated as follows:

$$R_{total} = \frac{L_i}{k_i} + \frac{1}{h_{amb}} \tag{3.21}$$

where

L_i is the thickness of the insulation surrounding the adsorber vessel (m), k_i is the thermal conductivity of the insulation surrounding the adsorber container (W/mºC) and h_{amb} is the overall heat transfer coefficient to the surroundings (W/m^{2}ºC). This latter term takes into account convection to the surrounding air and longwave radiation exchange with surfaces in the containing room.

The heat loss to the surroundings is then calculated as:

$$\dot{Q}_{loss} = \frac{T - T_{amb}}{R_{total}} * As_a \tag{3.22}$$

where

T_{amb} is the temperature of the surroundings (ºC) and

As_a is the surface area of the adsorber vessel (m^2).

The second term on the right hand side of the heat balance equations (3.16) and (3.17), $\dot{Q}_{h/x}$, represents the heat exchange between the adsorber and the heat transfer fluid

flowing through the heat exchanger. The relevant parameters are presented schematically in Figure 3.9.

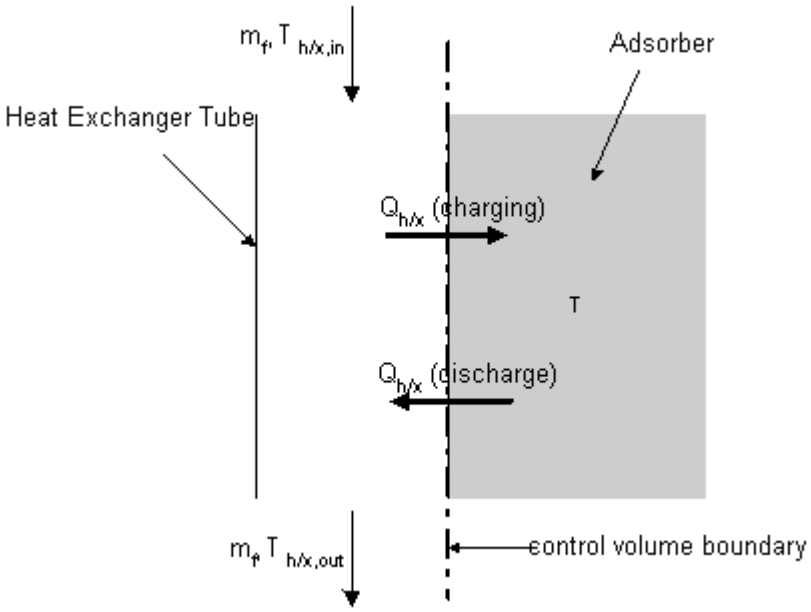

Figure 3.9 Schematic showing parameters involved in heat exchanger calculation

The amount of heat transferred between the heat exchanger and the adsorber can be calculated as follows:

Charging state: $\dot{Q}_{h/x} = \dot{m}_f Cp_f (T_{h/x,in} - T_{h/x,out})$ (3.23)

Discharge state: $\dot{Q}_{h/x} = \dot{m}_f Cp_f (T_{h/x,out} - T_{h/x,in})$ (3.24)

where

$\dot{m}_f$ is the mass flow rate of the heat exchanger fluid (kg/s);

Cp_f is the specific heat of the heat exchanger fluid (J/kgºC);

$T_{h/x,out}$ is the temperature of the fluid leaving the heat exchanger (ºC) and

$T_{h/x,\,in}$ is the temperature of the fluid entering the heat exchanger (ºC).

It is assumed that the heat exchanger fluid between the adsorber and the fuel cell (loop B in Figure 3.6), and between the adsorber and the main hot water storage tank (loop C in Figure 3.6) is pressurized water in order to accommodate the high temperatures at the fuel cell and at the adsorber. As the use of pressurized water loops may not be the most practical approach, the issue of alternative heat exchanger fluids should be addressed in the design of the system and in future research work. The pressure of the heat exchange loops will be such that boiling will be prevented at the plant operating temperatures. The specific heat Cp_f in equations (3.23) and (3.24) is a function of the pressure of the heat exchange loop and the temperature T_{in}. It is calculated by using an existing function in ESP-r based on (IAPWS, 1996). For brevity, the correlation for Cp_f is not provided in this document as it involves determining the ideal gas part and residual part of the dimensionless Helmholtz free energy and their derivatives; interested readers are advised to consult (IAPWS, 1996).

The effectiveness approach can be used to relate the temperature of the fluid leaving the heat exchanger and the temperature of the adsorber. The maximum heat exchange between the heat exchanger fluid and the adsorber, $\dot{Q}_{h/x,\max}$, occurs if the temperature of the fluid leaving the heat exchanger is equal to the temperature T of the adsorber, i.e.

Charging state: $\dot{Q}_{h/x,\max} = \dot{m}_f Cp_f (T_{h/x,in} - T)$ (3.25)

Discharge state: $\dot{Q}_{h/x,\max} = \dot{m}_f Cp_f (T - T_{h/x,in})$ (3.26)

If the heat exchanger effectiveness, ε, is defined as

$$\varepsilon = \frac{\dot{Q}_{h/x}}{\dot{Q}_{h/x,\max}} \quad (3.27)$$

then the heat transfer between the heat exchanger and the adsorber can be determined by:

Charging state: $\dot{Q}_{h/x} = \varepsilon_1 \cdot \dot{Q}_{h/x,\max} = \varepsilon_1 \cdot \dot{m}_f Cp_f (T_{h/x,in} - T)$ (3.28)

Discharge state: $\dot{Q}_{h/x} = \varepsilon_2 \cdot \dot{Q}_{h/x,\max} = \varepsilon_2 \cdot \dot{m}_f Cp_f (T - T_{h/x,in})$ (3.29)

The effectiveness approach is chosen because of the limited amount of data available in the literature regarding the characteristics of the adsorber's heat exchanger and because of its simplicity. As this research is not concerned with determining the optimum design characteristics of the adsorber, a simplified approach to quantify the heat exchange at the adsorber is appropriate.

It should be noted that the adsorber is connected to two plant components – the fuel cell during the charging phase and the main water storage tank during the discharge phase. As the heat exchanger fluid flow rate may differ depending on whether the adsorption storage unit is in charging or discharge mode, the heat exchanger effectiveness ε may also differ depending on the unit's operating mode. This will be taken into account by allowing two heat exchanger effectiveness values to be considered in the model, one constant efficiency (ε_1) that applies during the charging phase and another constant efficiency (ε_2) that applies during the discharge phase. A sensitivity analysis will be performed and presented in chapter 4 to investigate the importance of the variables ε_1 and ε_2 and the consequence of assuming that they are constant.

The final term in the adsorber heat balance equations (3.16) and (3.17), $\left| m_z \frac{\partial X}{\partial t} \Delta H \right|$, represents the heat of adsorption that is stored or released, during the charging and discharge phases, respectively. During the charging phase, the term is a sink term and thus negative. During the discharge phase, the term is a source term and thus positive.

Since the variable X is a function of temperature T and pressure P, the term $\frac{\partial X}{\partial t}$ can be expressed as:

$$\frac{\partial X}{\partial t} = \left.\frac{\partial X}{\partial T}\right|_P \frac{\partial T}{\partial t} + \left.\frac{\partial X}{\partial P}\right|_T \frac{\partial P}{\partial t} \tag{3.30}$$

If an ideal cycle is assumed, the pressure remains constant during the adsorption and desorption of vapour, when the valve between the adsorber and condenser/evaporator is opened, and therefore the last term in equation (3.30) disappears.

The value $\left.\frac{\partial X}{\partial T}\right|_P$ is calculated numerically at a temperature T as follows:

$$\left.\frac{\partial X}{\partial T}\right|_P = \frac{X(T_u, P) - X(T_l, P)}{\Delta T^*} \tag{3.31}$$

where

$\Delta T^* = 0.05°C$
$T_l = T - 0.5 * \Delta T^*$
$T_u = T + 0.5 * \Delta T^*$

The pressure P in the above equation is set to the condenser pressure during the charging phase and the evaporator pressure during the discharge phase, when the valve between the adsorber and condenser or evaporator is open.

The heat of adsorption ΔH is assumed constant in this model. (Leong and Liu, 2004b) provide a value of 3.2×10^6 J/kg for a zeolite NaX/water working pair.

All of the terms in the heat balance equations (3.16)-(3.18) for the adsorber control volume have been addressed in the preceding paragraphs.

3.5.3.2 Condenser/Evaporator Heat Balance

In order to simplify the model, thermal transients within the condenser and evaporator are ignored. The energy balance on the control volume surrounding the condenser or the control volume surrounding the evaporator leads to:

Condenser (Charging state): $-\dot{Q}_{c-e} - \dot{Q}_{loss} + \dot{m}_{vap,flow} h_{vap} - \dot{m}_{liq} h_{liq} = 0$ (3.32)

Evaporator (Discharge state): $\dot{Q}_{c-e} - \dot{Q}_{loss} - \dot{m}_{vap,flow} h_{vap} + \dot{m}_{liq} h_{liq} = 0$ (3.33)

The first term on the left hand side of the condenser/evaporator heat balances, $\dot{Q}_{c-e}$, represents the heat of condensation that is removed from the condenser when the unit is in charging mode or the heat input at the evaporator when the unit is in discharge mode. It can be calculated by considering the effectiveness value for the condenser/evaporator, $\varepsilon_{c\text{-}e}$:

Condenser (Charging state): $\dot{Q}_{c-e} = \varepsilon_c \dot{m}_{fl} Cp_{fl} (T_c - T_{c,in})$ (3.34)

Evaporator (Discharge state): $\dot{Q}_{c-e} = \varepsilon_e \dot{m}_{fl} Cp_{fl} (T_{e,in} - T_e)$ (3.35)

where

ε_c is the effectiveness of the condenser;

ε_e is the effectiveness of the evaporator;

$\dot{m}_{fl}$ is the mass flow rate of the heat transfer fluid flowing through the condenser or evaporator (kg/s);

Cp_{fl} is the specific heat of the heat transfer fluid flowing through the condenser or evaporator (J/kgºC);

$T_{c,in}$ is the temperature of the heat transfer fluid entering the condenser (ºC);

$T_{e,in}$ is the temperature of the heat transfer fluid entering the evaporator (ºC) ;

T_c is the temperature at the condenser (ºC) and

T_e is the temperature at the evaporator (ºC).

For this work, it is assumed that the condenser is air-cooled. Thus, the heat transfer fluid flowing through the condenser is air and the incoming air temperature is the outdoor temperature determined for the particular time (e.g., day, hour) from the weather file. The specific heat of the air flowing through the condenser and the water flowing through the evaporator is determined as a function of the incoming fluid temperature using ESP-r's existing SHTFLD function. The correlations for air and water as a function of temperature, T [ºC], are (Ham, 1984):

For air:

$$Cp_{fl} = 1006 + (\frac{T}{200}) + (\frac{T^2}{7500}) \tag{3.36}$$

For water:

$$Cp_{fl} = 4244 - 22.65\sqrt{T} + 1.95T \tag{3.37}$$

The second term on the right hand side of the condenser/evaporator heat balances, equations (3.32) and (3.33), $\dot{Q}_{loss}$, represents the sensible heat losses of the condenser/evaporator to the containing room due to convection to the surrounding air and longwave radiation exchange with surfaces in the containing room, expressed as:

Condenser (Charging state): $\dot{Q}_{loss} = h_{amb_c} \cdot As_c \cdot (T_c - T_{amb})$ (3.38)

Evaporator (Discharge state): $\dot{Q}_{loss} = h_{amb_e} \cdot As_e \cdot (T_e - T_{amb})$ (3.39)

where

$h_{amb,c}$ is the overall heat transfer coefficient from the condenser to the surroundings ($W/m^2°C$);

$h_{amb,e}$ is the overall heat transfer coefficient from the evaporator to the surroundings ($W/m^2°C$);

As_c is the surface area of the condenser (m^2);

As_e is the surface area of the evaporator (m^2) and

T_{amb} is the temperature of the surroundings (°C).

The term $\dot{m}_{vap,flow} h_{vap}$ in the heat balance equation (3.32) represents the heat contained in the vapour entering the condenser, while in the heat balance equation (3.33), it represents the heat contained within the vapour leaving the evaporator. Similarly, the term $\dot{m}_{liq} h_{liq}$ in

equation (3.32) represents the heat contained in the liquid leaving the condenser while in equation (3.33) it represents the heat contained in the liquid entering the evaporator.

The enthalpy terms h_{vap} and h_{liq} must be rearranged in order for them to be expressed in terms of temperature in the heat balance equations. The method described in (Beausoleil-Morrison, 2001) is used here. The specific heat of the vapour or liquid is related to enthalpy by the following expression:

$$Cp_{vap/liq} = \left(\frac{\partial h}{\partial T}\right)_P \tag{3.40}$$

Assuming that the enthalpy varies linearly with temperature, the specific heat of the vapour or liquid adsorbate at a temperature T can be approximated with respect to a reference temperature T_{ref}:

$$Cp_{vap/liq,T} = \frac{(h_{vap/liq})_T - (h_{vap/liq})_{Tref}}{T - T_{ref}} \tag{3.41}$$

Finally, the enthalpy terms h_{vap} and h_{liq} at a temperature T can be expressed in terms of temperature in the heat balance equations as:

$$(h_{vap/liq})_T = Cp_{vap/liq,T} \cdot (T - T_{ref}) + (h_{vap/liq})_{Tref} \tag{3.42}$$

The Shomate equations for liquid water and water vapour (NIST, 2003) are used to determine the numerator [J/kg] of equation (3.41):

$$\Delta h_{vap/liq} = \{A \cdot t + \frac{B}{2} \cdot t^2 + \frac{C}{3} \cdot t^3 + \frac{D}{4} \cdot t^4 - \frac{E}{t} + F - H\} \cdot 1000 / [Molweight]_{H2O} \qquad (3.43)$$

where

t = T[K]/1000

$[\text{Mol weight}]_{H2O}$ = 0.0180155 kg/mol

and the coefficients A-H are provided in Table 3.1.

Table 3.1 Coefficients of Shomate equation (3.43) for water vapour and liquid water

	A	B	C	D	E	F	H
vap	30.09200	6.832514	6.793435	-2.534480	0.082139	-250.8810	-241.8264
liq	-203.606	1523.980	-3196.413	2474.455	3.855326	-256.5478	-285.8304

The reference temperature T_{ref} is 25°C, the reference water vapour enthalpy $h_{vap,Tref}$ is 2546470 J/kg and the reference liquid water enthalpy $h_{liq,Tref}$ is 104830 J/kg.

For completeness, the terms $\dot{m}_{vap,flow} h_{vap}$ and $\dot{m}_{liq} h_{liq}$ appearing in the heat balance equations (3.32) and (3.33) are explicitly defined here:

Condenser (Charging state):

$$\dot{m}_{vap,flow} h_{vap} = \dot{m}_{vap,flow} \cdot [Cp_{vap,Ta} \cdot (T_a - T_{ref}) + h_{vap,Tref}] \qquad (3.44)$$

$$\dot{m}_{liq} h_{liq} = \dot{m}_{liq} \cdot [Cp_{liq,Tc} \cdot (T_c - T_{ref}) + h_{liq,Tref}] \quad (3.45)$$

Evaporator (Discharge state):

$$\dot{m}_{vap,flow} h_{vap} = \dot{m}_{vap,flow} \cdot [Cp_{vap,Te} \cdot (T_e - T_{ref}) + h_{vap,Tref}] \quad (3.46)$$

$$\dot{m}_{liq} h_{liq} = \dot{m}_{liq} \cdot [Cp_{liq,Tr} \cdot (T_r - T_{ref}) + h_{liq,Tref}] \quad (3.47)$$

where

T_a is the temperature of the adsorber (°C);

T_c is the temperature of the condenser (°C) and

T_r is the temperature of the reservoir (°C) where the liquid adsorbate is stored.

3.5.4 Mass Balance Equations

3.5.4.1 Adsorber Mass Balance

There are two mass balances for the adsorber component; one corresponding to periods when the valve connecting the adsorber and the condenser or evaporator is closed and the other corresponding to periods when the valve is open.

The valve connecting the adsorber and the condenser or evaporator is closed during the isosteric heating and cooling phases, respectively, during which the ratio of adsorbate

mass to adsorbent mass, X, is constant. There is no transfer of mass between the adsorber and the condenser/evaporator. The mass balance for the adsorber control volume is:

$$m_z \frac{\partial X}{\partial t} = 0 \tag{3.48}$$

where $m_z \frac{\partial X}{\partial t}$ represents the change in mass of the adsorbate within the adsorbent.

When the valve is open, the mass balance of the adsorber leads to:

Charging state: $m_z \frac{\partial X}{\partial t} = -\dot{m}_{vap,flow}$ (3.49)

Discharge state: $m_z \frac{\partial X}{\partial t} = \dot{m}_{vap,flow}$ (3.50)

where $\dot{m}_{vap,flow}$ is the mass flow rate of the vapour that flows between the adsorber and the condenser/evaporator. The value of $\dot{m}_{vap,flow}$ is negative when the adsorption unit is in charging mode (vapour flows out of the adsorber control volume) and positive when the unit is in discharge mode (vapour flows into the adsorber control volume).

3.5.4.2 Condenser/Evaporator Mass Balance

When the valve between the adsorber and the condenser/evaporator is closed, there is no mass transfer between the condenser and the adsorber or between the evaporator and the reservoir. When the valve between the adsorber and condenser/evaporator is opened, the mass balance is:

Condenser (Charging state): $0 = \dot{m}_{vap,flow} - \dot{m}_{liq}$ (3.51)

Evaporator (Discharge state): $0 = -\dot{m}_{vap,flow} + \dot{m}_{liq}$ (3.52)

That is, the mass of fluid entering the condenser/evaporator is equal to the mass of fluid leaving the condenser/evaporator.

3.6 Implementation of Mathematical Model in ESP-r

3.6.1 Adsorption Storage Unit

The mathematical model of the adsorption storage unit presented in Section 3.5 was implemented in ESP-r's plant domain. The adsorption storage unit is characterized as a plant component with 3 nodes: a node representing the adsorber, a node representing the condenser and a node representing the evaporator. Specifically, the following was done:

- An entry was added to ESP-r's plant component database for the adsorption storage unit. This allows users to select the adsorption storage unit as a component within the plant network via ESP-r's user interface and is required by the ESP-r simulation engine.
- A subroutine was added to ESP-r's plant domain to save the input data associated with the adsorption storage unit plant component into variables that are accessible to other subroutines. The subroutine also verifies that the correct number of inputs are specified and that for each node, the correct number and type of connections to other plant components are defined.
- A subroutine was added to ESP-r's plant domain to set up the matrix coefficients used by the plant domain equation solver to solve for nodal temperatures, first phase mass flows (i.e. water flow between nodes) and second phase mass flows (i.e. water vapour flow between nodes). The subroutine, commonly referred to as the coefficient generator, also defines the variables to be tracked for output. The determination of the energy balance matrix coefficients for each of the adsorption storage unit nodes is further explained below.

The subroutines and functions added to ESP-r were written in FORTRAN 77. Figure 3.10 shows the existing ESP-r plant domain subroutines that were modified, and the new subroutines that were created, for this work and how they interact with the plant component database and other subroutines in ESP-r's plant domain. It should be noted that for simplicity, the flowchart presented in Figure 3.10 does not present all of the

functions and subroutines in ESP-r's plant domain but rather only those that interact directly with the new and/or modified subroutines.

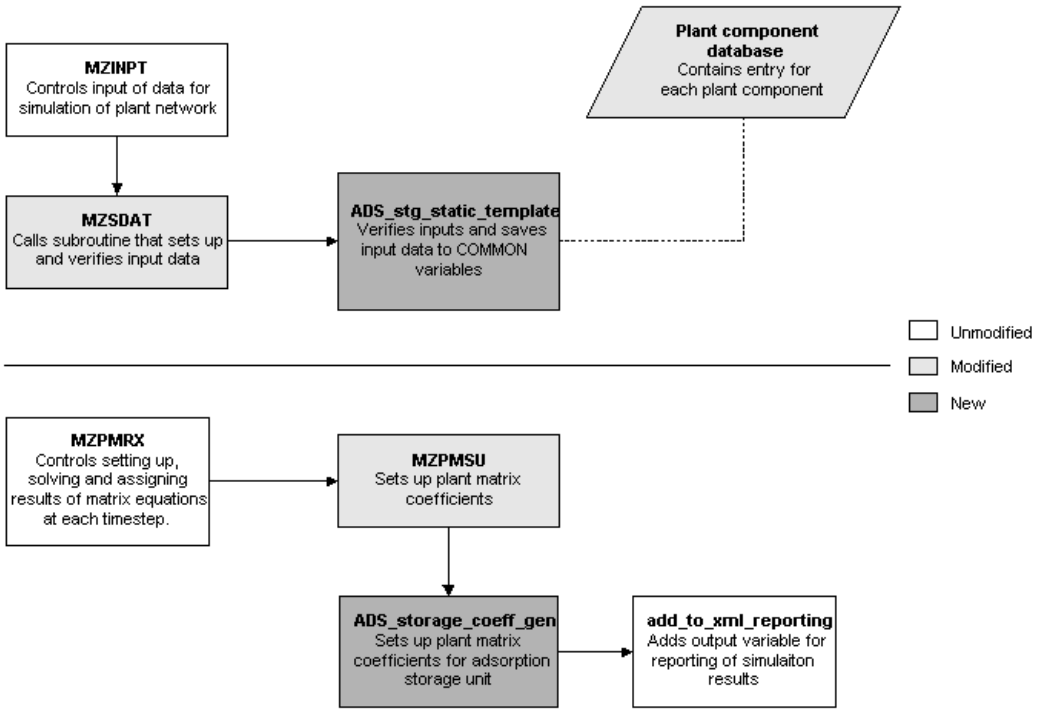

Figure 3.10 ESP-r plant domain subroutines

The plant matrix coefficients that apply to the solution of the energy balance at each of the nodes pertaining to the adsorption storage unit are derived below.

Node 1. Adsorber

Combining the heat balance equations (3.16), (3.17) and (3.18) that apply to the charging, discharge and storage modes, respectively, of the adsorber and assuming that the irrelevant terms in a particular mode are nil, leads to:

$$\frac{\partial E}{\partial t} = -\dot{Q}_{loss} + \dot{Q}_{fc} - \dot{Q}_{\tan k} \pm \left| m_z \frac{\partial X}{\partial t} \Delta H \right| \tag{3.53}$$

where

$\dot{Q}_{fc}$ represents the heat input to the adsorber from the fuel cell during the charging mode (W) and

$\dot{Q}_{\tan k}$ represents the heat output from the adsorber to the water tank during the discharge mode (W).

The last term in equation (3.53) is positive during the discharge mode (source term) and negative during the charging mode (sink term).

Substituting equations (3.19), (3.22), (3.28), (3.29) and (3.30) into equation (3.53) leads to:

$$\begin{aligned} &\left\{ m_z Cp_z + m_z X Cp_w + m_{vessel} Cp_{vessel} + m_{h/x} Cp_{h/x} - m_z \frac{\partial X}{\partial T_1} \Delta H \right\} \frac{\partial T_1}{\partial t} = \\ &- \left\{ \frac{T_1 - T_{amb}}{R_{total}} \right\} A s_a + \varepsilon_1 \dot{m}_{fc} Cp_{fc} (T_{fc} - T_1) - \varepsilon_2 \dot{m}_{\tan k} Cp_{\tan k} (T_1 - T_{\tan k}) \end{aligned} \tag{3.54}$$

where

T_1 denotes the temperature of node 1 (°C);

$\dot{m}_{fc}$ denotes the mass flow rate of the pressurized water entering the adsorber from the fuel cell heat exchanger (kg/s);

Cp_{fc} denotes the specific heat of the pressurized water entering the adsorber from the fuel cell heat exchanger (J/kg°C)

T_{fc} denotes the temperature of the pressurized water entering the adsorber from the fuel cell heat exchanger (°C);

$\dot{m}_{\tan k}$ denotes the mass flow rate of the pressurized water entering the adsorber from the hot water storage tank (kg/s);

Cp_{tank} denotes the specific heat of the pressurized water entering the adsorber from the hot water storage tank (J/kg°C) and

T_{tank} is the temperature of the pressurized water entering the adsorber from the hot water storage tank (°C).

The other variables appearing in equation (3.54) have been defined in section 3.5.

Representing the transient term in equation (3.54) with a forward difference scheme over a finite time-step Δt and representing the other terms at the present time-row leads to the explicit form of the heat balance on node 1:

$$\left\{m_z Cp_z + m_z[XCp_w]^t + m_{vessel}Cp_{vessel} + m_{h/x}Cp_{h/x} - m_z[\frac{\partial X}{\partial T_1}]^t \Delta H\right\}\frac{T_1^{t+\Delta t} - T_1^t}{\Delta t} = -\left\{\frac{T_1^t - T_{amb}^t}{R_{total}}\right\}As_a + \varepsilon_1[\dot{m}_{fc}Cp_{fc}]^t(T_{fc}^t - T_1^t) - \varepsilon_2[\dot{m}_{\tan k}Cp_{\tan k}]^t(T_1^t - T_{\tan k}^t) \quad (3.55)$$

The fully implicit form of the heat balance on node 1 is given by:

$$\left\{m_z Cp_z + m_z[XCp_w]^t + m_{vessel}Cp_{vessel} + m_{h/x}Cp_{h/x} - m_z[\frac{\partial X}{\partial T_1}]^t \Delta H\right\}\frac{T_1^{t+\Delta t} - T_1^t}{\Delta t} =$$
$$-\left\{\frac{T_1^{t+\Delta t} - T_{amb}^{t+\Delta t}}{R_{total}}\right\}As_a + \varepsilon_1[\dot{m}_{fc}Cp_{fc}]^{t+\Delta t}(T_{fc}^{t+\Delta t} - T_1^{t+\Delta t}) \qquad (3.56)$$
$$-\varepsilon_2[\dot{m}_{\tan k}Cp_{\tan k}]^{t+\Delta t}(T_1^{t+\Delta t} - T_{\tan k}^{t+\Delta t})$$

Multiplying equation (3.55) by a factor α (0< α<1) and equation (3.56) by (1- α), summing the two and rearranging so that future time-row self-coupling and cross-coupling terms appear on the left leads to a weighted average of the implicit and explicit forms of the heat balance on node 1:

$$\left\{\begin{array}{l}\frac{1}{\Delta t}\left[m_z Cp_z + m_z[XCp_w]^t + m_{vessel}Cp_{vessel} + m_{h/x}Cp_{h/x} - m_z[\frac{\partial X}{\partial T_1}]^t \Delta H\right] + \\ \alpha\frac{As_a}{Rtotal} + \alpha\varepsilon_1(\dot{m}_{fc}Cp_{fc})^{t+\Delta t} + \alpha\varepsilon_2(\dot{m}_{\tan k}Cp_{\tan k})^{t+\Delta t}\end{array}\right\}T_1^{t+\Delta t}$$
$$-\left[\alpha\varepsilon_1[\dot{m}_{fc}Cp_{fc}]^{t+\Delta t}\right]T_{fc}^{t+\Delta t} - \left[\alpha\varepsilon_2[\dot{m}_{\tan k}Cp_{\tan k}]^{t+\Delta t}\right]T_{\tan k}^{t+\Delta t} =$$
$$\left\{\begin{array}{l}\frac{1}{\Delta t}\left[m_z Cp_z + m_z[XCp_w]^t + m_{vessel}Cp_{vessel} + m_{h/x}Cp_{h/x} - m_z[\frac{\partial X}{\partial T_1}]^t \Delta H\right] - \\ (1-\alpha)\frac{As_a}{R_{total}} - (1-\alpha)\varepsilon_1(\dot{m}_{fc}Cp_{fc})^t - (1-\alpha)\varepsilon_2(\dot{m}_{\tan k}Cp_{\tan k})^t\end{array}\right\}T_1^t \qquad (3.57)$$
$$+(1-\alpha)\varepsilon_1(\dot{m}_{fc}Cp_{fc})^t T_{fc}^t + (1-\alpha)\varepsilon_2(\dot{m}_{\tan k}Cp_{\tan k})^t T_{\tan k}^t + (1-\alpha)\frac{As_a}{R_{total}}T_{amb}^t + \alpha\frac{As_a}{R_{total}}T_{amb}^{t+\Delta t}$$

Replacing the coefficients in equation (3.57) with the following expressions:

$$A_{11} = \frac{1}{\Delta t}\left[m_z Cp_z + m_z[XCp_w]^t + m_{vessel}Cp_{vessel} + m_{h/x}Cp_{h/x} - m_z\left[\frac{\partial X}{\partial T_1}\right]^t \Delta H\right] \qquad (3.58)$$
$$+\alpha\frac{As_a}{R_{total}} + \alpha\varepsilon_1(\dot{m}_{fc}Cp_{fc})^{t+\Delta t} + \alpha\varepsilon_2(\dot{m}_{\tan k}Cp_{\tan k})^{t+\Delta t}$$

$$A_{14} = -\alpha\varepsilon_1\left[\dot{m}_{fc}Cp_{fc}\right]^{t+\Delta t} \tag{3.59}$$

$$A_{15} = -\alpha\varepsilon_2\left[\dot{m}_{\tan k}Cp_{\tan k}\right]^{t+\Delta t} \tag{3.60}$$

$$\begin{aligned} R_1 = & \left\{ \begin{array}{l} \dfrac{1}{\Delta t}\left[m_z Cp_z + m_z\left[XCp_w\right]^t + m_{vessel}Cp_{vessel} + m_{h/x}Cp_{h/x} - m_z\left[\dfrac{\partial X}{\partial T_1}\right]^t \Delta H \right] - \\ (1-\alpha)\dfrac{As_a}{R_{total}} - (1-\alpha)\varepsilon_1(\dot{m}_{fc}Cp_{fc})^t - (1-\alpha)\varepsilon_2(\dot{m}_{\tan k}Cp_{\tan k})^t \end{array} \right\} T_1^t \\ & + (1-\alpha)\varepsilon_1(\dot{m}_{fc}Cp_{fc})^t T_{fc}^t + (1-\alpha)\varepsilon_2(\dot{m}_{\tan k}Cp_{\tan k})^t T_{\tan k}^t + (1-\alpha)\frac{As_a}{R_{total}}T_{amb}^t \\ & + \alpha\frac{As_a}{R_{total}}T_{amb}^{t+\Delta t} \end{aligned} \tag{3.61}$$

leads to the following form of equation (3.57):

$$A_{11}\cdot T_1^{t+\Delta t} + A_{14}\cdot T_{fc}^{t+\Delta t} + A_{15}\cdot T_{\tan k}^{t+\Delta t} = R_1 \tag{3.62}$$

The terms $T_1^{t+\Delta t}, T_{fc}^{t+\Delta t}$ and $T_{\tan k}^{t+\Delta t}$ are the variables that are being solved.

Node 2. Condenser

Substituting equations (3.34), (3.38), (3.44) and (3.45) in the heat balance equation for the condenser (3.32) and rearranging leads to the following:

$$\dot{m}_{vap,flow}[Cp_{vap,T1}(T_1 - T_{ref}) + h_{vap,Tref}] = \dot{m}_{liq}[Cp_{liq,T2}(T_2 - T_{ref}) + h_{liq,Tref}] + \varepsilon_c \dot{m}_{air} Cp_{air}(T_2 - T_{c,in}) + h_{amb} As_c (T_2 - T_{amb}) \quad (3.63)$$

where

T_2 is the temperature of node 2 (°C);

$\dot{m}_{air}$ is the mass flow rate of air entering the condenser (kg/s);

Cp_{air} is the specific heat of air entering the condenser (J/kg°C) and

$T_{c,in}$ is the temperature of the air entering the condenser (°C).

The other variables appearing in equation (3.63) have been defined in section 3.5.

Rearranging equation (3.63) so that the self-coupling and cross-coupling terms are on the left leads to:

$$(\dot{m}_{vap,flow} Cp_{vap,T1}) \cdot T_1 - [\dot{m}_{liq} Cp_{liq,T2} + \varepsilon_c \dot{m}_{air} Cp_{air} + h_{amb} As_c] \cdot T_2 = \dot{m}_{vap,flow} Cp_{vap,T1} T_{ref} - \dot{m}_{liq} Cp_{liq,T2} T_{ref} + \dot{m}_{liq} h_{liq,Tref} - \dot{m}_{vap,flow} h_{vap,Tref} - \varepsilon_c \dot{m}_{air} Cp_{air} T_{c,in} - h_{amb} As_c T_{amb} \quad (3.64)$$

Replacing the coefficients in equation (3.64) with the following expressions:

$$A_{21} = \dot{m}_{vap,flow} Cp_{vap,T1} \quad (3.65)$$

$$A_{22} = -[\dot{m}_{liq} Cp_{liq,T2} + \varepsilon_c \dot{m}_{air} Cp_{air} + h_{amb} As_c] \quad (3.66)$$

$$R_2 = \dot{m}_{vap,flow} Cp_{vap,T1} T_{ref} - \dot{m}_{liq} Cp_{liq,T2} T_{ref} + \dot{m}_{liq} h_{liq,Tref} - \dot{m}_{vap,flow} h_{vap,Tref} - \varepsilon_c \dot{m}_{air} Cp_{air} T_{c,in} - h_{amb} As_c T_{amb} \quad (3.67)$$

leads to the following form of equation (3.64):

$$A_{21} T_1^{t+\Delta t} + A_{22} T_2 = R_2 \quad (3.68)$$

The variables $T_1^{t+\Delta t}$ and T_2 are the variables that are being solved.

Node 3. Evaporator

Substituting equations (3.35), (3.39), (3.46) and (3.47) in the heat balance equation for the evaporator (3.33) and rearranging leads to the following:

$$\varepsilon_e \dot{m}_{aux-\tan k} Cp_{aux-\tan k} (T_{aux-\tan k} - T_3) + \dot{m}_{liq} [Cp_{liq,Tr} (T_r - T_{ref}) + h_{liq,Tref}] - \dot{m}_{vap,flow} [Cp_{vap,T3} (T_3 - T_{ref}) + h_{vap,Tref}] - h_{amb} As_e (T_3 - T_{amb}) = 0 \quad (3.69)$$

where

$\dot{m}_{aux-\tan k}$ is the mass flow rate of the water entering the evaporator from the auxiliary water tank (kg/s);

$Cp_{aux\text{-}tank}$ is the specific heat of the water entering the evaporator from the auxiliary water tank (J/kg°C);

$T_{aux\text{-}tank}$ is the temperature of the water entering the evaporator from the auxiliary water tank (°C);

T_3 is the temperature of node 3 (°C) and

T_r is the temperature of the liquid adsorbate entering the evaporator from the reservoir (°C).

The other variables appearing in equation (3.69) have been defined in section 3.5.

Rearranging equation (3.69) so that the self-coupling and cross-coupling terms are on the left leads to:

$$\begin{aligned}&-[\varepsilon_e \dot{m}_{aux-\tan k} Cp_{aux-\tan k} + \dot{m}_{vap,flow} Cp_{vap,T3} + h_{amb} As_e] \cdot T_3 + \\ &(\varepsilon_e \dot{m}_{aux-\tan k} Cp_{aux-\tan k}) \cdot T_{aux-\tan k} + (\dot{m}_{liq} Cp_{liq,Tr}) \cdot T_r = \\ &-h_{amb} As_e T_{amb} + \dot{m}_{liq} Cp_{liq,Tr} T_{ref} - \dot{m}_{vap,flow} Cp_{vap,T3} T_{ref} \\ &-\dot{m}_{liq} h_{liq,Tref} + \dot{m}_{vap,flow} h_{vap,Tref}\end{aligned} \tag{3.70}$$

Replacing the coefficients in equation (3.70) with the following expressions:

$$A_{33} = -[\varepsilon_e \dot{m}_{aux-\tan k} Cp_{aux-\tan k} + \dot{m}_{vap,flow} Cp_{vap,T3} + h_{amb} As_e] \tag{3.71}$$

$$A_{36} = \varepsilon_e \dot{m}_{aux-\tan k} Cp_{aux-\tan k} \tag{3.72}$$

$$A_{37} = \dot{m}_{liq} Cp_{liq,Tr} \tag{3.73}$$

$$\begin{aligned}R_3 = &-h_{amb} As_e T_{amb} + \dot{m}_{liq} Cp_{liq,Tr} T_{ref} - \dot{m}_{vap,flow} Cp_{vap,T3} T_{ref} \\ &-\dot{m}_{liq} h_{liq,Tref} + \dot{m}_{vap,flow} h_{vap,Tref}\end{aligned} \tag{3.74}$$

leads to the following form of equation (3.70):

$$A_{33}T_3 + A_{36}T_{aux-\tan k} + A_{37}T_r = R_3 \tag{3.75}$$

The variables T_3, $T_{aux\text{-}tank}$ and T_r are the variables that are being solved.

Assembling equations (3.62), (3.68) and (3.75) yields a matrix of energy balance equations for the adsorption storage unit that has the following form:

$$\left|\begin{array}{ccc:ccc} A_{11} & & & A_{14} & A_{15} & \\ A_{21} & A_{22} & & & & \\ & & A_{33} & & & A_{36} \quad A_{37} \end{array}\right| \text{X} \left|\begin{array}{c} T_1^{t+\Delta t} \\ T_2 \\ T_3 \\ T_{fc}^{t+\Delta t} \\ T_{\tan k}^{t+\Delta t} \\ T_{aux\text{-}tank} \\ T_r \end{array}\right| = \left|\begin{array}{c} R_1 \\ R_2 \\ R_3 \end{array}\right|$$

The matrix coefficients A_{ij} and R_i are determined in the coefficient generator subroutine for the adsorption storage unit and used to solve for T_j at each timestep.

3.6.2 Modifications to existing ESP-r plant component models

In order to model the system depicted in Figure 3.6, modifications were required to several existing plant component models in ESP-r and a new controller type was required in ESP-r's plant domain.

Two water storage tank models were available in ESP-r: a model of a gas-fired storage tank and a model of an electrically heated storage tank (Beausoleil-Morrison, 2002b). For both models, the node representing the storage tank's water and casing allowed for two connections: a connection to a heat source, such as a fuel cell's exhaust-to-water heat exchanger, and a connection to a heat sink, such as an air handling unit's heating coil. The two water storage tank models were modified to allow for an additional connection so that the main water storage tank depicted in Figure 3.6 could be modelled. The new gas-fired storage tank model and electrically heated storage tank models now allow for three connections: one to the fuel cell's exhaust-to-water heat exchanger, a second to the air handling unit's heating coil and a third to the adsorption storage unit's adsorber.

The existing SOFC plant component model in ESP-r allows one connection to the fuel cell's exhaust-to-water heat exchanger (Beausoleil-Morrison, 2001). The model was modified to permit an additional connection between the fuel cell's exhaust-to-water heat exchanger and the adsorption storage unit's adsorber.

A modification was also made to the model of a wet central heating pipe and the model of a wet central heating pump in ESP-r (Hensen, 1991). Specifically, an input was added

to both models for pressure in order to allow the modelling of pressurized water loops, as discussed in section 3.5.3.1. The pressure was used to determine the thermophysical properties, namely the density and specific heat, of the pressurized water flowing through the pipe and pump.

A new controller type was created in ESP-r's plant domain for this work. The new controller subroutine obtains and verifies inputs, senses the required plant conditions, such as the temperature in the main water storage tank, and according to the controller algorithm, sets the charging/discharging signal for the adsorption storage unit and the flow rates for pumps A, B, C and D of Figure 3.6. Several inputs required by the controller subroutine are listed in Table 3.2 (those not listed in Table 3.2 pertain to index numbers required by the controller to identify specific plant components).

The algorithm used by the controller to set the charging/discharging signal of the adsorption storage unit and the pump flow rates is depicted in Figure 3.11. For brevity, the condition whereby the adsorption storage unit is full during the cooling season and therefore cannot be charged is not depicted in Figure 3.11. Similarly, the condition whereby the adsorption storage unit is empty during the heating season and therefore cannot be discharged is not depicted in Figure 3.11.

Table 3.2 Inputs required by adsorption storage controller

Input	Example values
Start date of heating season during which discharging is permitted	October 1
End date of heating season during which discharging is permitted	April 30
Start date of cooling season during which charging is permitted	May 1
End date of cooling season during which charging is permitted	September 30
Water tank upper (ON) set-point temperature for charging of unit (°C)	65
Water tank lower (OFF) set-point temperature for charging of unit (°C)	55
Water tank lower (ON) set-point temperature for discharging of unit (°C)	65
Water tank upper (OFF) set-point temperature for discharging of unit (°C)	75

Figure 3.11 Adsorption storage unit controller algorithm

4 MODEL VALIDATION

In order to validate the mathematical model of the adsorption storage unit described in the previous chapter, and its implementation in ESP-r, a simple plant network that consists of the adsorption storage unit, circulating pumps and pipes is considered. It is assumed that the heat source and heat sink connected to the adsorber are at a constant temperature, as is the evaporator's heat source and the liquid adsorbate stored in the reservoir. Finally, the air entering the condenser is assumed to be at the outdoor temperature for the particular time of year considered for the simulation. A comparison of simulation results to published data is done in section 4.1 and a sensitivity analysis of certain model input parameters is undertaken in section 4.2. The conclusions of the model validation are presented in section 4.3.

4.1 Comparison with published data

The literature review was undertaken to find experimental data or simulation results from other models that could be used to validate the model of the adsorption storage unit created for this study. The literature review did not focus solely on adsorption systems used in storage applications but also encompassed adsorption heat pumps used for heating and/or cooling applications. The literature review was limited to the zeolite-water adsorbent-adsorbate pair. A summary of published work that discusses or provides information on the performance of zeolite-water adsorption systems is presented in Table 4.1.

Table 4.1 Summary of published data

Author(s)	Input data available	Assumptions	Results
(Lachance, 2003)	-Coefficients Wo, D and n of Dubinin-Astakhov equation -Specific heat of adsorbent -Specific heat of steel containers -Mass of adsorbent -Mass of adsorber vessel, condenser and evaporator -Operating temperatures of heat pump: desorption temperature, condenser temperature, evaporator temperature and adsorption temperature -Maximum cycle time	-Uniform temperature and pressure in each system component modelled -Water vapour behaves like an ideal gas -Heat losses in piping are neglected -Energy consumption of circulating pumps is neglected -Circulating pump flow rates are constant	-Cooling coefficient of performance (COP) -Specific cooling power (SCP) -Plot of adsorber temperature versus time -Clausius-Clapeyron diagram -Plot of heat transfer at adsorber/condenser/evaporator versus time -Plot of adsorber pressure versus time
(Cacciola and Restuccia, 1995)	-Operating temperatures of cycle: desorption temperature, condenser temperature, adsorption temperature and evaporator temperature	-Ideal thermodynamic cycle -Equilibrium conditions of adsorbent-adsorbate pair represented with parametric equations	-Plots showing influence of desorption and evaporation temperatures on the COP in heating operation -Plots showing influence of desorption and evaporation temperatures on the useful heat produced in heating operation - Plots showing influence of desorption and condensation temperatures on the COP in cooling operation -Plots showing influence of desorption and condensation temperatures on useful cold produced in cooling operation
(Nùñez et al., 1999)	-Operating conditions of adsorption storage system: desorption, condensation and evaporation temperatures	-Ideal thermodynamic cycle	-Plot of energy density versus adsorption temperature
(Leong and Liu, 2004a)	-Heat transfer fluid inlet temperature to adsorber during heating -Heat transfer fluid inlet temperature during cooling -Operating temperatures of cycle: desorption, adsorption, evaporator and condenser temperatures -Initial adsorber pressure and temperature -Specific heat of adsorbent bed -Heat of adsorption	-Adsorbed phase is considered to be liquid -Adsorbate gas is assumed to be an ideal gas -Adsorbent bed is composed of uniformly sized particles and has isotropic properties -Thermal properties of the heat transfer fluid, metal tube and adsorbate vapour are constant -No heat losses in the adsorption cycle -Thermal resistance between the metal tube and adsorbent bed is neglected	-Plot of pressure versus temperature for cycle -Plot of average temperature and average pressure versus time -Cooling COP -SCP
(Ülkü and Mobedï, 1989)	-Condenser and evaporator operating pressures	-Ideal thermodynamic cycle	-Energy density of adsorbent pair -Plot of energy density versus desorption temperature -Plot of cooling COP versus desorption temperature -Plot of heating COP versus desorption temperature
(Lang et al., 1999)	-Operating temperatures of heat pump cycle	-Thermodynamic model takes into account thermal gradient between heat source/sink and adsorber	-Clausius-Clapeyron diagram -Plot of relative water content versus time -Plot of adsorber, condenser and evaporator temperatures versus time

(Lachance, 2003) and (Leong and Liu, 2004a) provide the most input data and have similar assumptions to the model of the adsorption unit created in this work. Therefore, the data from these two sources are used to validate the model of the adsorption unit created for this work.

4.1.1 Comparison with (Lachance, 2003)

(Lachance, 2003) compares simulation results, obtained using his model, with experimental data for three sets of operating conditions. The model input parameters provided by (Lachance, 2003) for one set of operating conditions and used in the present comparison are provided in Table 4.2.

Table 4.2 Model input parameters provided by (Lachance, 2003)

Input parameter	Input value
Coefficient Wo of D-A equation (m^3/kg)	0.000148
Coefficient D of D-A equation (-)	1.5563E-07
Coefficient n of D-A equation (-)	2
Adsorber mass (kg)	40.24
Adsorbent mass (kg)	7.21
Specific heat of metal (J/kgK)	544
Specific heat of adsorbent (J/kgK)	850.829
Desorption temperature (°C)	180
Condenser pressure (kPa)[1]	8
Adsorption temperature (°C)	40
Evaporator pressure (kPa)[1]	1.5

[1] 1 kPa = 10 mbar

The input parameters not provided by (Lachance, 2003) that are required by the model, namely the mass flow rates of the circulation pumps, the pressure of the heat exchange loops, the effectiveness of the adsorber, condenser and evaporator heat exchangers and

the mass flow rate of the air flowing through the condenser, are assumed. The assumed inputs were either determined from published data provided by other authors in their investigation of adsorption heat pumps or chosen by the author. The complete set of model inputs are provided in Table A.1 of Appendix A. The heat losses from the adsorber to the ambient are neglected in the present model, however they are taken into account by (Lachance, 2003). The heat losses from the adsorber are not taken into account in the present model since an overall heat loss coefficient is not provided by (Lachance, 2003). It is expected that the performance results determined using the present model will be greater than those determined by (Lachance, 2003) since the present model assumes that the adsorption system behaves ideally and no heat losses are taken into account.

It should be noted that (Lachance, 2003) uses a timestep of 0.1 to 0.5 seconds depending on the phase of the cycle to obtain his simulation results. In comparison, the simulation results presented in this section are obtained using a timestep of 1 minute. Using a shorter timestep is not feasible for the model developed for this work since simulation times in this case were very long (a trial simulation was performed for a 1 second timestep. After two hours, only 2% of the simulation was complete).

Figure 4.1 shows the variation of the adsorber pressure for a complete adsorption cycle, as obtained by using the model presented in this thesis. In Figure 4.1, the results for three convergence criteria are presented as differences are due to numerical convergence. The '0.05% convergence' curve represents the results whereby the simulation is assumed to be converged when the heat transfer between the adsorber and the heat source or heat

sink is less than 0.05% of the maximum heat transfer between the adsorber and heat source/heat sink. Similarly, the '0.075% convergence' curve and the '1% convergence' curve represent the results whereby the simulation is assumed to be converged when the heat transfer between the adsorber and the heat source or heat sink is less than 0.075% and 1%, respectively, of the maximum heat transfer between the adsorber and heat source/heat sink. The different convergence criteria are applied in order to match the cycle time obtained with the present model to the cycle time determined by (Lachance, 2003). The corresponding plot of adsorber pressure versus time obtained by (Lachance, 2003) is presented in Figure 4.2 (experimental and simulation results are shown for two cycles). If the 1% convergence criterion is used, the cycle time obtained using the present model (56 minutes) matches more closely the cycle time obtained by (Lachance, 2003) (approximately 70 minutes). The other convergence criteria lead to a longer cycle time, since both the desorption and adsorption phases are extended.

Figure 4.1 shows how the pressure increases quickly during the isosteric heating phase, remains constant during the desorption phase, decreases quickly during the isosteric cooling phase and is constant during the adsorption phase. Qualitatively, the curve of Figure 4.1 is similar to the experimental and simulation results presented in Figure 4.2 during the isosteric heating, isosteric cooling and adsorption phases. However, during the desorption phase, (Lachance, 2003) shows that the pressure decreases slightly and does not remain constant. The present adsorption system model does not predict this pattern as an ideal cycle is assumed. No explanation is provided by (Lachance, 2003) as to the cause of the non-uniform pressure during the desorption phase.

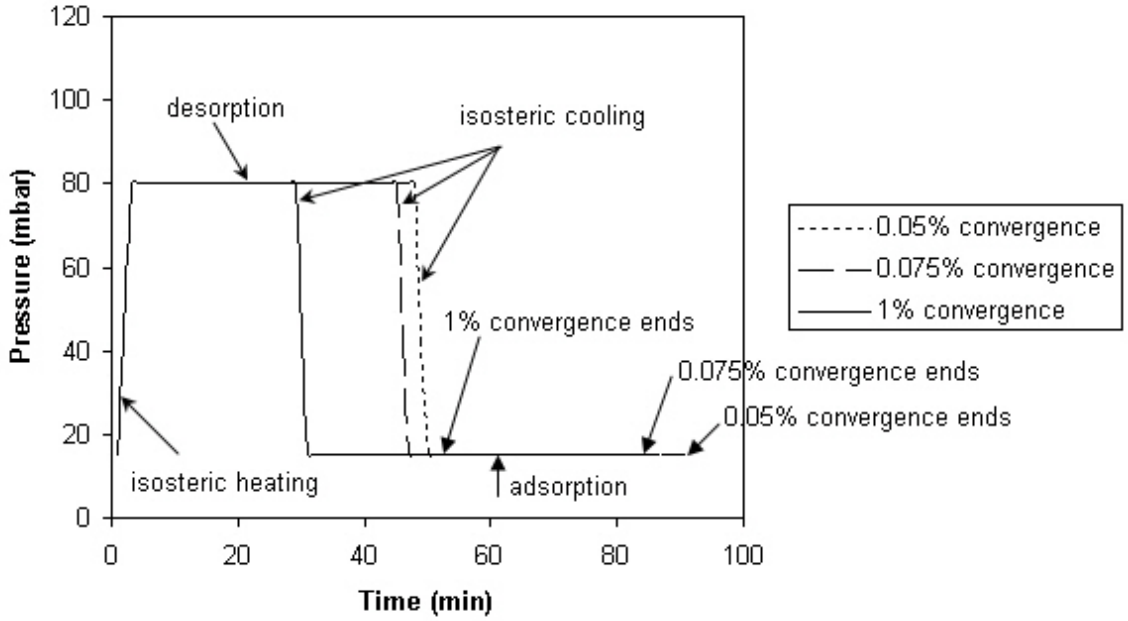

Figure 4.1 Adsorber pressure versus time predicted by the present model

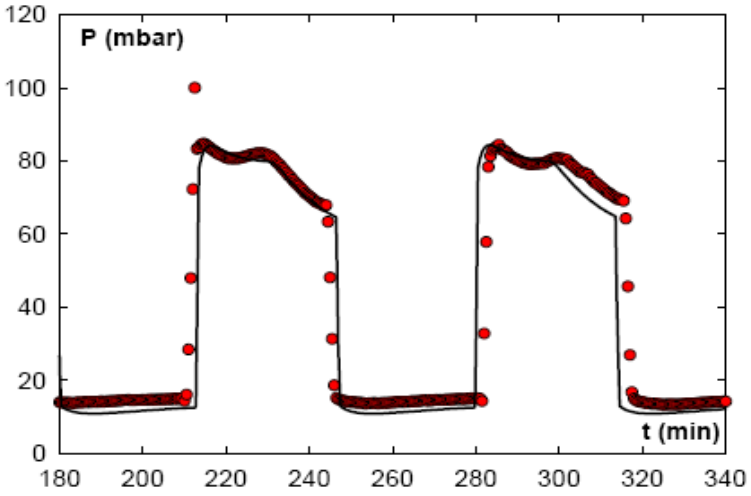

Figure 4.2 Adsorber pressure versus time for 2 cycles; experimental (•) and simulation (-) (Lachance, 2003)

Both studies presented in Figures 4.1 and 4.2 show that the isosteric heating phases and isosteric cooling phases are short in relation to the total cycle time; each isosteric phase is approximately 3.6% of the total cycle time.

Figure 4.3 shows the variation of the adsorber temperature for a complete adsorption cycle as predicted by the model presented in this thesis. The results provided by (Lachance, 2003) are reproduced in Figure 4.4. Qualitatively, Figure 4.3 is similar to Figure 4.4, especially for the case where the 1% convergence criterion is used since the cycle times predicted by the two models in this case are closer. The present model predicts the cycle time to be 56 minutes, 25% less than the cycle time predicted by (Lachance, 2003)'s model (70 minutes).

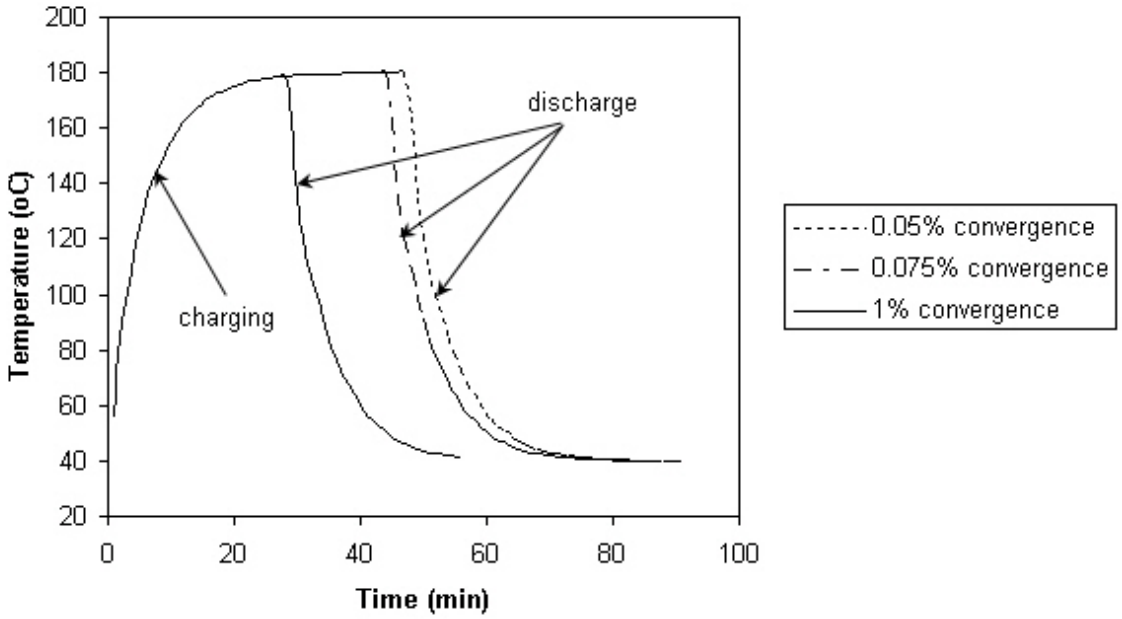

Figure 4.3 Adsorber temperature versus time predicted by the present model

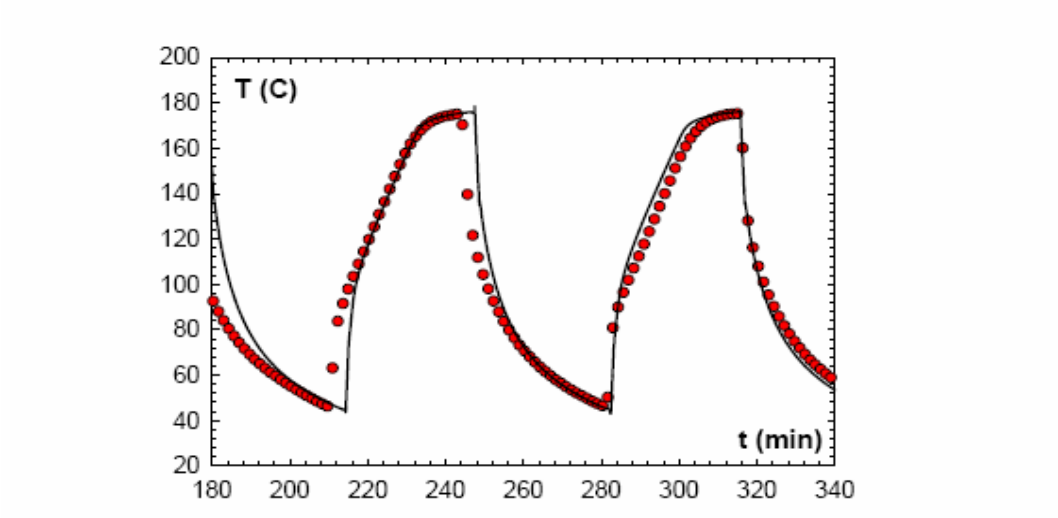

Figure 4.4 Adsorber temperature versus time for 2 cycles; experimental (•) and simulation (-) (Lachance, 2003)

Figure 4.5 shows the Clapeyron-Clausius diagram for the adsorber as obtained by using the model presented in this thesis and the 1% convergence criterion, while Figure 4.6 shows the Clapeyron-Clausius diagram obtained by (Lachance, 2003).

Figure 4.5 is similar to Figure 4.6 in that the pressure remains constant during the desorption and adsorption phases. However, during the isosteric heating and cooling phases, the curves in Figures 4.5 and 4.6 differ. Because the isosteric heating and cooling phases are relatively short, approximately 2 minutes long each, and a 1-minute timestep is used in the present simulation, only two points are available on the Clausius-Clapeyron diagram of Figure 4.5 during these phases. This explains why the isosteres in Figure 4.5 are not parallel and not perfectly straight lines, though an ideal cycle is assumed.

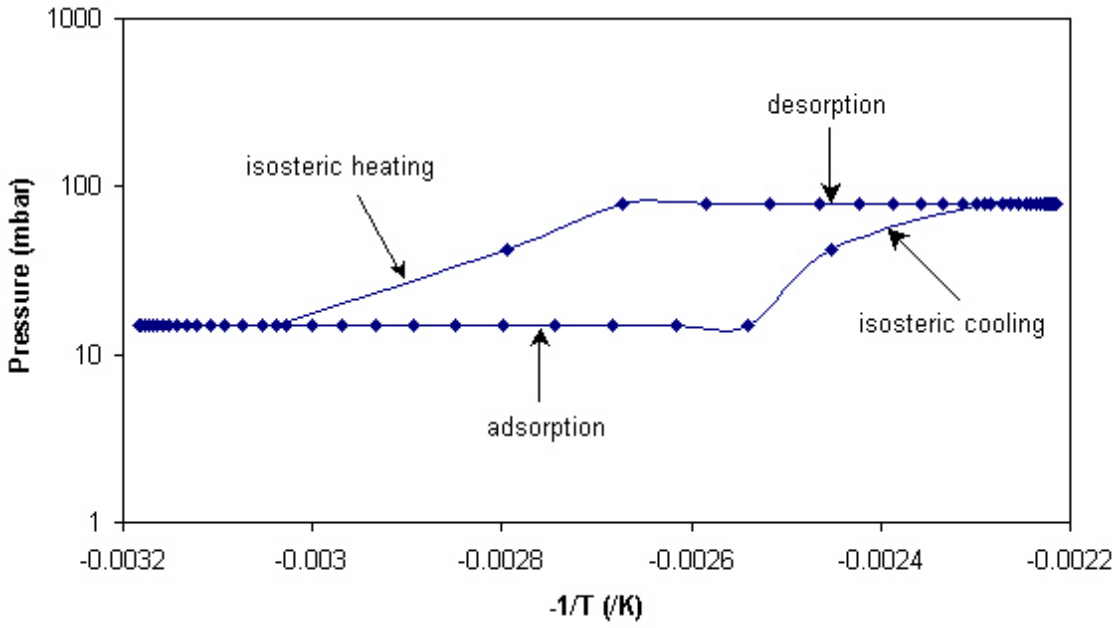

Figure 4.5 Clausius-Clapeyron diagram (1% convergence criterion) predicted by the present model

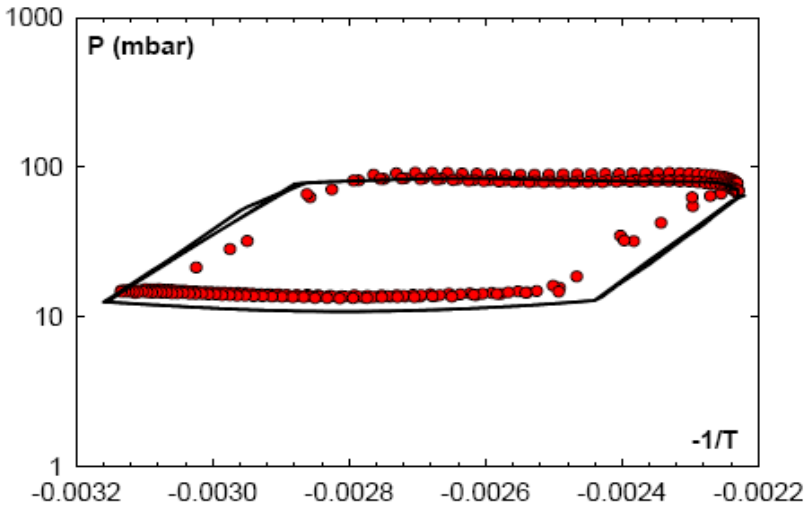

Figure 4.6 Clausius-Clapeyron diagram for entire cycle: experimental (•) and simulation (-) (Lachance, 2003)

Figure 4.7 presents the heat flows during a complete adsorption cycle obtained using the model developed in this thesis and the 1% convergence criterion. Specifically, Figure 4.7 presents the heat transferred between the heat source and the adsorber, $Q_{desorption}$, and the heat rejected by the condenser, Q_{cond}, during the charging process that lasts for approximately 28 minutes; and the heat transferred between the adsorber and the heat sink, $Q_{adsorption}$, and the heat input to the evaporator, Q_{evap}, during the discharge process. The total cycle time is approximately 56 minutes. Figure 4.8 presents the corresponding plot provided by (Lachance, 2003). In Figure 4.8, (Lachance, 2003) uses the term $\dot{Q}_{reg}$ to represent the heat transferred from the heat source to the adsorber, the term $\dot{Q}_{cond}$ to represent the heat rejected by the condenser, the term $\dot{Q}_{ads}$ to represent the heat transferred between the adsorber and the heat sink and the term $\dot{Q}_{ev}$ to represent the heat input to the evaporator.

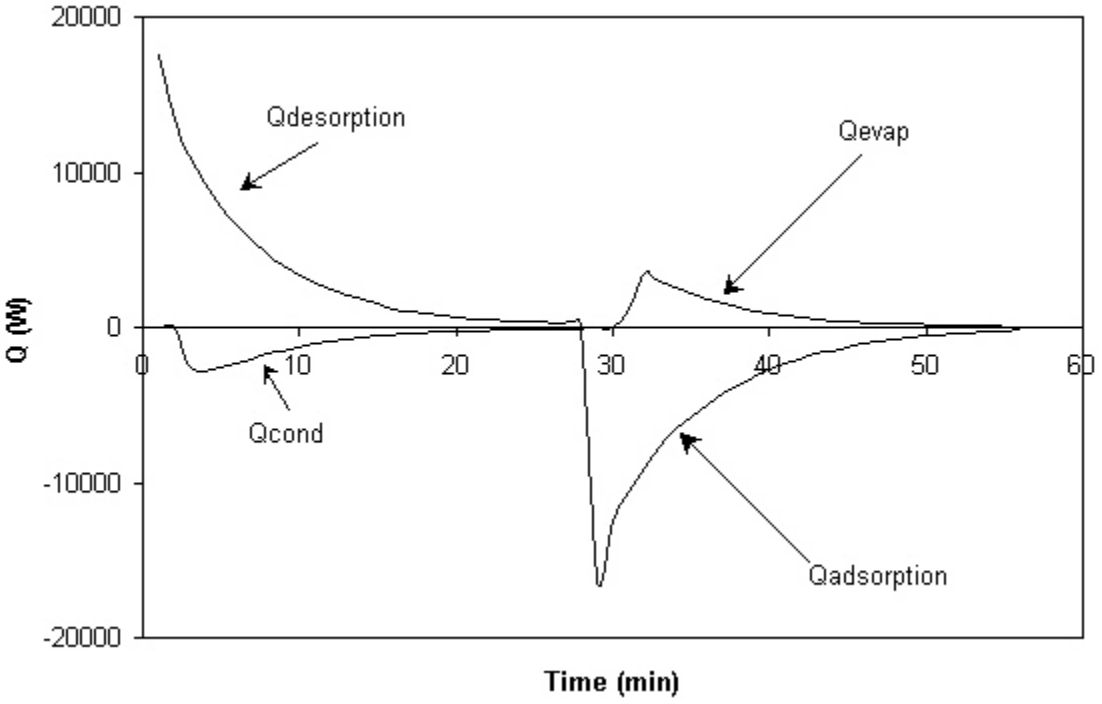

Figure 4.7 Heat flows during a complete adsorption cycle (1% convergence criterion) predicted by the present model

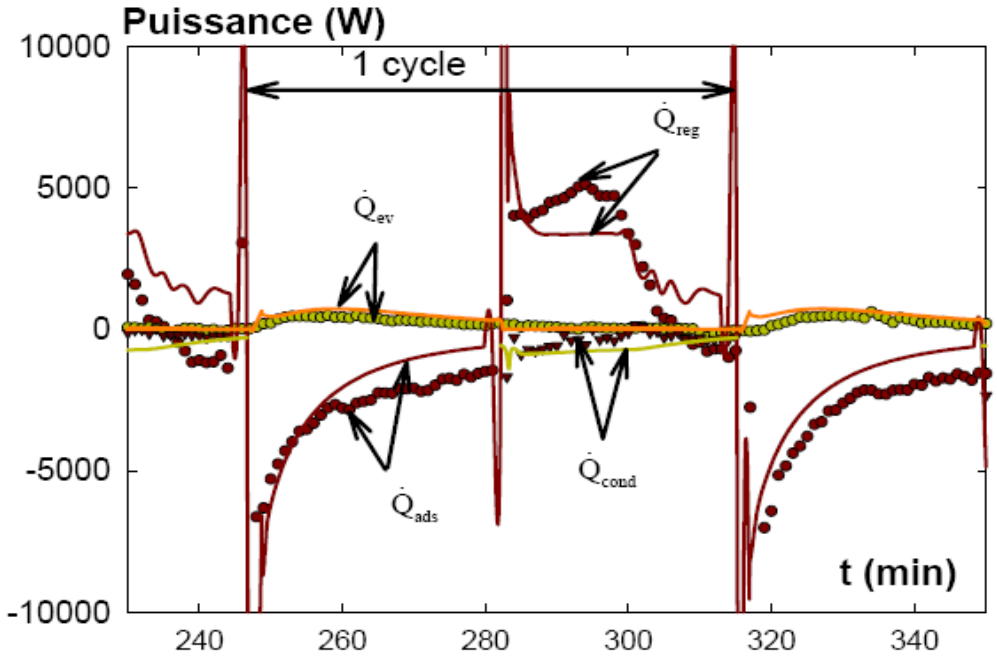

Figure 4.8 Heat flows: experimental (•) and simulation (-) (Lachance, 2003)

Comparing Figures 4.7 and 4.8 qualitatively, it is seen that the trend of the heat flows versus time predicted by the two models is similar. However, the predicted maximum amounts of heat transferred using the model developed in this thesis (peaks in Figure 4.7) are greater than those predicted by (Lachance, 2003); this is expected since many inputs to the model are assumed.

(Lachance, 2003) evaluated the performance of the adsorption heat pump using the coefficient of performance (COP) and specific cooling power (SCP) parameters. They are defined, respectively, as:

$$COP = \frac{Q_{evap}}{Q_{reg}} \tag{4.1}$$

$$SCP = \frac{Q_{evap}}{t_{cycle} \cdot m_z} \tag{4.2}$$

where Q_{evap} is the amount of heat input to the evaporator during the discharge process [J], Q_{reg} is the amount of heat input to the adsorber during the charging process [J], t_{cycle} is the length of the complete cycle [s] and m_z is the mass of adsorbent [kg].

Table 4.3 compares the performance characteristics of the adsorption system determined by (Lachance, 2003) experimentally and using his model with those determined using the present model for the different convergence criteria considered.

Table 4.3 Comparison of performance results with (Lachance, 2003)

	(Lachance, 2003)		Present model		
	Experimental	Model	0.05% conv.	0.075% conv.	1% conv.
t_{cycle} (min)	approximately 70		91	86	56
COP	0.13	0.16	0.23	0.23	0.23
SCP(W/kg)	30	41	36	38	58
vapour transferred (kg)	0.335	0.427	0.569	0.569	0.563

The cycle time predicted by the model developed for this thesis is greatly affected by the convergence criterion that is used. The COP predicted by the present model is 76.9% greater than the COP determined experimentally by (Lachance, 2003) and 43.8% greater than the COP predicted by (Lachance, 2003)'s model. This is expected since the present model assumes an ideal cycle with no heat losses. The SCP predicted by the present model is within the range of the experimental and simulation results obtained by (Lachance, 2003) for the 0.05% and 0.075% convergence criteria. However, for the case of the 1% convergence criterion, the present model predicted an SCP 93.3% and 41.5% greater than the SCP determined experimentally and calculated, respectively, by (Lachance, 2003) since for this criterion the cycle time is shorter. Finally, the amount of vapour transferred between the adsorber and condenser during the charging process, which is equal to the amount of vapour transferred between the adsorber and the evaporator during the discharge process, predicted using the present model (and the 1% convergence criterion) is 68.1% and 31.9% greater than the experimental and simulation results, respectively, provided by (Lachance, 2003). This is most likely because an ideal cycle is assumed.

The differences between the performance results of the adsorption heat pump found by (Lachance, 2003) and those found using the present model are to be expected given the use of the ideal cycle approach and the number of model inputs that are assumed.

4.1.2 Comparison with (Leong and Liu, 2004a)

The model input parameters provided by (Leong and Liu, 2004a) and used in the present comparison are provided in Table 4.4.

Table 4.4 Model input parameters provided by (Leong and Liu, 2004a)

Input parameter	Input value
Initial adsorber temperature (°C)	45
Initial adsorber pressure (kPa)	1
Adsorption temperature (°C)	45
Generation temperature (°C)	200
Fluid inlet temperature during heating (°C)	210
Fluid inlet temperature during cooling (°C)	25
Evaporator temperature (°C)	6
Condenser temperature (°C)	45
Specific heat of adsorbent bed (J/kgK)	836
Enthalpy of adsorption (J/kg)	3.2E06

The input parameters that are not provided by (Leong and Liu, 2004a) are assumed based on information obtained from other published data. The complete set of model inputs are provided in Table A.2 of Appendix A. The model developed by (Leong and Liu, 2004a) is a two-dimensional non-equilibrium numerical model that takes into account the heat and mass transfer within the adsorbent bed. Therefore, it is expected that the performance of the adsorption system predicted using the model developed for this work will be

greater than the performance predicted by (Leong and Liu, 2004a). Both (Leong and Liu, 2004a)'s model and the model developed for this work assume that there are no heat losses from the adsorption system to the ambient.

(Leong and Liu, 2004a) choose a timestep between 0.01 and 0.1 second in their analysis while a timestep of 1 minute is used to obtain the simulation results using the model developed for this work. A shorter timestep is not feasible due to very long simulation times.

Figure 4.9 shows the variation of pressure and temperature for a complete adsorption cycle using the model created for this work while the corresponding plot obtained by (Leong and Liu, 2004a) is shown in Figure 4.10.

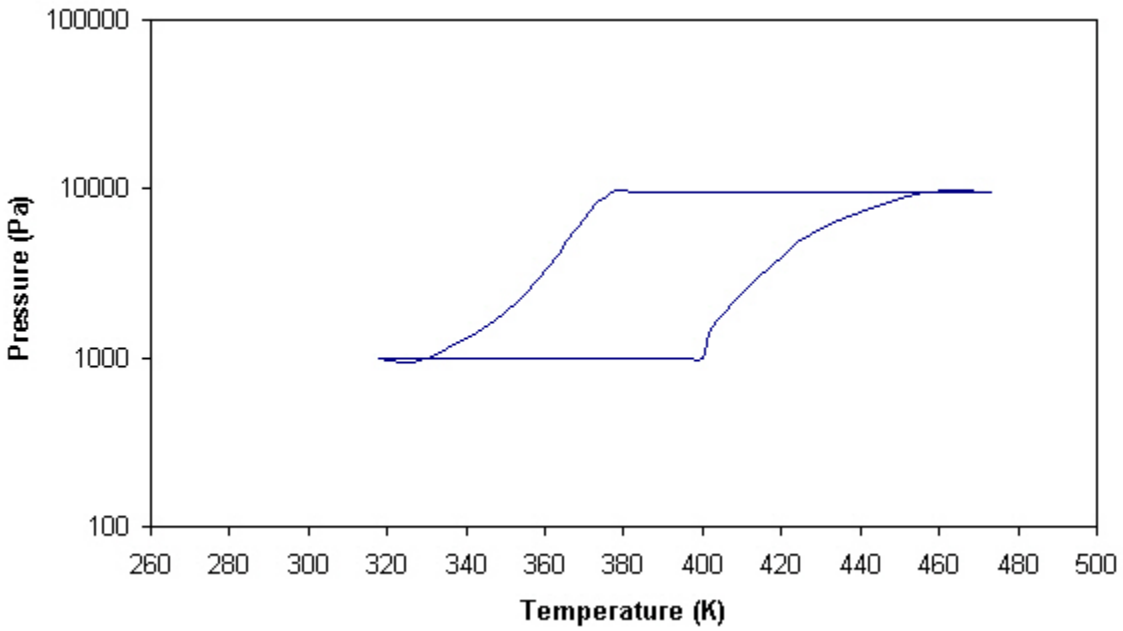

Figure 4.9 Pressure versus temperature for complete adsorption cycle predicted by the present model

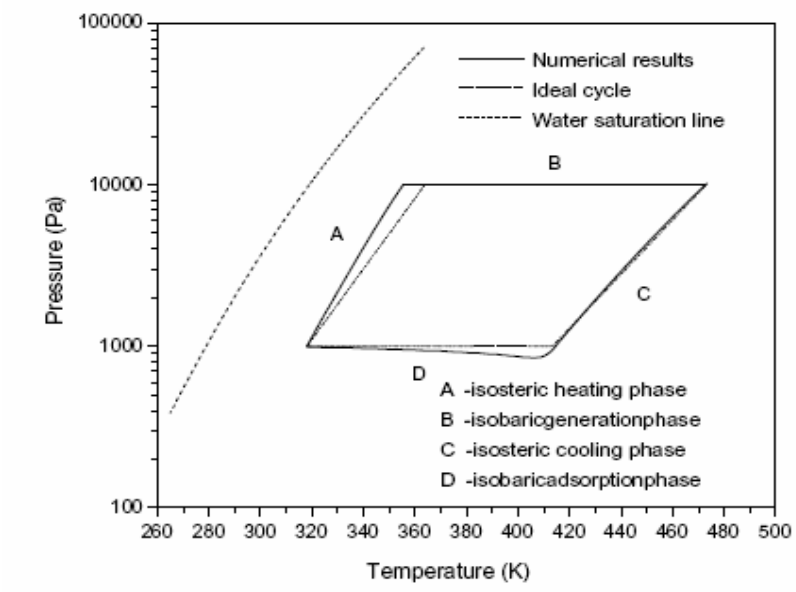

Figure 4.10 Pressure versus temperature for complete adsorption cycle (Leong and Liu, 2004a)

The shape of a complete adsorption cycle of Figure 4.9 is similar to the shape of the cycle predicted by (Leong and Liu, 2004a), presented in Figure 4.10. It should be noted that in the latter case, the authors presented both the numerical results obtained with their model and the curve obtained if an ideal cycle is assumed.

Figure 4.11 presents the variation of the adsorber temperature with time obtained using the model developed for this work. Figure 4.12 presents the variation of average temperature with time obtained by (Leong and Liu, 2004a). The authors present the average temperature of the adsorbent bed, metal tube and heat exchanger fluid as in their model each of these is represented by several control volumes. The results of Figure 4.11, however, were obtained by incorporating the adsorbent bed, metal tube and heat exchanger fluid in one single control volume. The letters A, B, C and D in Figures 4.11 and 4.12 denote the isosteric heating, desorption, isosteric cooling and adsorption phases of the cycle, respectively. The shape of the curves presented in Figures 4.11 and 4.12 are similar. Both studies predict that the adsorbent bed reaches about 470 °C at the end of the desorption phase (B) and the charging phase (A+B) lasts for approximately 3300 seconds.

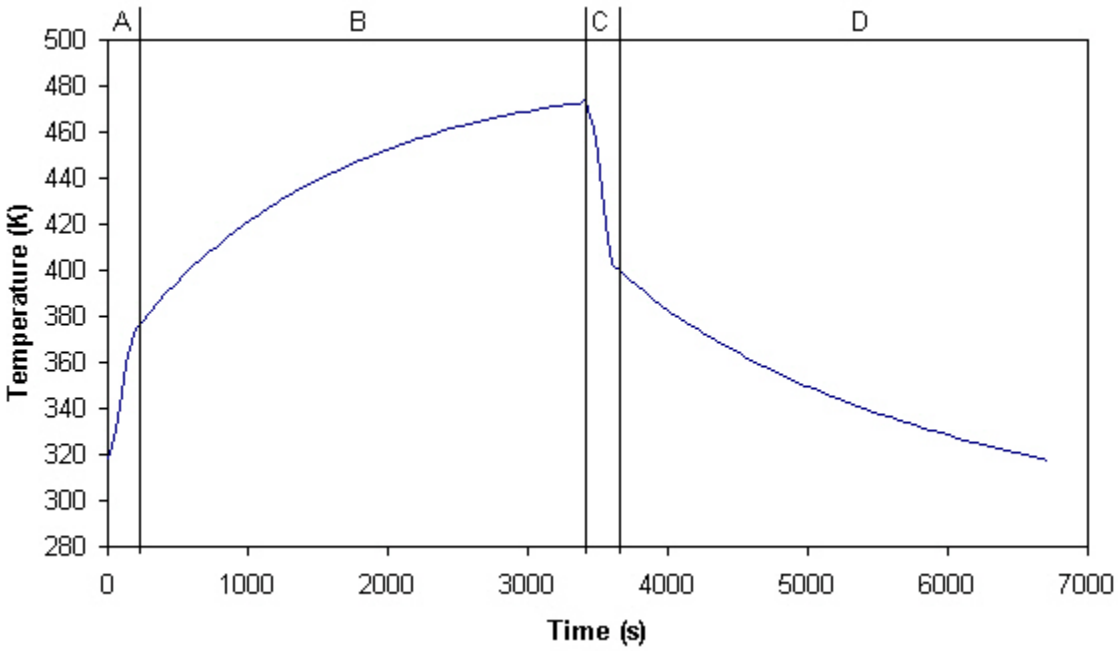

Figure 4.11 Adsorber temperature versus time predicted by the present model

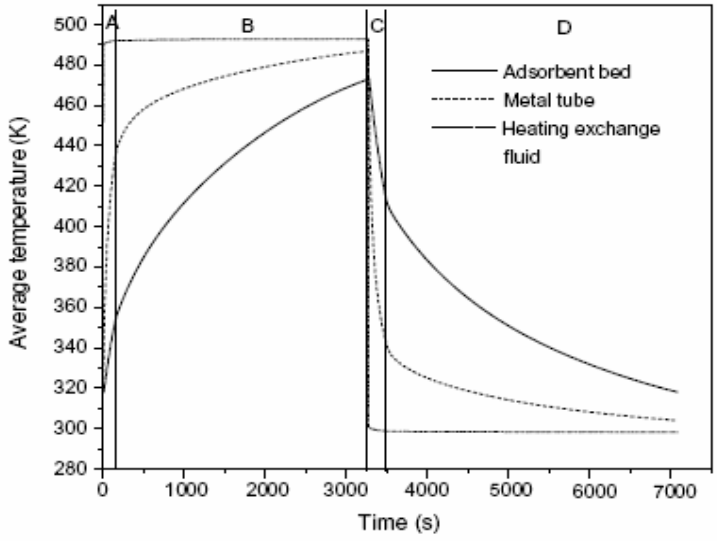

Figure 4.12 Variation of average temperature with time (Leong and Liu, 2004a)

Figure 4.13 presents the variation of the adsorber pressure with time while Figure 4.14 presents the variation of the adsorbed amount (mass of adsorbate per mass of adsorbent) with time predicted by the model developed for this work. The corresponding results by (Leong and Liu, 2004a) are presented in Figure 4.15.

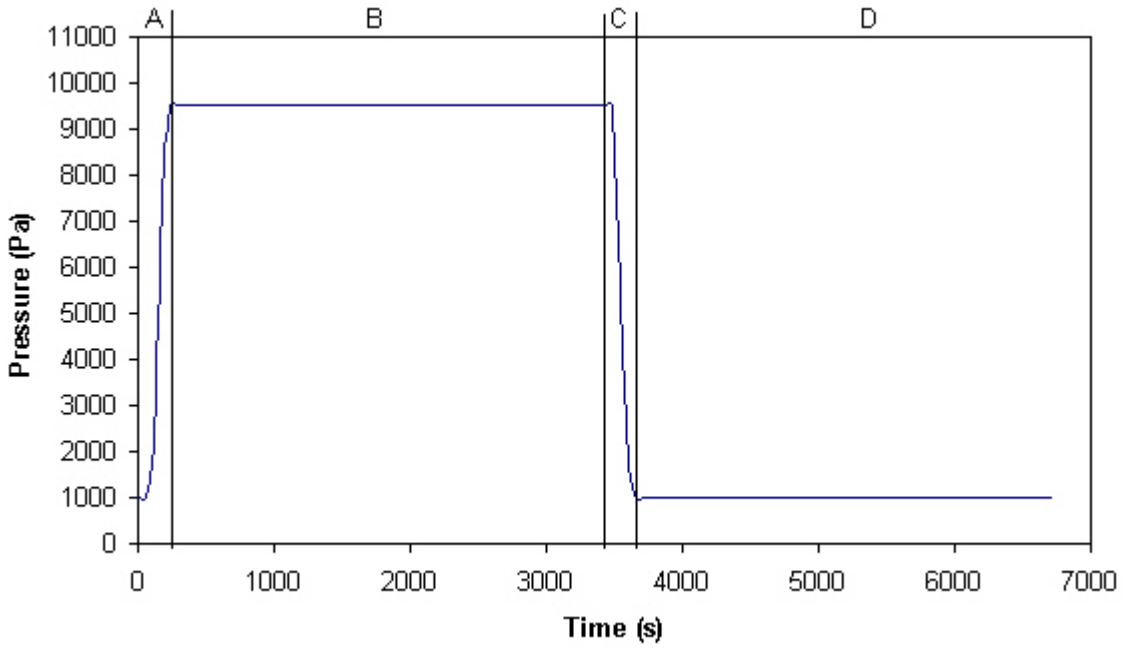

Figure 4.13 Adsorber pressure versus time predicted by the present model

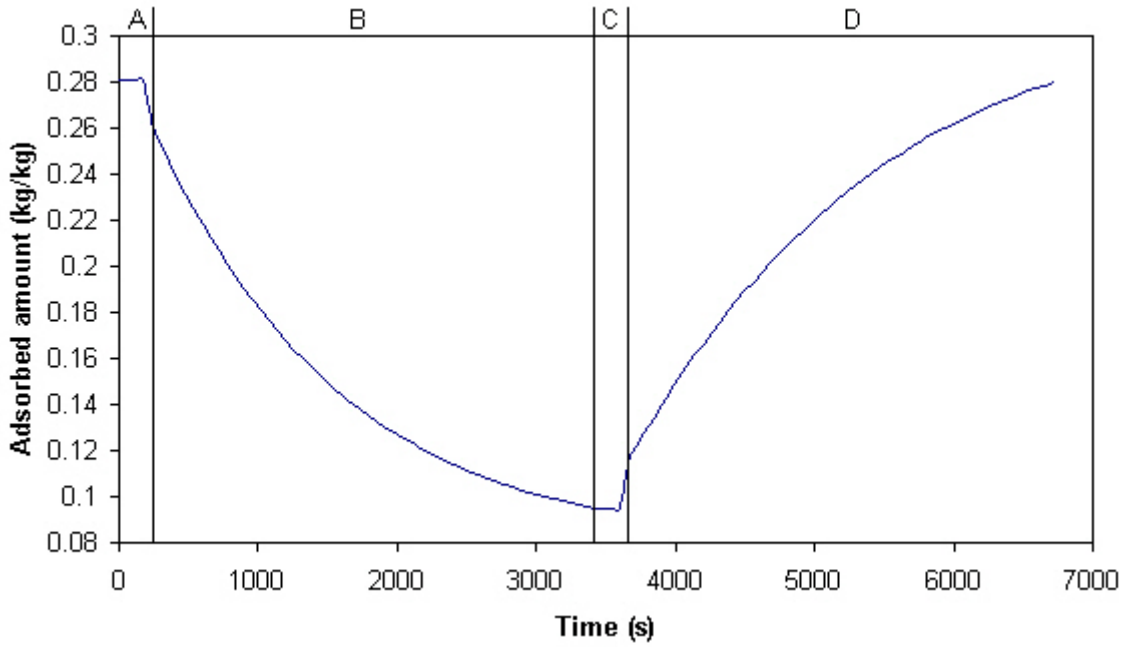

Figure 4.14 Adsorbed amount versus time predicted by the present model

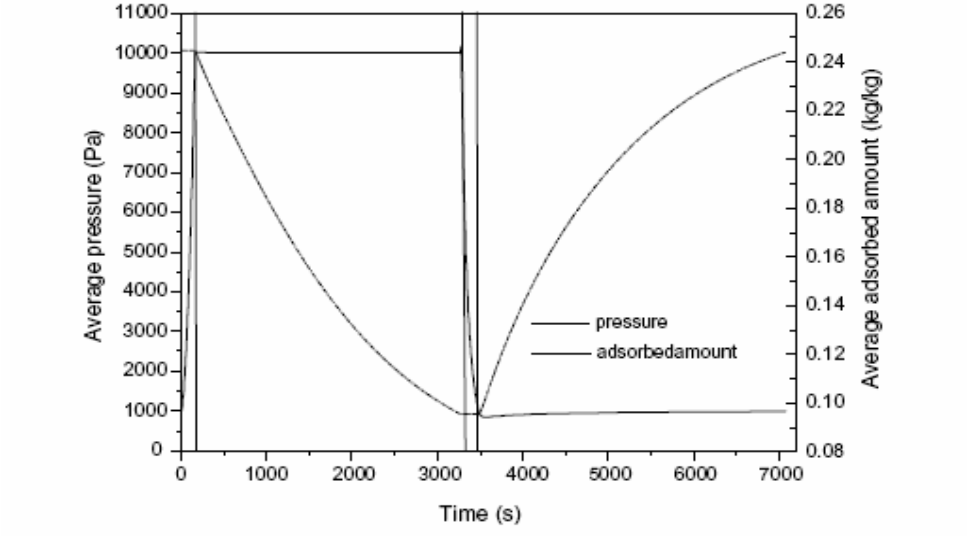

Figure 4.15 Average pressure and adsorbed amount versus time (Leong and Liu, 2004a)

(Leong and Liu, 2004a) evaluate the performance of the adsorption heat pump using the same parameters as (Lachance, 2003), that is the COP and SCP, defined by equations (4.1) and (4.2), respectively. Table 4.5 compares the performance characteristics of the adsorption system determined by (Leong and Liu, 2004a) with those determined using the present model.

Table 4.5 Comparison of performance results with (Leong and Liu, 2004a)

	(Leong and Liu, 2004a)	Present model
COP	0.473	0.556
SCP (W/kg)	52.2	68.8

As expected, the performance of the adsorption system predicted by the model created for this work is greater than the performance predicted by (Leong and Liu, 2004a) – the present model overestimates the COP and SCP by 17.5% and 31.8%, respectively.

4.2 Sensitivity analysis

A list of the inputs required by the model of the adsorption storage unit and the other component models that are considered in the simple network created for this validation exercise is presented in Table 4.6.

Table 4.6 Model inputs

Adsorption storage unit	
Adsorber characteristics	**Mass of adsorbent (kg)**
	Specific heat of adsorbent (J/kgK)
	Coefficient Wo of D-A equation (m^3/kg)
	Coefficient D of D-A equation (-)
	Coefficient n of D-A equation (-)
	Mass of adsorber vessel (kg)
	Specific heat of adsorber vessel (J/kgK)
	Mass of adsorber heat exchanger (kg)
	Specific heat of adsorber heat exchanger (J/kgK)
	Enthalpy of adsorption (J/kg)
	Surface area of adsorber (m^2)
	Thickness of adsorber insulation layer (m)
	Thermal conductivity of adsorber insulation (W/mK)
	Overall heat transfer coefficient adsorber-surroundings (W/m^2K)
Condenser	**Condenser pressure (kPa)**
	Condenser heat exchanger effectiveness (-)
	Mass flow rate of air entering condenser (kg/s)
	Surface area of condenser (m^2)
	Overall heat transfer coefficient condenser-surroundings (W/m^2K)
	Condenser fan power rating (W)
	Temperature of air entering condenser (°C)
Evaporator	**Evaporator pressure (kPa)**
	Evaporator heat exchanger effectiveness (-)
	Surface area of evaporator (m^2)
	Overall heat transfer coefficient evaporator-surroundings (W/m^2K)
	Temperature of heat source to evaporator (°C)
Other	Delta T for determining dX/dT (°C)
	Ambient temperature (°C)
Heat source (fuel cell)	
	Temperature of heat source (°C)
	Adsorber-fuel cell heat exchanger effectiveness (-)
	Pressure of adsorber-fuel cell heat exchange loop (kPa)
	Minimum temperature of heat source for charging unit (°C)
Heat sink (water tank)	
	Temperature of heat sink (°C)
	Adsorber-water tank heat exchanger effectiveness (-)
	Pressure of adsorber-water tank heat exchange loop (kPa)
	Minimum temperature difference between adsorber and heat sink/source (°C)

Reservoir	
	Temperature of liquid adsorbate (°C)
Circulating pump(s)	
	Component total mass (kg)
	Mass weighted average specific heat (J/kgK)
	UA modulus from wall to environment (W/K)
	Rated total absorbed power (W)
	Rated volume flow rate (m^3/s)
	Overall efficiency (-)
	Pressure (kPa)
	Water volume flow rate (m^3/s)
Circulating pipe(s)	
	Component total mass (kg)
	Mass weighted average specific heat (J/kgK)
	UA modulus from wall to environment (W/K)
	Hydraulic diameter of pipe (m)
	Length of pipe section (m)
	Cross-sectional face area (m^2)
	Pressure (kPa)

The input parameters that are likely to have the greatest impact on the simulation results, specifically on the performance of the adsorption storage unit, are highlighted in bold text in Table 4.6. These parameters have been chosen based on similar analyses found in the literature, including those identified in Table 4.1, that examine the sensitivity of different characteristics on the performance of an adsorption heat pump.

In this section, the model of the adsorption storage unit is verified by investigating the impact of several input parameters on the performance of the unit as predicted by the model, considering the charging and discharge modes of operation separately before considering a complete adsorption cycle. This verification approach assumes that a valid model of the system will produce the expected impact on the predicted system performance when an input is modified. For example, one would expect that increasing

the thickness of the adsorber's insulation layer would increase the COP of the unit since the amount of heat lost to the ambient would be reduced.

When the adsorption unit is in charging mode, the performance of the system will be evaluated by considering the following definition of COP:

$$COP_{charge} = \frac{Q_{cond}}{Q_{charge}} \tag{4.3}$$

where Q_{cond} is the amount of heat rejected by the condenser [J] and Q_{charge} is the amount of heat exchanged with the heat source [J] during the charging cycle. COP_{charge} considers the thermal output that is available during the charging process, and is a ratio of the heat leaving the unit to the heat entering the unit.

When the adsorption unit is in discharge mode, the performance of the system is evaluated using the following definition of COP:

$$COP_{discharge} = \frac{Q_{discharge}}{Q_{evap}} \tag{4.4}$$

where $Q_{discharge}$ is the amount of heat exchanged with the heat sink [J] and Q_{evap} is the amount of heat input at the evaporator [J] during the discharge cycle. The variable $COP_{discharge}$ focuses on the upgraded heat that is available during the discharge process (Ogura et al., 2003).

Finally, when considering the entire adsorption cycle including the charging and discharge modes, the COP of the unit is defined as:

$$COP = \frac{Q_{discharge}}{Q_{charge} + Q_{evap}} \tag{4.5}$$

The definition of COP provided by equation (4.5) is suggested by (Ogura et al., 2003) as it defines the efficiency of the system based on the useful energy available during the discharge process and the energy that is required to obtain the useful heat during both the charging and discharge processes. It should be noted that the work of the circulation pumps and fans is not included in the COP defined by equation (4.5).

4.2.1 Charging mode

The model input values that correspond to the basecase simulation of the adsorption storage unit are provided in Table A.3 of Appendix A. The model predicts a charging COP of 0.13, as defined by equation (4.3), for the adsorption storage unit with the basecase inputs. The unit completes the charging process when the temperature of the adsorber reaches 195°C (heat source temperature of 200°C minus minimum temperature difference between adsorber and heat source of 5°C for proper heat transfer), and subsequently remains in storage mode.

The impact of the following four parameters on the performance of the adsorption system operating in charging mode, COP_{charge}, is investigated:

- condenser effectiveness;
- mass flow rate of air entering the condenser;
- effectiveness of the adsorber – heat source (fuel cell) heat exchanger;
- volume flow rate of the pump between the adsorber and the heat source (fuel cell).

Figure 4.16 presents the variation of COP_{charge} with the condenser effectiveness.

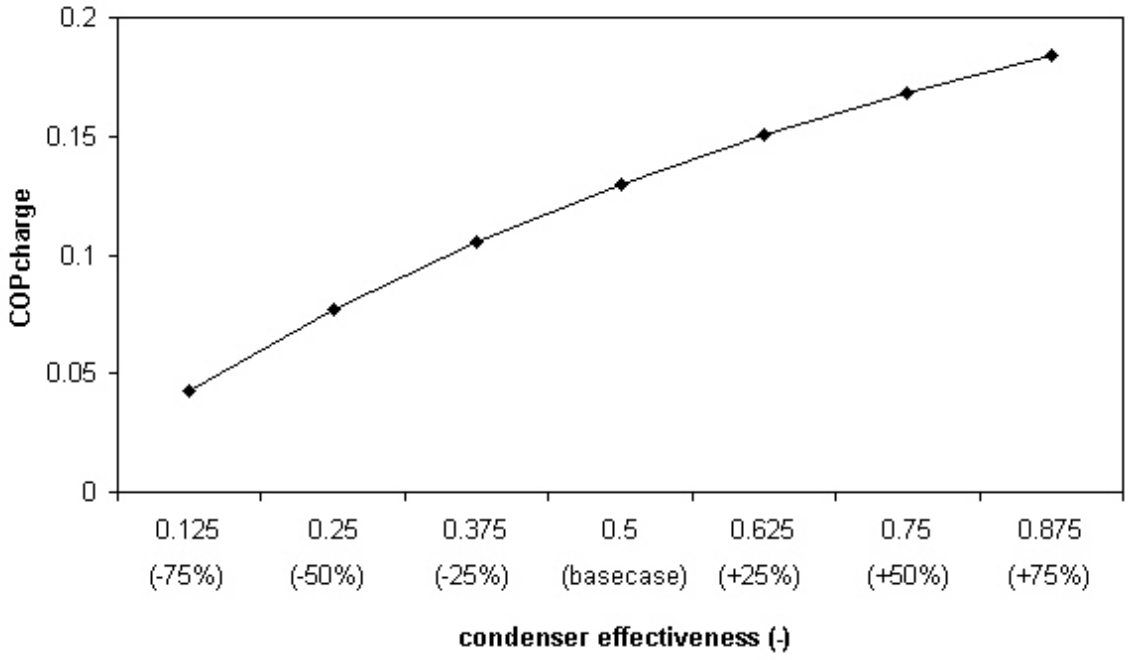

Figure 4.16 COP_{charge} versus condenser effectiveness

As one would expect, an increase in the condenser effectiveness results in an increase of COP_{charge} due to a greater amount of heat being rejected by the condenser. Figure 4.17 presents the variation of the system COP in charging mode with the mass flow rate of air entering the condenser. The mass flow rate of air entering the condenser has a similar impact on COP_{charge} as the condenser effectiveness. This is expected since both input parameters are directly proportional to the heat released from the condenser, and thus to COP_{charge}.

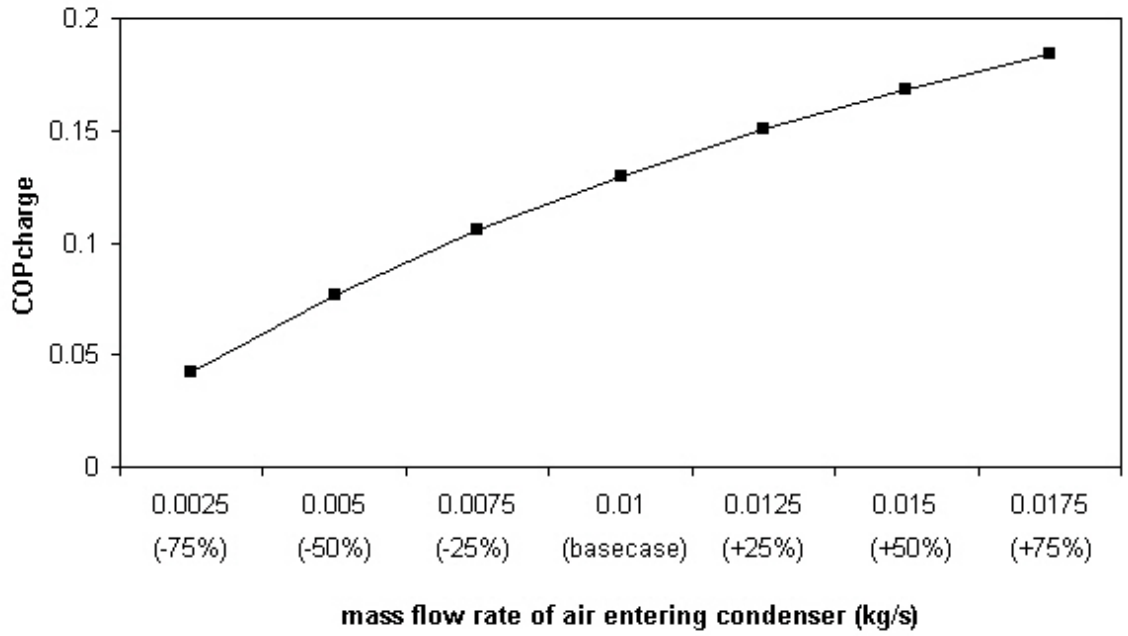

Figure 4.17 COP_{charge} versus mass flow rate of air entering condenser

Figure 4.18 shows the variation of COP_{charge} with the effectiveness of the adsorber-heat source (fuel cell) heat exchanger. Two curves are presented in Figure 4.18 to indicate the different states of the adsorber at the end of the simulations. For the simulations with

effectiveness values of 0.125 and 0.25 (–75% and –50% of the basecase, respectively), the adsorber reaches a steady state temperature less than 195°C, the temperature that is required for the unit to switch from the charging mode to the storage mode of operation. However, for the simulations with effectiveness values equal to or greater than 0.375, an adsorber temperature of 195°C is reached and the unit switches from the charging mode of operation to the storage mode.

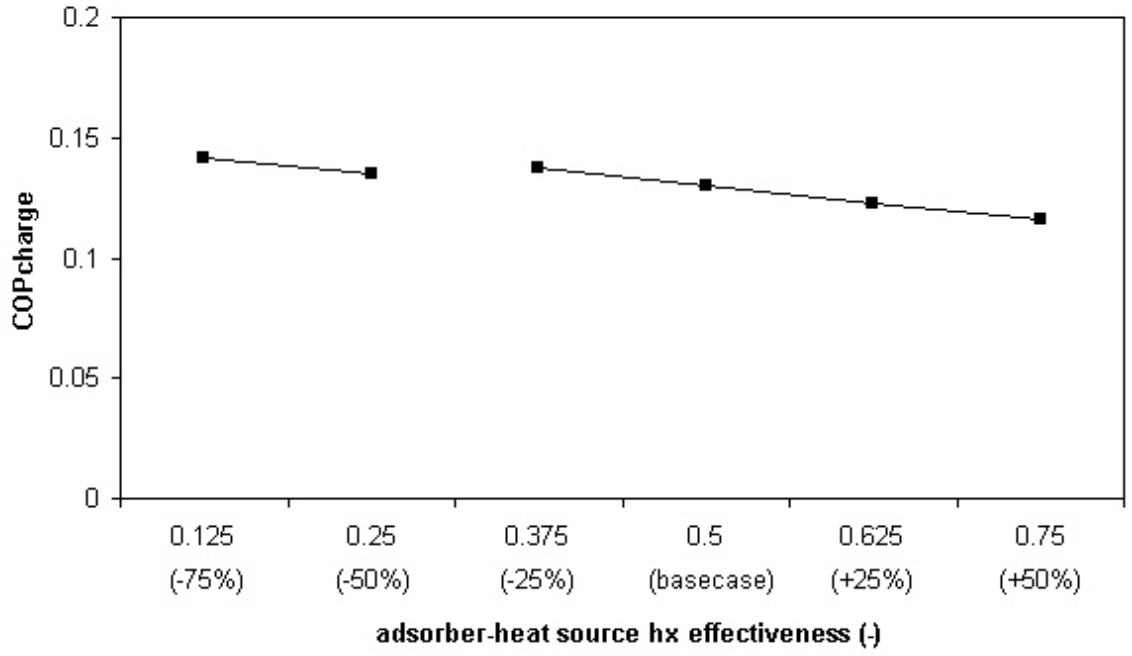

Figure 4.18 COP_{charge} versus adsorber-heat source h/x effectiveness

Figure 4.18 shows that the adsorber-heat source heat exchanger effectiveness has a slight impact on the system performance during the charging process. COP_{charge} decreases slightly as the effectiveness increases. This is mostly because a higher effectiveness results in a shorter charging period and therefore less heat is rejected at the condenser.

It should be noted that a simulation could not be carried out with a heat exchanger effectiveness value of 0.875 (+75% of the basecase value) as this case led to a convergence error.

Figure 4.19 presents the variation of COP_{charge} with the volume flow rate of the pump that circulates the heat exchanger fluid between the heat source (fuel cell) and the adsorber.

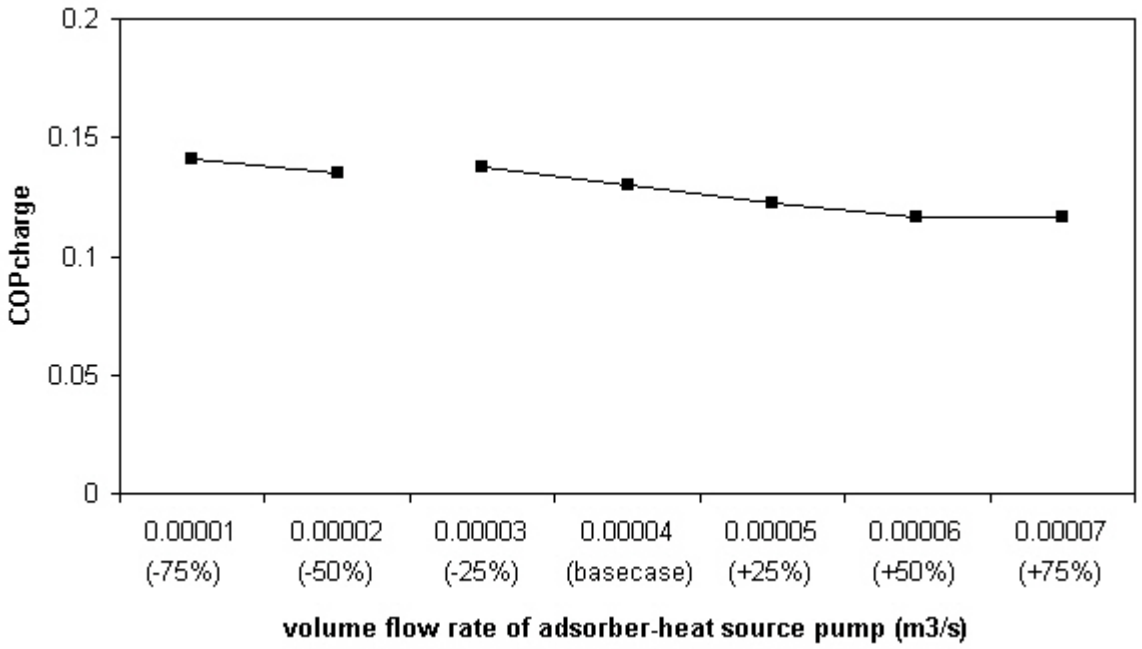

Figure 4.19 COP_{charge} versus adsorber-heat source pump flow rate

As in Figure 4.18, the two curves presented in Figure 4.19 indicate the different states of the adsorber at the end of the simulations. For the simulations with pump flow rates equal to 0.00001 m^3/s and 0.00002 m^3/s (–75% and –50% of the basecase, respectively), the adsorber reaches a steady state temperature less than 195°C, the temperature that is required for the unit to switch from the charging mode to the storage mode of operation.

However, for the simulations with pump flow rates equal to or greater than 0.00003 m^3/s, this temperature is reached and the unit switches from the charging mode of operation to the storage mode.

The volume flow rate of the adsorber/heat source pump has a similar impact on COP_{charge} as the adsorber/heat source heat exchanger effectiveness. A greater pump flow rate results in a shorter charging period and therefore less heat rejected at the condenser.

4.2.2 Discharge mode

The model predicts a discharge COP of 2.15, as defined by equation (4.4), for the adsorption storage unit with the basecase inputs, provided in Table A.3 of Appendix A. The unit completes its discharge process when the temperature of the adsorber reaches 45°C (heat sink temperature of 40°C plus minimum temperature difference between adsorber and heat sink of 5°C for proper heat transfer), and subsequently remains idle, that is in storage mode.

The impact of the following five parameters on the performance of the adsorption system operating in the discharge mode, $COP_{discharge}$, is investigated:

- evaporator effectiveness;
- temperature of the evaporator's heat source (auxiliary water tank);
- volume flow rate of the pump connecting the evaporator and its heat source (auxiliary water tank);
- effectiveness of the adsorber – heat sink (main water storage tank) heat exchanger;

- volume flow rate of the pump between the adsorber and the heat sink (main water storage tank).

Figure 4.20 presents the variation of $COP_{discharge}$ with the effectiveness of the evaporator. $COP_{discharge}$ decreases as more energy is input to the evaporator, which occurs as the evaporator effectiveness increases. It should be noted that the performance parameter $COP_{discharge}$ does not give an indication of the minimum temperature that is reached at the evaporator at the beginning of the adsorption phase. For example, for the basecase simulation, the temperature at the evaporator reaches a minimum temperature of 9.7°C. However, for the simulation with the evaporator effectiveness set to 0.125 (-75% of the basecase), the evaporator reaches a minimum temperature of –3.5°C, which may or may not be realistic depending on the heat exchanger fluid used between the evaporator and its heat source (auxiliary water tank). It should also be noted that there is no provision in the model to verify that the heat input to the evaporator is sufficient to evaporate the liquid adsorbate. It is assumed that the required amount of vapour adsorbate enters the adsorber from the evaporator at the evaporator temperature.

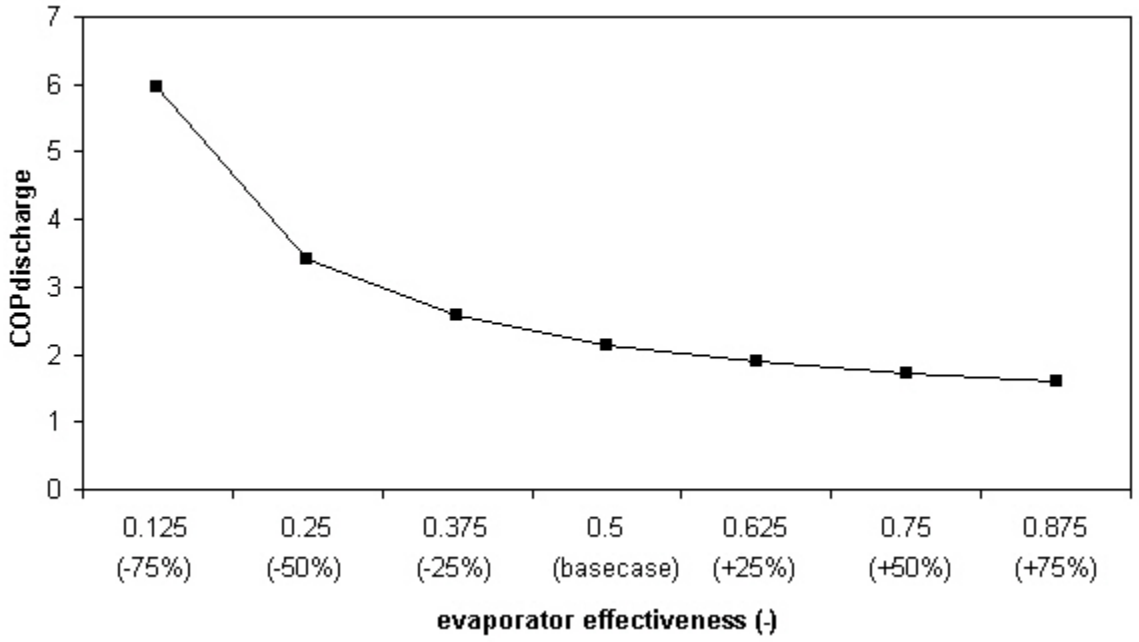

Figure 4.20 $COP_{discharge}$ versus evaporator effectiveness

Figure 4.21 presents the variation of $COP_{discharge}$ with the temperature of the evaporator's heat source (auxiliary water tank). As the temperature of the heat source increases, $COP_{discharge}$ decreases since a higher temperature results in more heat input to the evaporator (the denominator in equation (4.4)). As one would expect, the minimum evaporator temperature that is reached (at the beginning of the adsorption phase) increases as the temperature of the evaporator's heat source increases. For example, for the basecase simulation, the minimum evaporator temperature is 9.7°C, while the minimum temperature is 16.8°C if the temperature of the heat source is increased to 70°C (+75% of the basecase value).

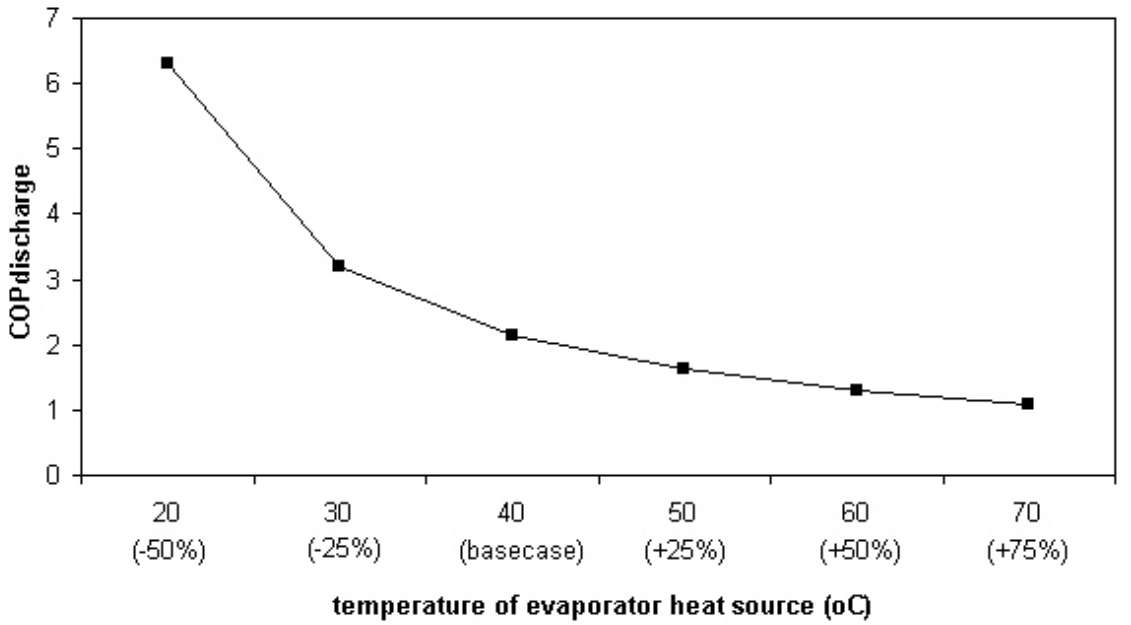

Figure 4.21 $COP_{discharge}$ versus temperature of evaporator heat source

Figure 4.22 presents the variation of $COP_{discharge}$ with the volume flow rate of the pump circulating fluid between the evaporator and its heat source (the auxiliary water tank). The flow rate of the evaporator pump has a similar impact on $COP_{discharge}$ as the evaporator effectiveness. This is expected since both variables are directly proportional to the heat input at the evaporator.

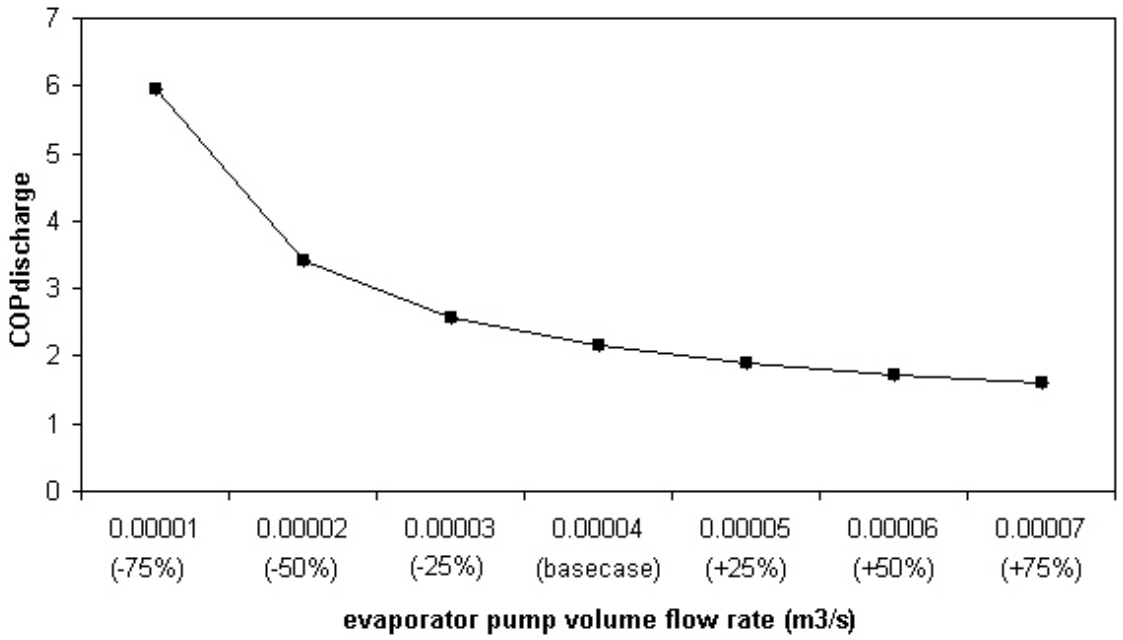

Figure 4.22 $COP_{discharge}$ versus evaporator pump flow rate

Figure 4.23 presents the variation of $COP_{discharge}$ with the effectiveness of the adsorber - heat sink (the main water storage tank) heat exchanger. The effectiveness of the adsorber-heat sink heat exchanger has a considerable impact on the COP of the unit during the discharge process. According to the simulation results, a $COP_{discharge}$ equal to 3.0 can be reached if the heat exchanger effectiveness is 0.875 (+75% of the basecase). This is somehow misleading, however, as the minimum evaporator temperature (at the start of the adsorption phase) for this case is very low, approximately –9.2°C, which may be unrealistic if the evaporator heat exchange fluid does not permit such low temperatures.

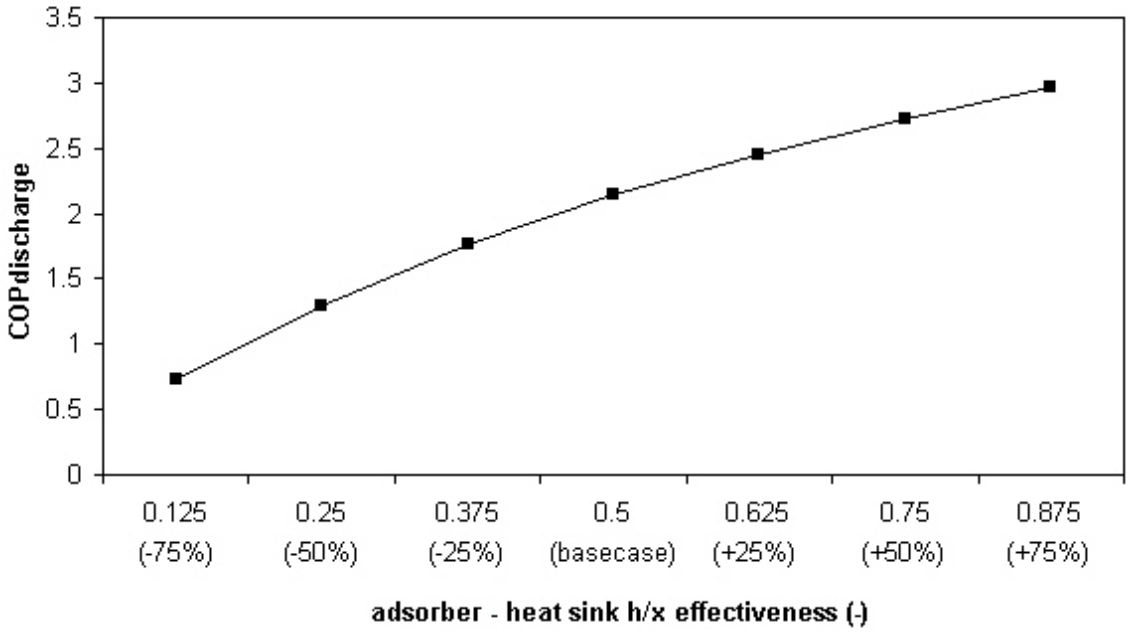

Figure 4.23 $COP_{discharge}$ versus adsorber-heat sink heat exchanger effectiveness

Figure 4.24 presents the variation of $COP_{discharge}$ with the volume flow rate of the pump circulating fluid between the adsorber and the heat sink (main water storage tank). The value of $COP_{discharge}$ increases as the pump flow rate increases since a greater pump flow rate results in a shorter discharge period and thus less amount of heat required at the evaporator. The results presented in Figure 4.23 and 4.24 are similar since both the effectiveness of the adsorber-heat sink heat exchanger and the flow rate of the adsorber-heat sink circulating pump are directly proportional to the heat transfer at the adsorber, and inversely proportional to the length of the discharge period and thus to the heat input to the evaporator.

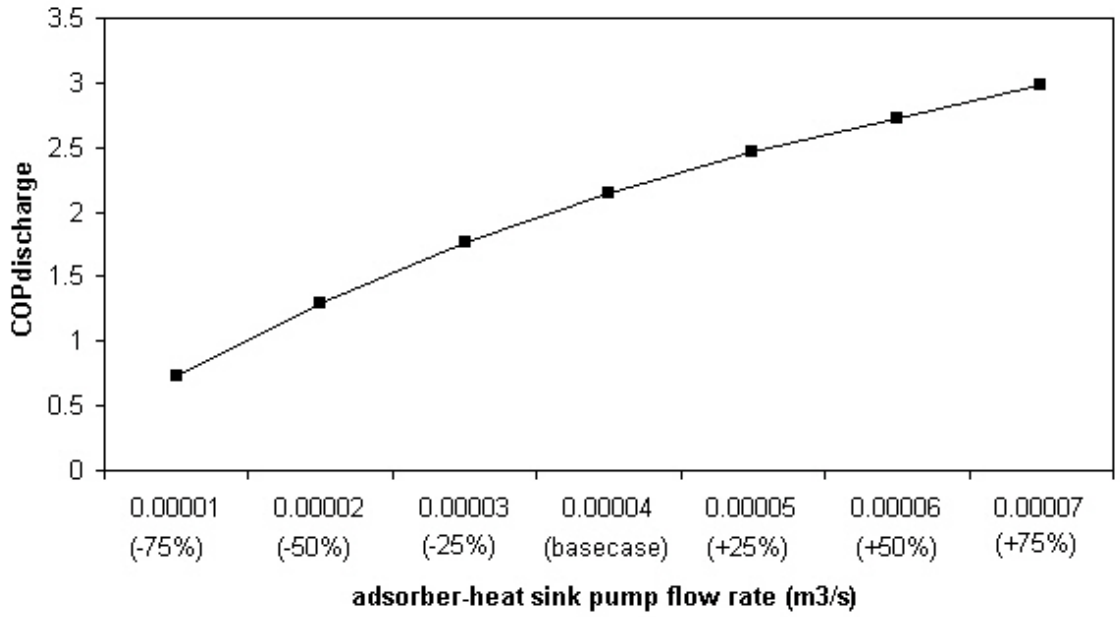

Figure 4.24 $COP_{discharge}$ versus adsorber-heat sink pump flow rate

4.2.3 Complete adsorption cycle

In this section, the impact of several parameters on the COP of a complete adsorption cycle, as defined by equation (4.5), is investigated. A complete adsorption cycle includes the isosteric heating, desorption, isosteric cooling and adsorption phases. The COP predicted for the basecase inputs, presented in Table A.3 of Appendix A, is 0.62.

The impact of the following parameters on the COP of the adsorption storage unit is investigated:

- mass of adsorbent;
- thickness of the adsorber's insulation layer;
- temperature of the heat source (fuel cell);

- temperature of the heat sink (main water storage tank);
- condenser pressure;
- evaporator pressure.

Figure 4.25 presents the variation of the unit's COP with the mass of adsorbent contained within the adsorber. An increase in the mass of adsorbent leads to an increase in the heat input to the unit during the charging process as well as an increase in the heat output from the unit during the discharge process. As well, the amount of heat input to the evaporator increases, since the discharge period lasts for a longer period of time. The result is a negligible impact on the COP of the adsorption storage unit.

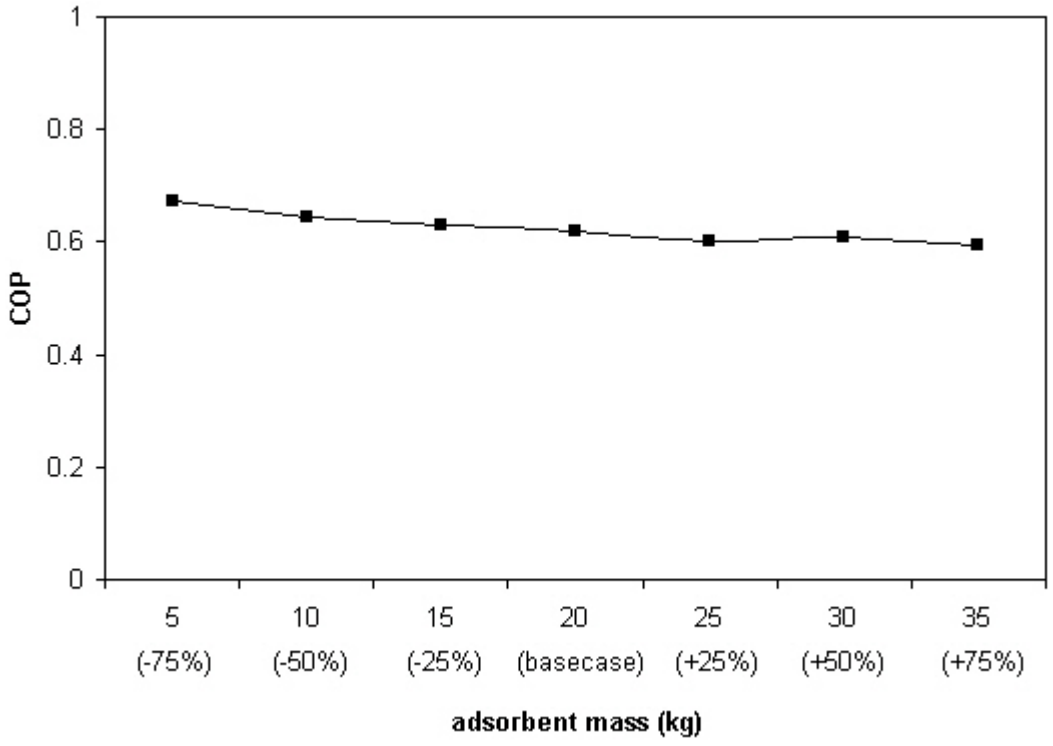

Figure 4.25 COP versus mass of adsorbent

Figure 4.26 presents the variation of the COP with the thickness of the insulation layer surrounding the adsorber.

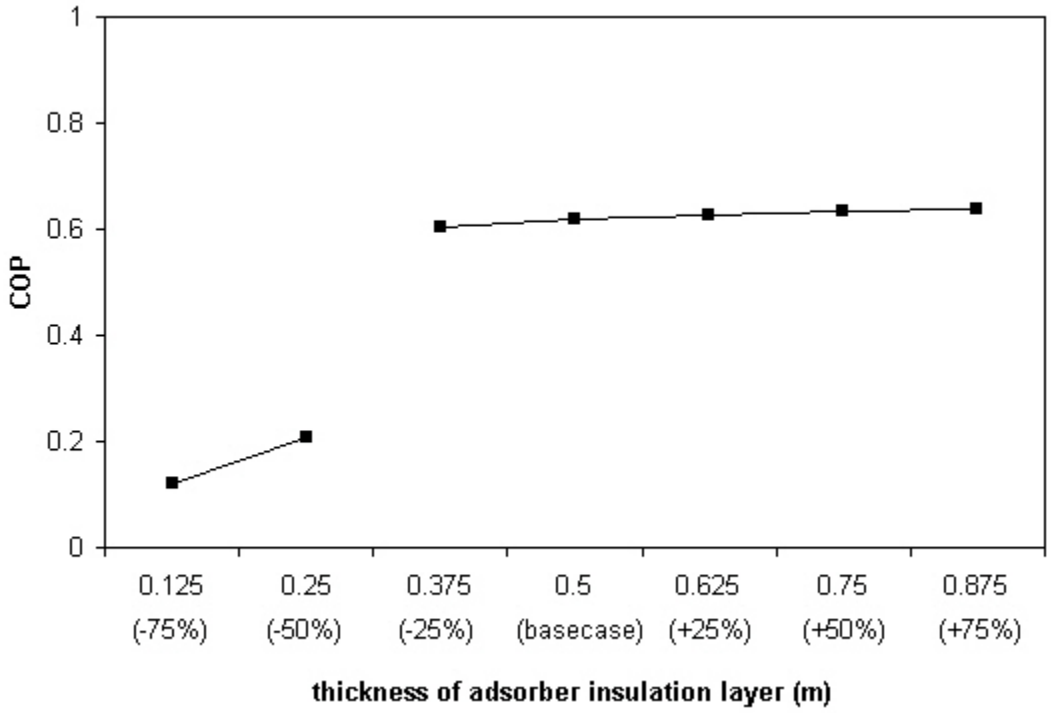

Figure 4.26 COP versus thickness of adsorber insulation layer

For the cases where the insulation layer thickness is set to 0.125mm and 0.250mm (-75% and –50% of the basecase, respectively), the adsorber temperature required for the unit to go from the charging mode of operation to the storage mode is not reached. Rather, a steady-state temperature below the required temperature is reached as heat that continues to be exchanged between the adsorber and the heat source is lost to the ambient. This explains the low COP predicted for these two values of insulation layer thickness.

When considering the cases where the charging mode is completed and the unit goes into storage mode, the COP is seen to increase slightly as the thickness of the insulation layer increases. A thicker insulation layer reduces the losses from the adsorber to the ambient leading to a decrease in the amount of heat input to the adsorber during the charging process and an increase in the heat output from the adsorber during the discharge process.

Figure 4.27 presents the variation of the COP with the temperature of the adsorber's heat source (fuel cell) during the charging process.

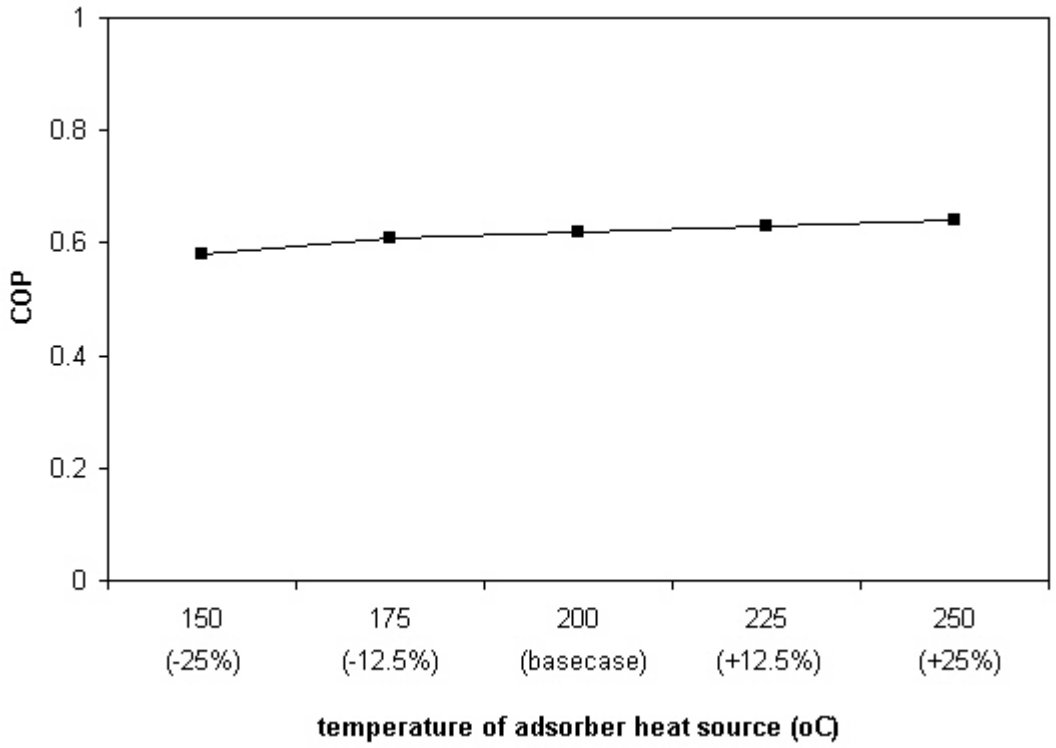

Figure 4.27 COP versus adsorber heat source temperature

An increase in the temperature of the adsorber's heat source leads to an increase in the heat input to the adsorber during the charging process and an increase in the heat output from the adsorber during the discharge process. As well, the heat input to the evaporator increases. The result is a fairly constant COP, indicating that heat at a higher temperature can be stored in the adsorption storage unit without a significant reduction in the COP.

It should be noted that in Figure 4.27, temperatures less than 150°C are not considered since they would be below the minimum charging temperature required for a zeolite-water adsorption system. Also, COP values are not provided for an adsorber heat source temperatures greater than 250°C since the simulation led to convergence errors (due to temperatures going out of bounds at the condenser).

Figure 4.28 presents the variation of COP with the temperature of the adsorber's heat sink (main water storage tank) during the discharge process. The temperature of the heat sink has little impact on the COP of the unit. As the temperature of the heat sink increases, the heat output from the adsorber during the discharge process decreases, as does the heat input to the evaporator. As well, the heat input to the adsorber during the charging process decreases since it is assumed that the initial temperature of the unit is equal to the heat sink temperature. The result is little variation in the COP as the temperature of the heat sink increases. Heat sink temperatures less than 40°C are disregarded in Figure 4.28 since they are of little practical significance.

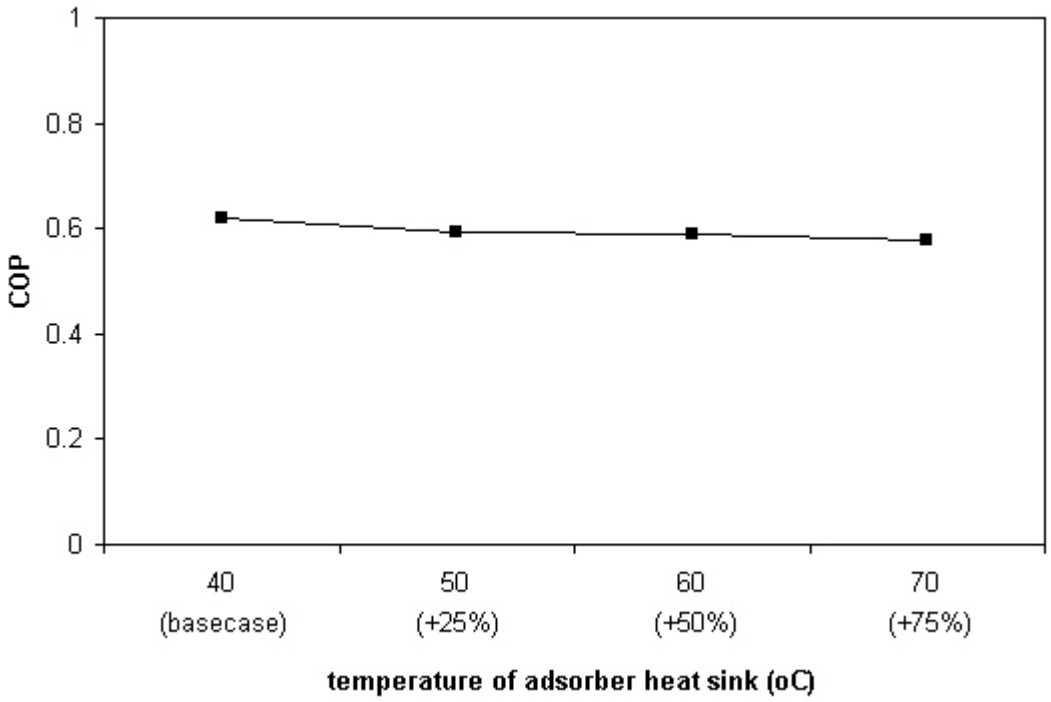

Figure 4.28 COP versus adsorber heat sink temperature

Figure 4.29 presents the variation of the COP with condenser pressure. The condenser pressure is seen to have a negligible impact on the performance of the unit. The ratio of adsorbate mass to adsorbent mass at the end of the charging phase, X_{min}, increases for a higher condenser pressure thus resulting in a smaller change in X during the charging and discharge phases and therefore less heat being exchanged between the adsorber and heat sink/heat source. As well, as the condenser pressure increases, less heat is required at the evaporator since the isosteric cooling phase is longer and thus the adsorption phase shorter. All these factors combine to result in little variation of the COP of the system.

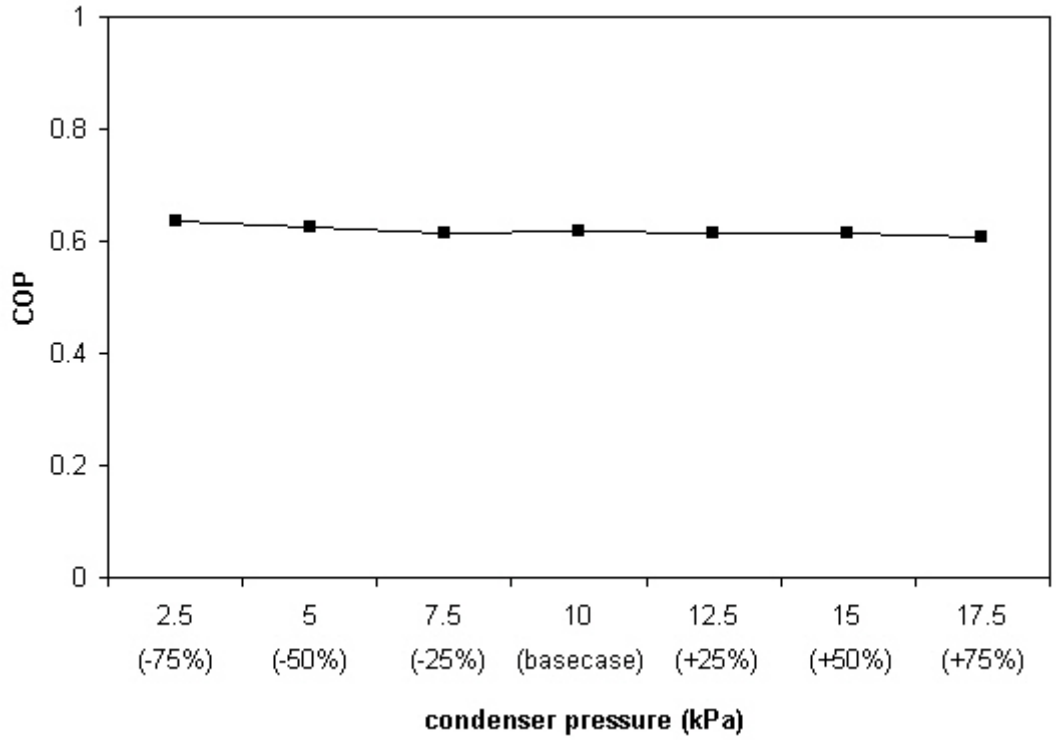

Figure 4.29 COP versus condenser pressure

Figure 4.30 presents the variation of COP with evaporator pressure. The evaporator pressure also has a negligible impact on the performance of the system. As the evaporator pressure is increased, the ratio of adsorbate mass to adsorbent mass at the end of the discharge phase, X_{max}, increases thus resulting in a greater change in X during the charging and discharge phases. Therefore, more heat is exchanged between the adsorber and the heat sink and the adsorber and the heat source during the discharge and charging processes, respectively. Also, a greater evaporator pressure results is a shorter isosteric cooling phase and thus a longer adsorption phase, resulting in a greater amount of heat input to the evaporator. All these factors combine to cause little variation in the COP of the system as the evaporator pressure is increased.

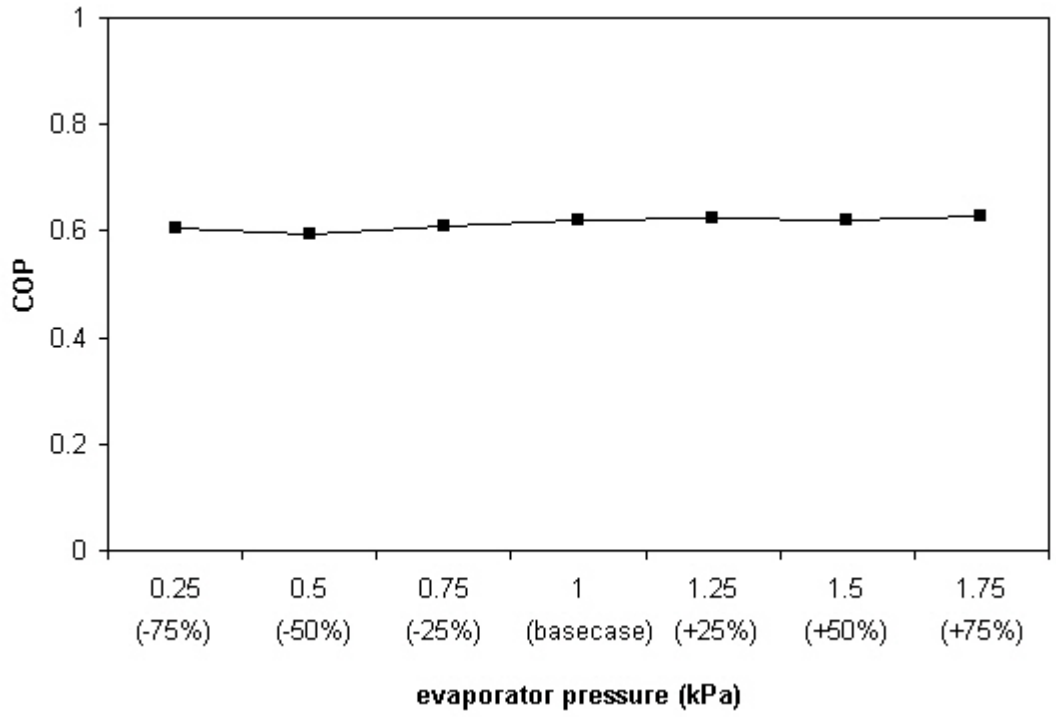

Figure 4.30 COP versus evaporator pressure

4.3 Conclusions of model validation

The simulation results obtained using the model of the adsorption storage unit developed and implemented in ESP-r are qualitatively similar to the results obtained by (Lachance, 2003) and (Leong and Liu, 2004a) in their investigation of adsorption heat pumps. The performance parameters of the system, namely the COP and SCP, that are predicted using the model developed for this work are greater than the values predicted by (Lachance, 2003), which is to be expected since (Lachance, 2003) considers the heat losses from the system's components (adsorber, condenser and evaporator) while no heat losses are assumed in this work. Similarly, the COP and SCP predicted by the model developed for this work are greater than the results reported by (Leong and Liu, 2004a), which is to be

expected since (Leong and Liu, 2004a) consider both the heat and mass transfer effects within the adsorbent bed while this model assumes that there is no resistance to heat or mass transfer within the adsorbent bed. The differences in the performance results in both cases are also expected given the number of inputs that are required by the model developed for this work, but not provided by (Lachance, 2003) and (Leong and Liu, 2004a), and therefore assumed. Qualitatively, the variation of the adsorber's temperature and pressure with time, during a complete adsorption cycle, predicted by the model developed for this work, is similar to that predicted by both (Lachance, 2003) and (Leong and Liu, 2004a). Other simulation results, such as the variation of the system heat flows and the adsorbed amount of vapour within the adsorbent bed are also qualitatively similar.

The results of the sensitivity analysis suggest that the model of the adsorption storage unit developed for this work is valid, since variations of several key model inputs result in the expected impact on the predicted COP of the system, evaluated during the charging cycle, the discharge cycle and a complete charging/discharge cycle. The simulation results show that the condenser and evaporator pressures have a negligible impact on the COP of the unit during a complete charging/discharge cycle, as does the temperature of the adsorber's heat sink (main water storage tank) or adsorber's heat source (fuel cell). When considering the charging and discharge cycles separately, the effectiveness of the adsorber's heat exchanger (whether to the heat source or heat sink) and the flow rate of the pump circulating the heat exchanger fluid between the adsorber and the heat source/sink have a significant impact on the performance of the unit. Results of the

sensitivity analysis also show that the effectiveness of the adsorber/heat source heat exchanger, the flow rate of the pump circulating fluid between the adsorber and its heat source and the thickness of the adsorber's insulation layer influence whether the adsorption storage unit completes its charging cycle. If the values assigned to the three aforementioned variables are not high enough, the adsorber does not reach the required temperature for the unit to switch from the charging mode of operation to the storage mode; rather, a steady-state temperature less than the adsorber's maximum temperature is reached.

5 APPLICATION

The purpose of this chapter is to demonstrate the application of the model of the adsorption storage unit that has been implemented in ESP-r and to investigate the performance of the adsorption storage unit under a certain set of operating conditions. The model of the adsorption storage unit is combined with existing plant component models of a solid-oxide fuel cell (SOFC), water tanks, pipes, pumps, a heating coil and a fan, within ESP-r, to form a plant network. The plant network is configured to provide the space heating and domestic hot water requirements of a house, with the adsorption storage unit providing a means to store the surplus thermal output from the SOFC on a seasonal basis. This plant configuration is compared to two alternate plant configurations: 1) the case where the house's space heating load is served by a conventional natural gas-fired furnace and the domestic hot water load is served by an electric boiler, and 2) the case where the house's space heating and domestic hot water requirements are met by a SOFC cogeneration system but there is no adsorption storage unit for the seasonal storage of heat.

The input parameters that are required by the plant component model of the adsorption storage unit are based on data available in the literature. It should be noted that most of the published data that is available pertains to adsorption systems used in heat pump applications and therefore the input parameters may not represent the actual operating characteristics of an adsorption system used for a storage application. No attempt is made in this analysis to optimize the characteristics of the adsorption storage unit, or of any of the components within the plant network. Optimal system parameters should be

determined in future work when actual characteristic data for the adsorption system as well as the other components within the plant network are available.

In section 5.1, the characteristics of the house and the three different heating, ventilation and air-conditioning (HVAC) systems are described. The simulation results are presented in section 5.2.

5.1 House model description

The house model used in this study is a modern energy-efficient house built to the R-2000 standard (Natural Resources Canada, 2005) and located in Montréal. This same house model was used to demonstrate the ESP-r model of a SOFC cogeneration system by (Beausoleil-Morrison et al., 2002a). The house is modelled using four zones: one zone comprising the basement, a second zone comprising the main living area, a third comprising the attached garage and a fourth zone comprising the attic. Several characteristics of the house model are presented in Table 5.1.

The domestic hot water (DHW) loads and non-HVAC electrical loads were selected to be typical of a family of four. Sensible heat gains due to lighting and occupants are modelled in the main living-area zone.

Table 5.1 House model characteristics

Zone 1: Basement	
Floor Area (m^2)	84
Volume (m^3)	218
Thermal resistance of walls ($m^2°C/W$)	2.10
Thermal resistance of floor slab ($m^2°C/W$)	0.83
Zone 2: Main living area	
Floor Area (m^2)	84
Volume (m^3)	554
Window Area (m^2)	22
Thermal resistance of walls ($m^2°C/W$)	3.23
Thermal conductance of windows ($W/ m^2°C$)	1.53
Zone 3: Attic	
Floor Area (m^2)	122
Volume (m^3)	175
Thermal resistance of roof ($m^2°C/W$)	0.26
Zone 4: Garage	
Floor Area (m^2)	38
Volume (m^3)	115
Thermal resistance of floor slab ($m^2°C/W$)	0.83

Infiltration was modelled in the basement and main living-area zones using 1.5 ach at 50 Pa and an equivalent leakage area of 523.7 m^2 at 10 Pa.

Ventilation is provided to the house by a heat-recovery ventilator (HRV) with a nominal efficiency of 85%. The power draw of the HRV's fan and pre-heater is 117 W.

Each of the three heating systems that are considered in this analysis is described below.

5.1.1 Case 1: Conventional Natural-Gas Furnace

In this case, the house is heated with a natural gas furnace. The characteristics of the furnace are provided in Table 5.2. The indoor temperatures in the attic and garage zones are allowed to free-float. However, temperatures are controlled in the basement and main living-area zones. In these zones, the heating setpoint is 21°C during the day (8h00 to 20h00) and set back to 18°C during the night (20h00 to 8h00). It is assumed that an electrically-heated water tank provides domestic hot water.

Table 5.2 Furnace characteristics

Heating fuel	Natural gas
Capacity (W)	19800
Steady-state efficiency (%)	85
Circulation fan mode	Auto
Circulation fan power (W)	385

5.1.2 Case 2: SOFC cogeneration system with no seasonal heat storage

The heating system configuration considered in this case is adapted from (Beausoleil-Morrison et al., 2002a). The HVAC plant network consists of a SOFC, a gas-fired water storage tank, pumps, pipes and an air-handling unit, comprised of a heating coil and a fan. The plant network is depicted in Figure 5.1.

In this case, the SOFC cogeneration unit is operated to meet the house's electrical load. Thermal energy that is available from the SOFC is transferred to a water storage tank via a pump that circulates water from the SOFC's heat exchanger to the water storage tank.

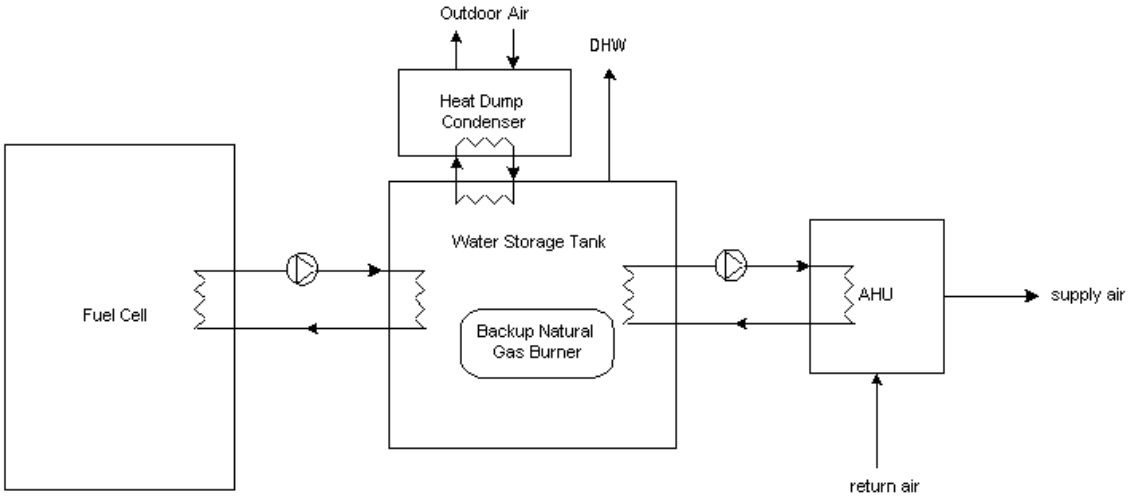

Figure 5.1 HVAC configuration for Case 2

The water storage tank meets the house's space heating load, via an air-handling unit, as well as its domestic hot water requirement. The water storage tank contains a backup natural gas burner that operates when the SOFC does not provide sufficient thermal energy to the tank to meet the house's space heating and domestic hot water loads. A pump circulates hot water from the storage tank to the air-handling unit's heating coil when a space heating load exists, in which case the air handling unit's fan also operates. For safety concerns, a safety device rejects heat from the water storage tank when the temperature in the tank is above a maximum set-point temperature.

Several characteristics of the SOFC and water tank plant components are listed in Table 5.3. Also listed in Table 5.3 are the set-point temperatures for the water tank's natural gas burner and heat dump feature.

Table 5.3 Characteristics of SOFC and water tank plant components

SOFC	
Fuel source	Natural gas
Minimum net electric output (W)	500
Maximum net electric output (W)	5000
Parasitic loads (W)	0
Heat leakage from SOFC to basement (W)	100
Water storage tank	
Fuel source	Natural gas
Total (water and tank) mass (kg)	300
UA to surroundings (W/°C)	1.1750
Nominal burner capacity when ON (W)	29300
Nominal burner capacity when OFF (W)	0
Combustion and flue efficiency (%)	80
Natural gas burner ON set-point (°C)	50
Natural gas burner OFF set-point (°C)	60
Heat-dump set-point (°C)	90

Space heating is permitted between October 1st and April 30th, inclusive. During this period, the air-handling unit's fan and the pump circulating water between the water storage tank and the air-handling unit's heating coil switch on when the temperature in the main-living area drops below 19.5°C and switch off when the temperature in the zone rises above 20.5°C. No setback conditions are modelled in this case. The burner capacity in Table 5.3 is chosen to match the capacity investigated by (Beausoleil-Morrison et al., 2002a).

5.1.3 Case 3: SOFC cogeneration system with an adsorption storage system

In this case, the plant network consists of the same components as in Case 2, that is, a SOFC, a water storage tank, pumps and an air-handling unit, with the addition of the following components: an adsorption storage system for the seasonal storage of heat, an auxiliary water tank and additional pumps. The auxiliary water tank and the additional

pumps are required for the operation of the adsorption storage system. A schematic of the plant network is presented in Figure 5.2.

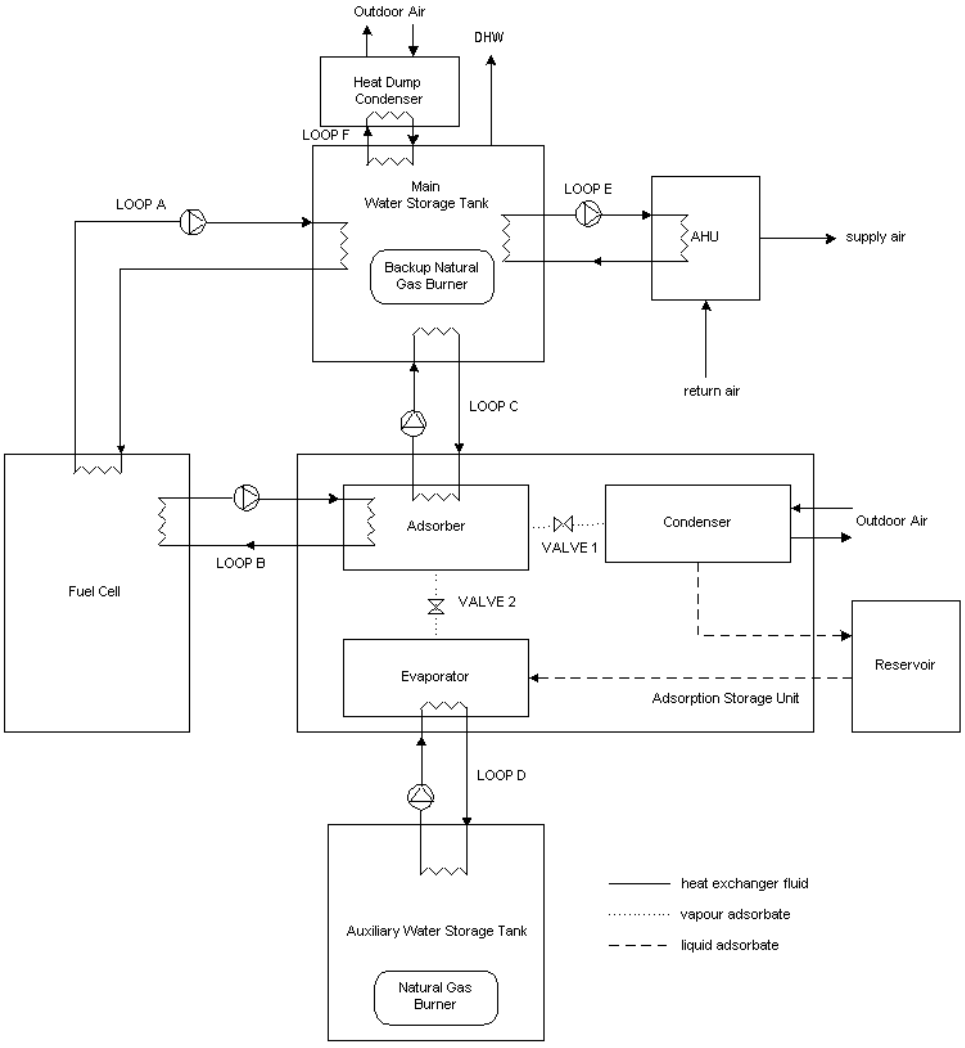

Figure 5.2 HVAC configuration for Case 3

As in Case 2, the SOFC operates to meet the house's electrical load. However, in Case 3, the SOFC's thermal output is either transferred to the adsorption storage unit or to the

main water storage tank, depending on the sensed control parameters. The control logic for the plant network is presented in section 3.3.

As in Case 2, the main water storage tank meets the house's space heating load and its domestic hot water requirement. When the SOFC does not provide sufficient thermal energy to the tank to meet the house's space heating and domestic hot water loads, either the adsorption storage unit is discharged and/or the natural gas burner within the water storage tank cycles on, depending on the sensed control parameters (the adsorption storage controller algorithm is depicted in Figure 3.11).

As in Case 2, a pump circulates hot water from the storage tank to the air-handling unit's heating coil when a space heating load exists, in which case the air handling unit's fan also operates. For safety concerns, a safety device rejects heat from the water storage tank when the temperature in the tank is above a maximum set-point temperature.

When the adsorption storage unit is discharging, the evaporator requires heat, which is provided by the auxiliary water tank. An existing ESP-r plant component model of a boiler is used to represent the auxiliary water tank in the plant network; the model only requires that the heating capacity of the boiler be specified.

In order to simplify the plant network, the reservoir that contains the liquid adsorbate is not explicitly modelled. Rather, it is assumed that the liquid adsorbate transferred to the

adsorption system's evaporator when the adsorption storage unit is discharging is at a constant temperature of 20°C.

For this analysis, heat losses from the adsorption storage unit to the surroundings are not modelled, for several reasons: (1) input data such as the overall heat transfer coefficient and the surface area of the unit's individual components (adsorber, condenser and evaporator) are not available; (2) although the heat losses from the unit's individual components to the ambient are taken into account in the mathematical model presented in Chapter 3, it is not known, in the actual operation of the system, if and how the pressure in the unit would be kept constant when the temperature of the unit decreases due to heat losses to the ambient; (3) if the simulation results show that even for the ideal case in which the heat losses from the unit's individual components to the ambient are ignored, the adsorption storage unit is not able to store or recover sufficient amounts of thermal energy to improve the overall performance of the cogeneration system, then it follows that the adsorption storage unit will likely not be feasible in the actual case.

The characteristics of the SOFC and water storage tank presented in Table 5.3 also apply for Case 3. The characteristics and control parameters of the adsorption storage unit and auxiliary water tank are listed in Table 5.4 (for brevity, not all inputs pertaining to the adsorption storage unit are listed in Table 5.4; the complete set of inputs are provided in Appendix B).

Table 5.4 Characteristics of adsorption storage unit and auxiliary water tank components

Adsorption storage unit		
Mass of adsorbent (kg)	Case 3A	Case 3B
	7500	22500
Mass of adsorber vessel (kg)	20	
Mass of adsorber heat exchanger (kg)	50	
Adsorber/fuel-cell heat-exhanger effectiveness (-)	0.5	
Adsorber/water tank heat-exchanger effectiveness (-)	0.5	
Minimum temperature difference between adsorber and heat source/sink (°C)	5	
Condenser pressure (kPa)	10	
Condenser heat exchanger effectiveness (-)	0.5	
Condenser fan power rating (W)	200	
Evaporator pressure (kPa)	1	
Evaporator heat exchanger effectiveness (-)	0.5	
Adsorption storage unit controller inputs		
Period during which charging is permitted	May 1 - September 30	
Period during which discharging is permitted	October 1 - April 30	
Water tank upper (ON) set-point temperature for charging of unit (°C)	65	
Water tank lower (OFF) set-point temperature for charging of unit (°C)	55	
Water tank lower (ON) set-point temperature for discharging of unit (°C)	65	
Water tank upper (OFF) set-point temperature for discharging of unit (°C)	75	
Auxiliary water tank		
Total mass (kg)	50	
Heating capacity (W)	1000	
ON set-point temperature (°C)	40	
OFF set-point temperature (°C)	50	

Two different adsorber volumes are considered. In the first instance (case 3A) an adsorber volume of 8.4 m^3 is considered since equipment of this volume can be placed in a house's basement. Assuming the bulk density for zeolite 13X is 896.3 kg/m^3 (Nùñez et

al., 1999), the adsorber contains 7500 kg of adsorbent. In the second instance (case 3B), the adsorber volume was increased threefold, to 25.2 m^3, representing an adsorbent mass of 22500 kg. Although equipment of this size is most likely not suitable for a residential application (only the adsorber volume is 25.2 m^3, this does not include volumes of the condenser or evaporator that are required), the analysis is carried out to determine the effect of an increased adsorber capacity on the performance of the overall system.

The operating pressures of the adsorption storage unit are chosen based on those cited for an adsorption system used in a heat pump application (Leong and Liu, 2004a).

It is assumed that the pumps required for the operation of the adsorption storage unit (loops B, C and D in Figure 5.2) each have a power draw of 150W. The flow rates that are assumed for the pumps in Figure 5.2 are listed in Table 5.5. The flow rates for the pumps that are common for cases 2 and 3 (loops A and E in Figure 5.2) are set equal in the two cases. For case 3, it is assumed that loops B and C are pressurized to 2000 kPa in order to permit temperatures greater than 100°C for the charging and discharging of the adsorption storage unit.

Table 5.5 Pump flow rates

Volume flow rate of fuel cell-water tank pump (loop A) (m^3/s)	1.26E-04
Volume flow rate of fuel cell-adsorber pump (loop B) (m^3/s)	5.0E-06
Volume flow rate of adsorber-water tank pump (loop C) (m^3/s)	1.0E-05
Volume flow rate of auxiliary water tank-evaporator pump (loop D) (m^3/s)	3.0E-05
Volume flow rate of water tank-heating coil pump (loop E) (m^3/s)	3.0E-04

It is assumed that on January 1 (the start date of the simulation), the adsorption storage unit is fully charged, the adsorber's temperature is 200°C and its pressure is equal to the condenser pressure.

5.2 Simulation results

Simulations of the house model served by each of the three heating systems that are considered in this analysis are carried out for an entire year (January 1 – December 31) using 5-minute time-steps and a 3-day start-up period. The time required to run a one-year simulation on a computer with 1.5 GB of RAM and a CPU speed of 3 GHz varied for each case. For Case 1, an annual simulation was completed in approximately 5 minutes while for Case 2, an annual simulation required approximately 15 minutes. For Case 3, an annual simulation was completed in 30 hours. The cause of the long run-times for the Case 3 simulations could not be found but further investigation is recommended for future work.

The house's annual heating load is 56.5 GJ/year. The house's monthly heating load is presented in Figure 5.3.

In the subsequent sections, the simulation results for each case are presented, followed by a comparison of the simulation results for the three cases.

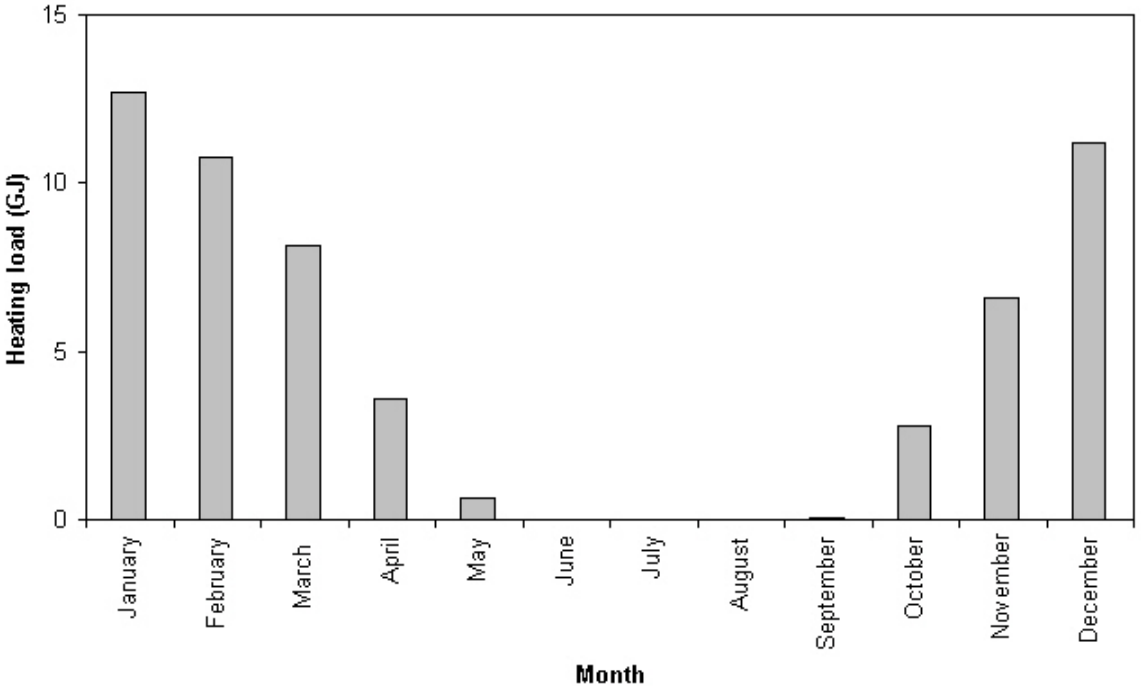

Figure 5.3 Monthly heating load

5.2.1 Case 1: Conventional Natural-Gas Furnace

For the case where the house is served by a conventional natural gas-fired furnace, ESP-r predicts an annual energy consumption of 127.2 GJ/year, including electric loads and heating needs. The monthly energy consumption of the house is presented in Figure 5.4. In Figure 5.4, the non-HVAC electrical load includes the base energy consumed by lights and appliances while the HVAC electrical load includes the energy consumed by the HRV, electric domestic hot water heater and the furnace's circulation fan.

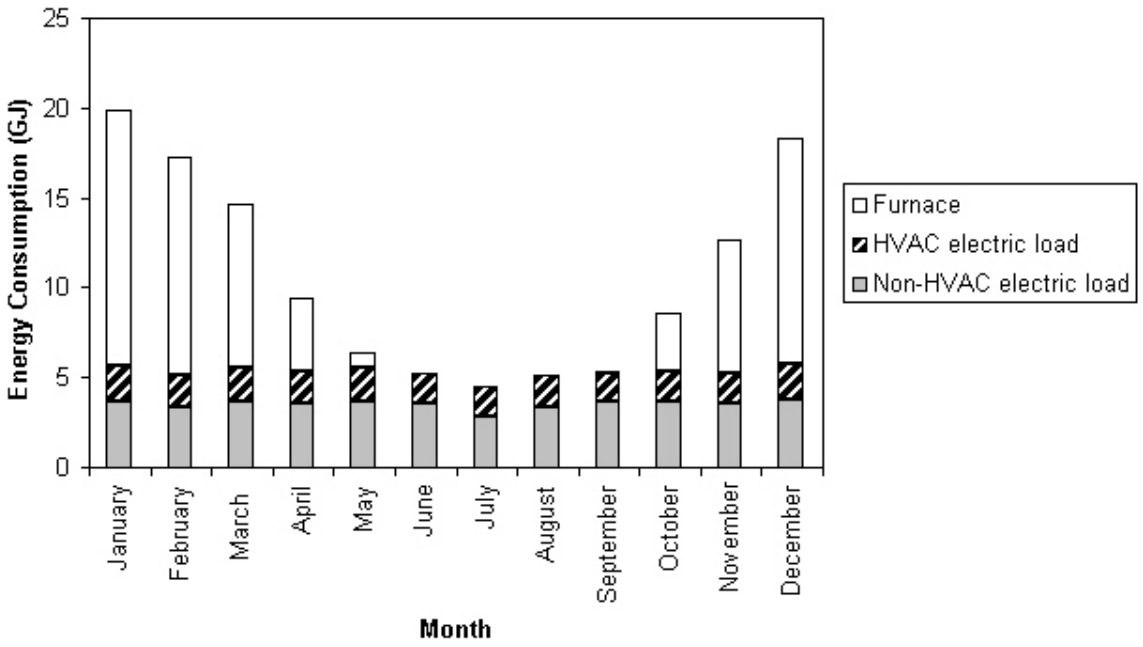

Figure 5.4 Monthly energy consumption for Case 1

The house's annual natural gas consumption is 1769.6 m^3, based on a lower heating value (LHV) equal to 35.9 MJ/m^3. The monthly natural gas consumption for the house is shown in Figure 5.5.

An average annual efficiency, $\eta_{sys\text{-}1}$, for the system can be calculated as a ratio of the annual energy loads and the annual energy consumption:

$$\eta_{sys-1} = \frac{Htg - load + DHW - load + Elec - load}{Nat - gas - cons \cdot LHV_{nat-gas} + Elec - cons} \tag{5.1}$$

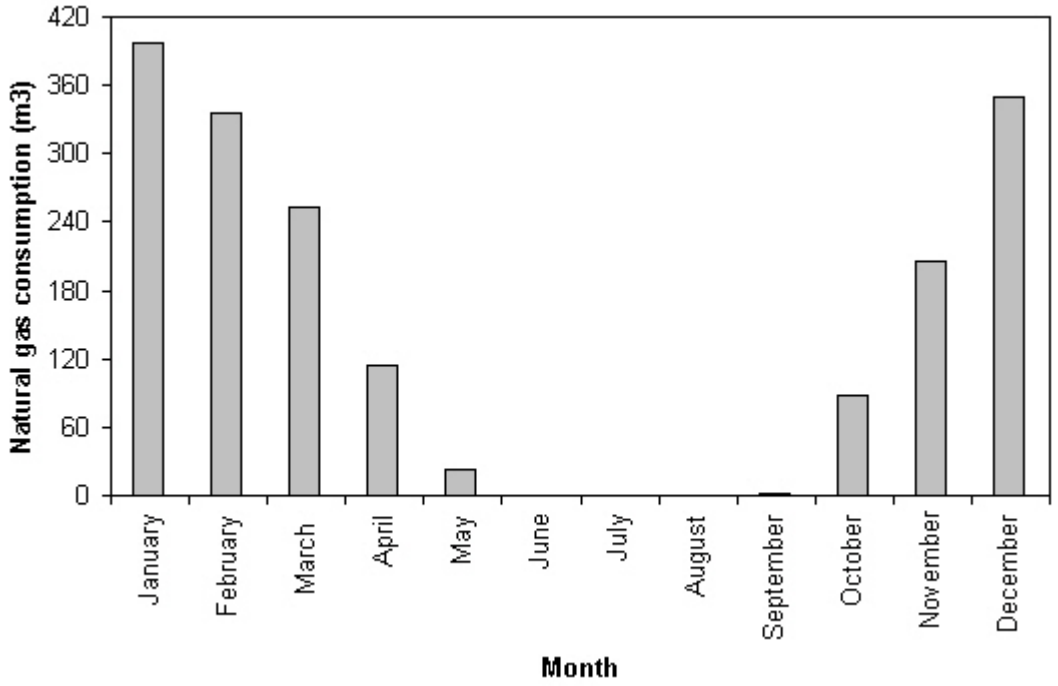

Figure 5.5 Monthly natural gas consumption for Case 1

where

Htg-load is the annual space-heating load (GJ);

DHW-load is the annual domestic hot water heating load (GJ);

Elec-load is the annual non-HVAC electrical load (GJ);

Nat-gas-cons is the annual natural gas consumption of the furnace (m^3);

$LHV_{\text{nat-gas}}$ is the lower heating value of natural gas (GJ/m^3);

Elec-cons is the annual total electricity consumption (GJ).

The average system efficiency for this case, calculated using equation (5.1), is 90.7%.

The house's annual energy consumption reported above is in fact the secondary energy consumed by the house. If the primary energy requirement of the house is considered so that the efficiency of the generation source supplying the electric power and the transmission losses are taken into account, the house's annual energy consumption and average system efficiency are much different.

If we assume that the electricity supplied to the house is generated from a hydro-electric source (applicable to Montréal) and that the efficiency of the generation and transmission of electricity is 85% (Zmeureanu, 2005), the primary energy consumption of the house is 138.5 GJ. Considering the primary, versus secondary, electric consumption of the house in equation (5.1), the average system efficiency is 83.4%.

If we assume that the electricity supplied to the house is generated from oil (applicable to Alberta for example) and that the efficiency of the generation and transmission of electricity is 30% (Zmeureanu, 2005), the primary energy consumption of the house is 275.9 GJ. Considering the primary, versus secondary, electric consumption of the house in equation (5.1), the average system efficiency is 41.8%.

5.2.2 Case 2: SOFC cogeneration system with no seasonal heat storage

For the case where the house is served by a SOFC and there is no seasonal storage of the SOFC's thermal output, ESP-r predicts an annual energy consumption of 164.6 GJ, which includes the energy required for the operation of the SOFC to meet the house's electrical load and for the operation of the water tank's natural gas burner. The estimated

annual energy consumption for Case 2 is 18.8% greater than the estimated primary annual energy consumption for Case 1 if it is assumed that power is generated from a hydro-electric source in the latter case. The monthly energy consumption for Case 2 is presented in Figure 5.6.

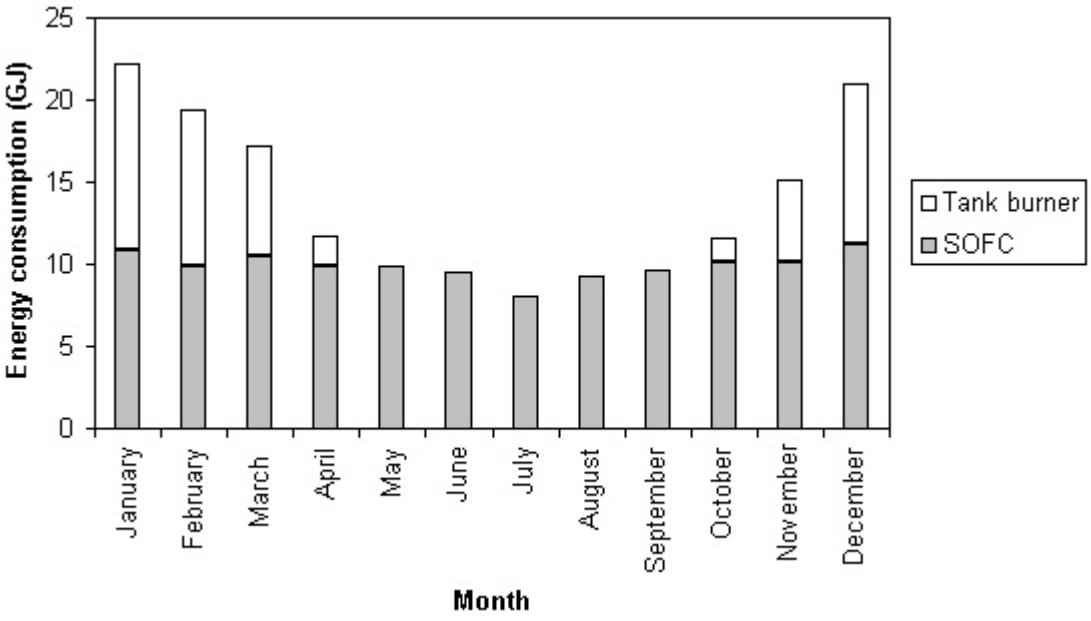

Figure 5.6 Monthly energy consumption for Case 2

The house's annual natural gas consumption is 4591.3 m^3, based on a LHV of 35.9 MJ/m^3. The annual natural gas consumption for Case 2 is 1.6 times greater than the annual natural gas consumption of Case 1, keeping in mind that for Case 2 natural gas is used to fuel the SOFC, in response to the house's electrical demand, and the water tank's natural gas burner. The monthly natural gas consumption for the house for Case 2 is shown in Figure 5.7.

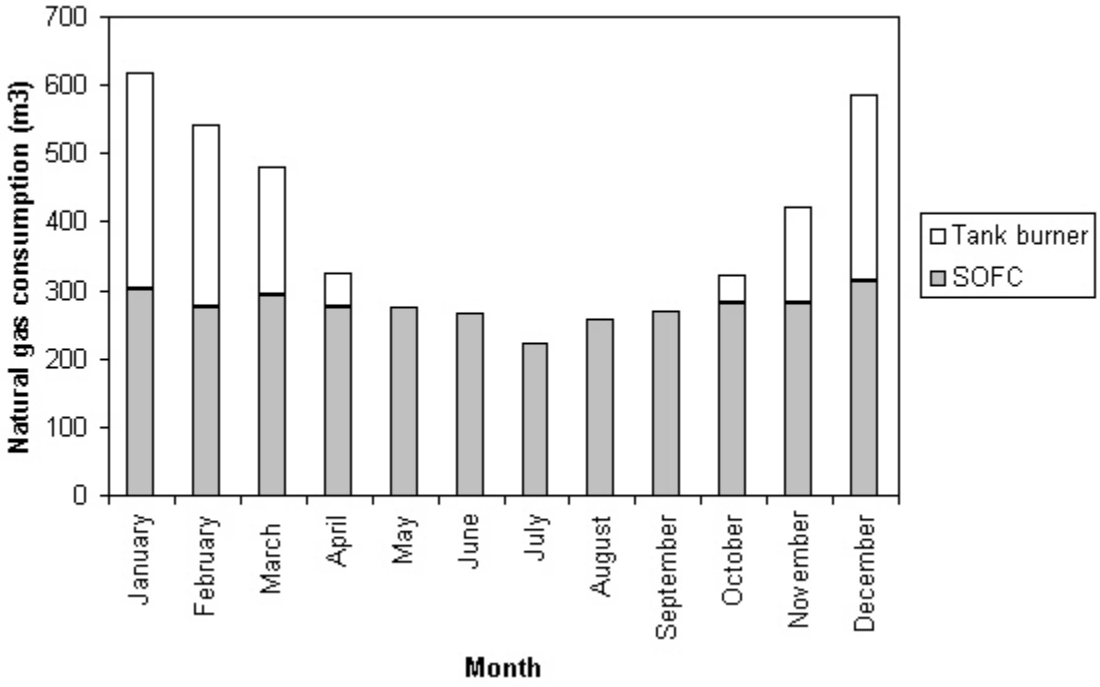

Figure 5.7 Monthly natural gas consumption for Case 2

Figure 5.8 presents the thermal energy added to the water tank by the SOFC, the thermal energy added to the water tank by the natural gas burner and the thermal energy rejected by the tank's safety device, on a monthly basis. Consistent with the findings of (Beausoleil-Morrison et al., 2002a) for a similar case, the water tank's burner is inactive between May and September when the SOFC's thermal output is sufficient to meet the house's thermal load. The only thermal load on the tank between May and September is due to heating of domestic hot water. Thermal energy is rejected by the water tank's safety device during the summer months when there is no space-heating load and during the swing months when space-heating loads are minimal.

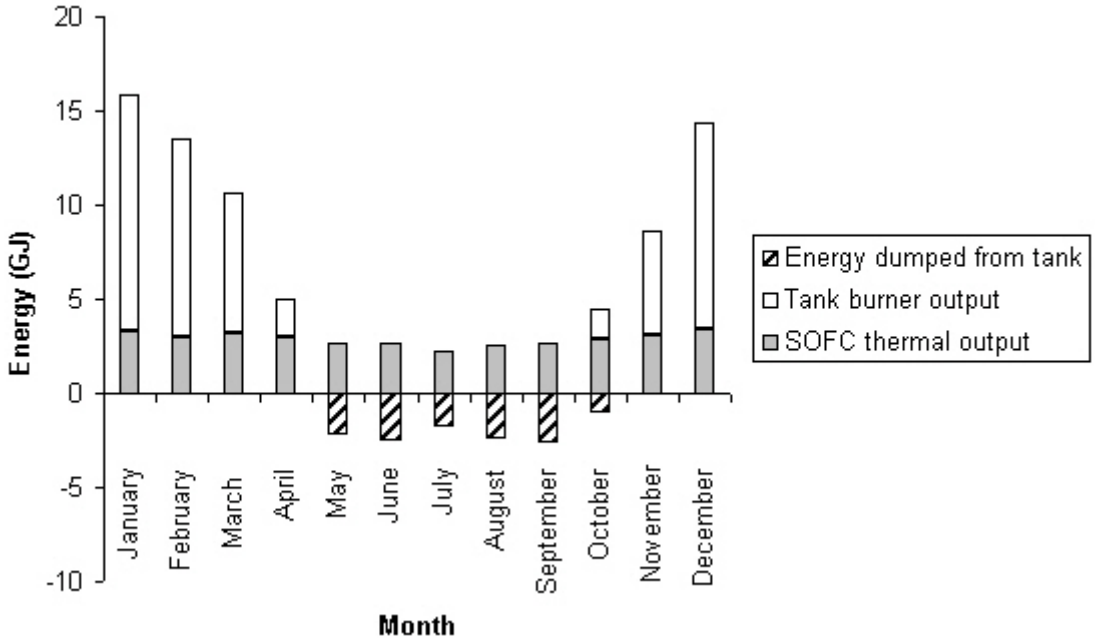

Figure 5.8 Monthly thermal energy balance on water tank for Case 2

The SOFC delivers 34.5 GJ of thermal energy to the water tank over the year. However, 12.9 GJ of energy is rejected from the water tank to maintain the temperature in the water tank below its maximum set-point temperature. Therefore, the SOFC's net thermal contribution is 21.6 GJ. The water tank's burner must provide 50.6 GJ of thermal energy during the year to maintain the water in the tank above its minimum set-point temperature. Therefore, for this specific case the SOFC provides 29.9% of the house's thermal requirement.

(Beausoleil-Morrison et al., 2002a) defines the total (electrical plus thermal) efficiency of the SOFC cogeneration system, η_{cogen}, in terms of the LHV of natural gas, $LHV_{nat\text{-}gas}$ [GJ/m^3]:

$$\eta_{cogen} = \frac{SOFC_{elec-out} + SOFC_{thermal-out} - Tank_{rej-heat}}{SOFC_{nat-gas} \cdot LHV_{nat-gas}} \quad (5.2)$$

where

$SOFC_{elec\text{-}out}$ is the annual electrical energy delivered by the SOFC (GJ);

$SOFC_{thermal\text{-}out}$ is the annual thermal energy delivered by the SOFC (GJ);

$Tank_{rej\text{-}heat}$ is the annual energy rejected from the water tank by the safety device (GJ) and

$SOFC_{nat\text{-}gas}$ is the annual natural gas consumption of the SOFC (m^3).

In this case, the SOFC delivers 52.9 GJ of electrical energy over the year and consumes 3317.7 m^3 of natural gas to deliver its electrical and thermal output. Therefore, the total cogeneration efficiency of the system is 62.6%.

The thermal state of the water storage tank on a typical winter day (January 6) is depicted in Figure 5.9. The SOFC's thermal output is not sufficient to meet the space heating and DHW loads of the house. The natural gas burner cycles on when the temperature within the water tank is less than 50°C and cycles off when the temperature reaches 60°C, approximately every hour.

Figure 5.10 presents the temperature in the water storage tank on October 16, when the SOFC's thermal output is sufficient and no backup heating by the tank's natural gas burner is required. Although the temperature within the water storage tank decreases during the day, it does not fall below the natural gas burner's ON set-point (50°C).

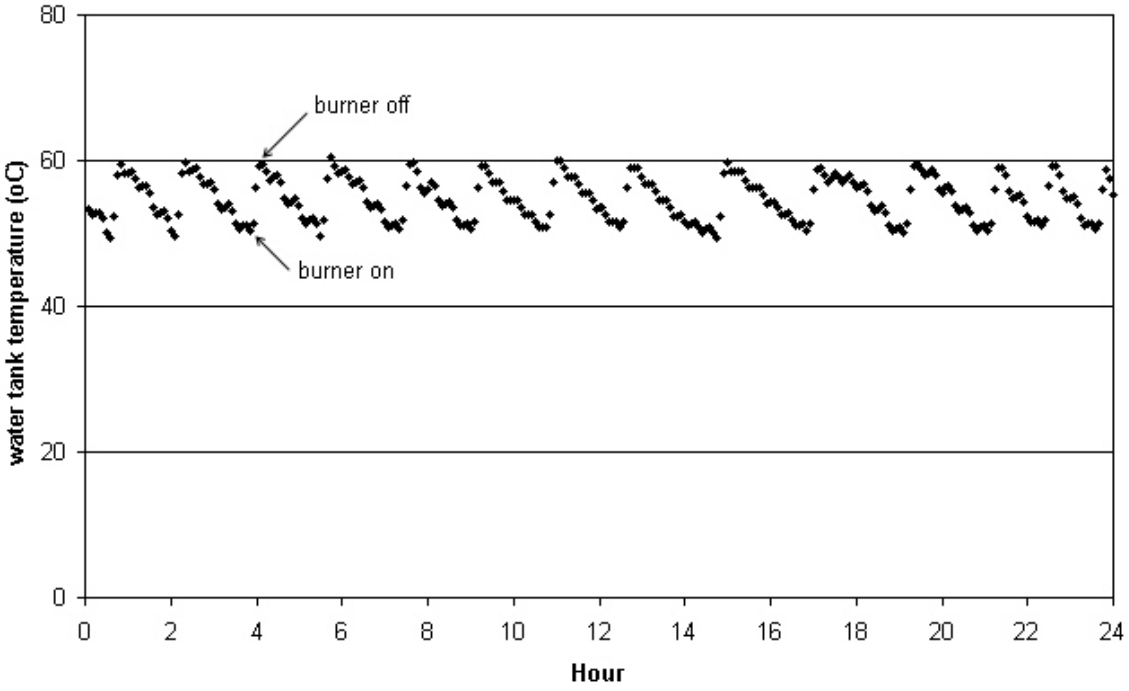

Figure 5.9 Temperature of water storage tank on January 6 (Case 2)

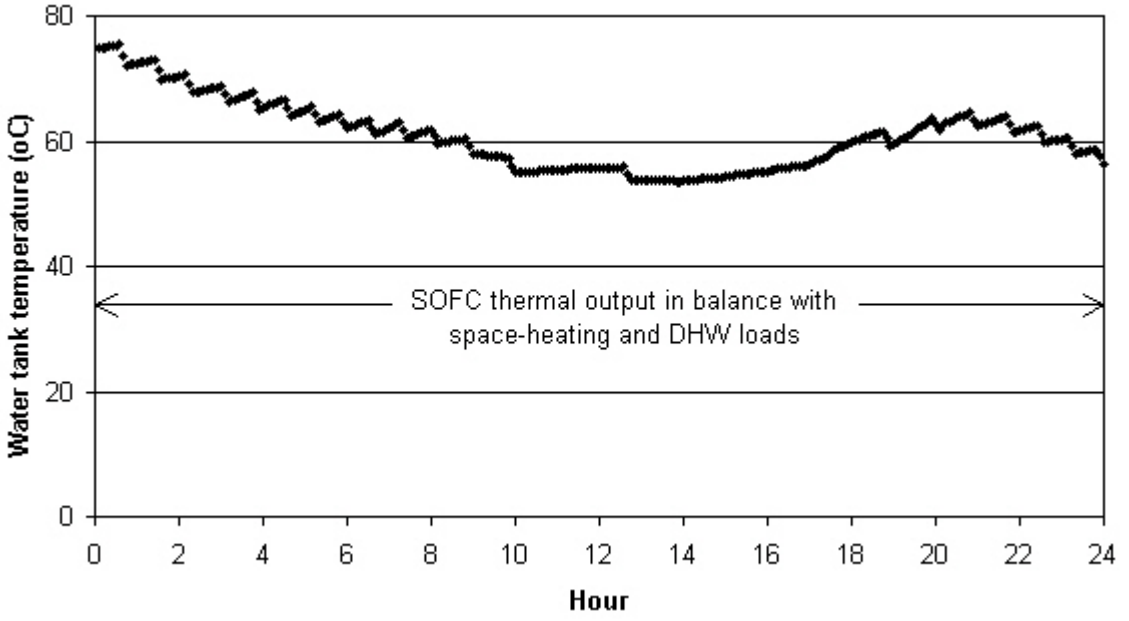

Figure 5.10 Temperature of water storage tank on October 16 (Case 2)

Figure 5.11 depicts the thermal state of the tank on a spring day (May 1). The SOFC's thermal output is greater than the thermal requirements of the house and therefore energy is rejected by the tank's safety device frequently throughout the day. The safety device rejects energy from the tank when the water reaches a temperature of 90°C.

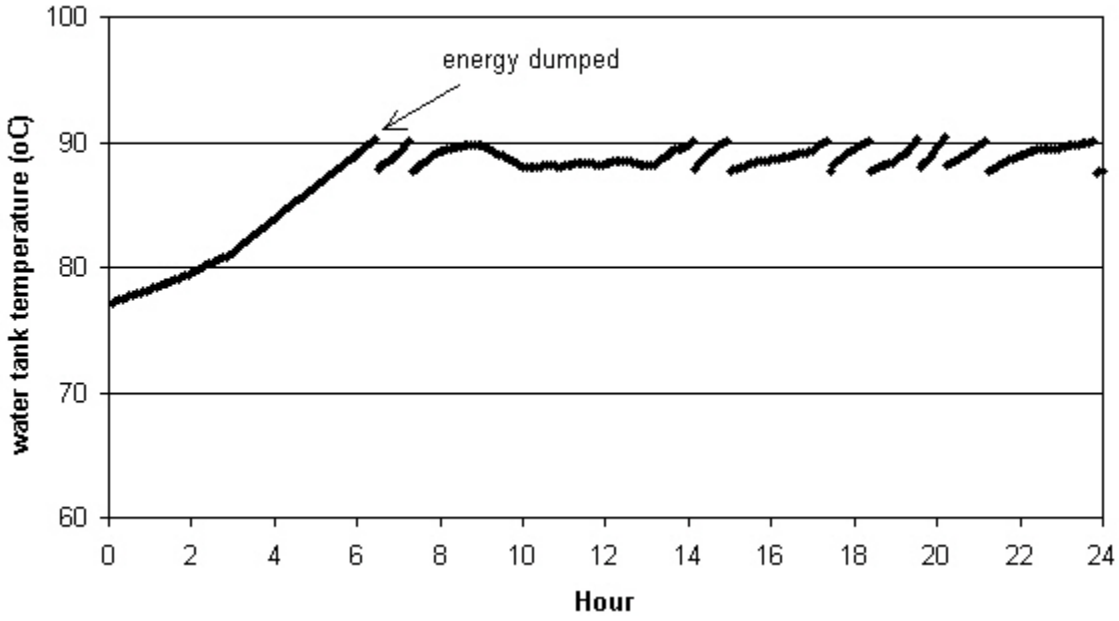

Figure 5.11 Temperature of water storage tank on May 1 (Case 2)

5.2.3 Case 3: SOFC cogeneration system with an adsorption storage system

5.2.3.1 Case 3A: Mass of adsorbent = 7500 kg

For the case where the house is served by a SOFC and an adsorption storage system, with an adsorbent mass of 7500 kg, is available to store the SOFC's surplus thermal output on a seasonal basis, ESP-r predicts the house's annual energy consumption to be 147.4 GJ,

10.4% less than the annual energy consumption predicted for Case 2 and 6.4% greater than the amount predicted for Case 1, if it is assumed that power is generated from a hydro-electric source in the latter case. The monthly energy consumption for Case 3A is presented in Figure 5.12. The presence of the adsorption storage unit reduces the monthly energy consumption significantly in the months of January (34.5%), February (16.5%), March (12.7%) and October (12.0%).

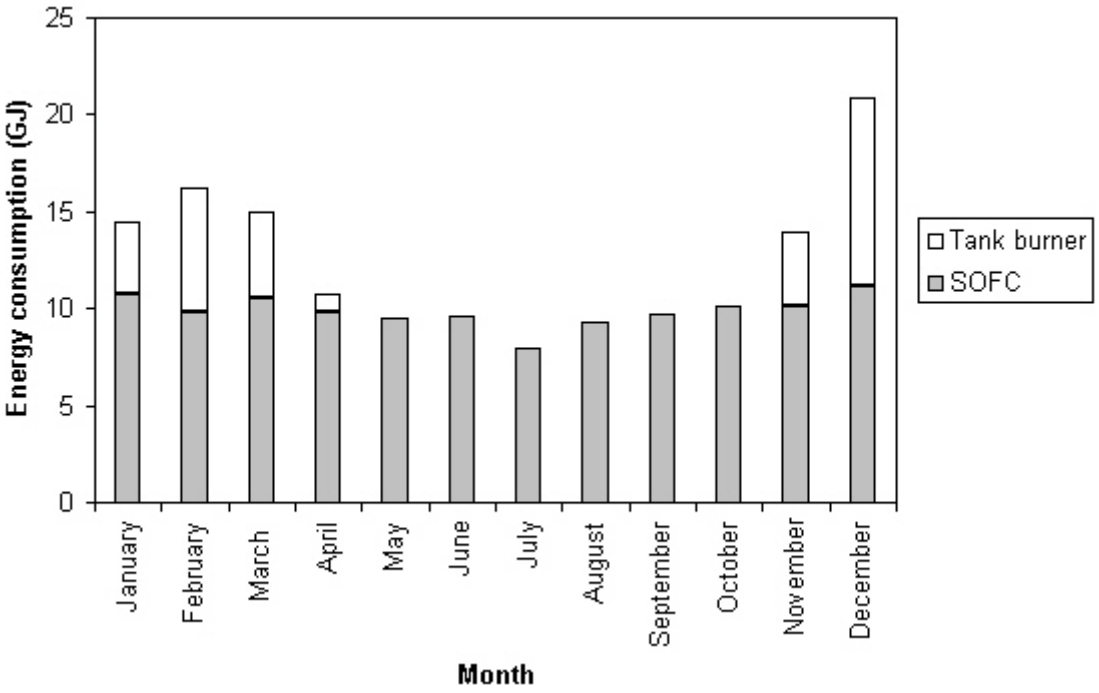

Figure 5.12 Monthly energy consumption for Case 3A

The house's annual natural gas consumption is 4110.9 m^3 (based on a LHV of 35.9 MJ/m^3), 10.5% less than the annual natural gas consumption for Case 2. The monthly natural gas consumption for Case 3A is presented in Figure 5.13. The natural gas consumption is notably reduced between January and March and in October.

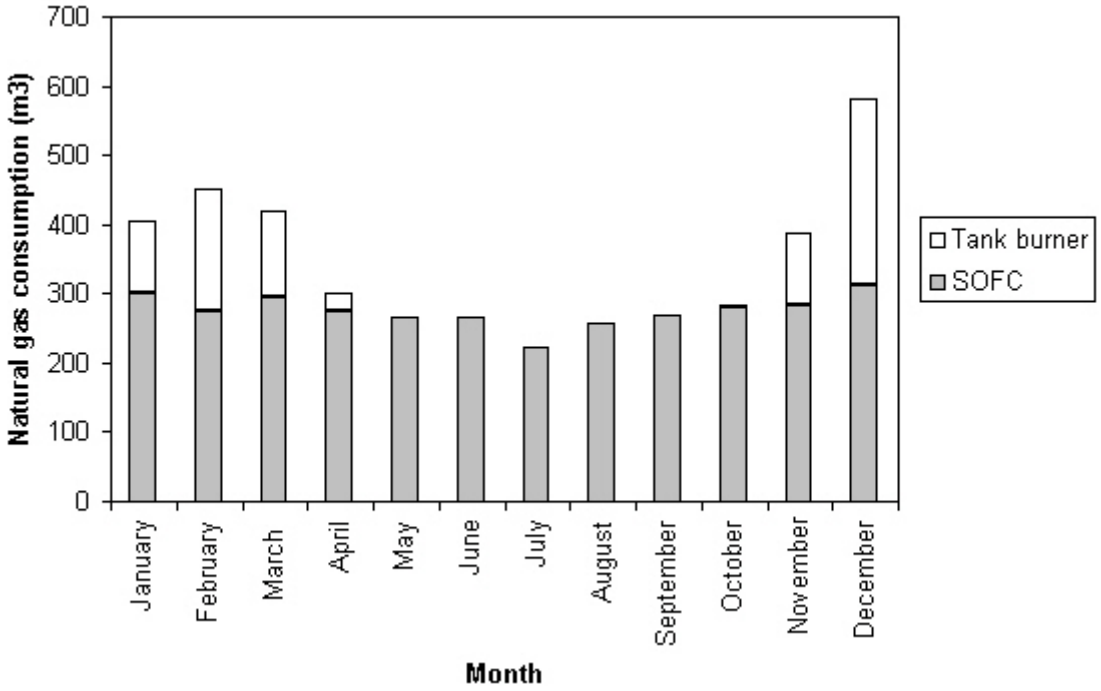

Figure 5.13 Monthly natural gas consumption for Case 3A

The adsorption storage unit delivers 6.0 GJ of energy during the heating season and stores 0.5 GJ of energy during the cooling season. Figure 5.14 presents the energy flows into and out of the adsorption storage unit for each month.

The adsorption storage unit discharges most of its stored energy in January; the amount of thermal energy discharged to the water tank decreases between January 1 and April 30. An examination of the simulation results shows that on April 30, the temperature of the adsorber is 59.2°C, suggesting that the adsorption storage unit is no longer a significant source of thermal energy for the water storage tank which is maintained at a temperature above 50°C.

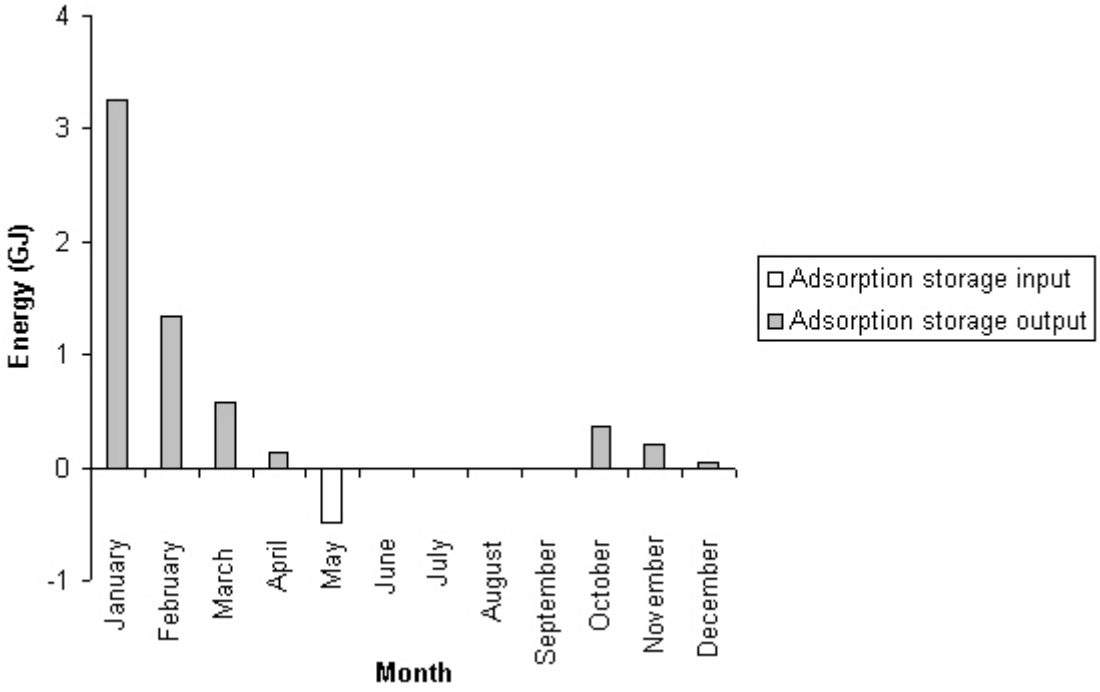

Figure 5.14 Monthly energy flows into and out of adsorption storage unit (Case 3A)

Although the adsorption storage unit is available for charging between May and September, only 0.5 GJ of energy is stored in the unit, all in May. An analysis of the simulation results shows that the adsorption storage unit has sufficient capacity to store more heat however the temperature of the water entering the adsorber from the SOFC's exhaust-to-water heat exchanger is not high enough to complete the charging of the unit. An examination of the simulation results shows that the adsorber reaches a temperature of 94.5°C on May 27 and maintains this temperature until September 30, the last day of the year that the adsorption storage unit is permitted to operate in charging mode. Although surplus thermal energy is available from the SOFC after May 27, the temperature of the water leaving the SOFC's heat exchanger does not exceed 94.5°C and no thermal energy is directed to the absorber. An analysis of the simulation results also

shows that only sensible heat is stored in the adsorption storage unit and no desorption takes place in the adsorber. It is recommended that in future work, the flow rates of the pumps circulating fluid through the SOFC's heat exchanger (pumps A and B in Figure 5.2) be modified to determine the values that would lead to optimal temperatures of the fluid leaving the heat exchanger for the charging of the adsorption storage unit.

In October, the adsorption storage unit is allowed to discharge but of course, can only discharge a limited amount of energy since a small amount of energy was stored in the unit during the previous summer. The adsorption storage unit discharges approximately 0.6 GJ of energy between October and December. The temperature of the adsorber on December 31 is 56.1°C.

Figure 5.15 presents the thermal energy added to the water tank by the SOFC, the thermal energy added to the water tank by the natural gas burner, the thermal energy added to the water tank by the adsorption storage unit and the thermal energy rejected from the tank by the safety device on a monthly basis.

The SOFC delivers 34.3 GJ of thermal energy to the water tank over the year. However, 12.4 GJ of energy is rejected from the water tank to maintain the temperature in the water tank below its maximum set-point temperature. Therefore, the SOFC's net thermal contribution is 21.9 GJ. The water tank's burner must provide 32.1 GJ of thermal energy during the year to maintain the water in the tank above its minimum set-point temperature. The adsorption storage unit provides 6.0 GJ of thermal output to the tank.

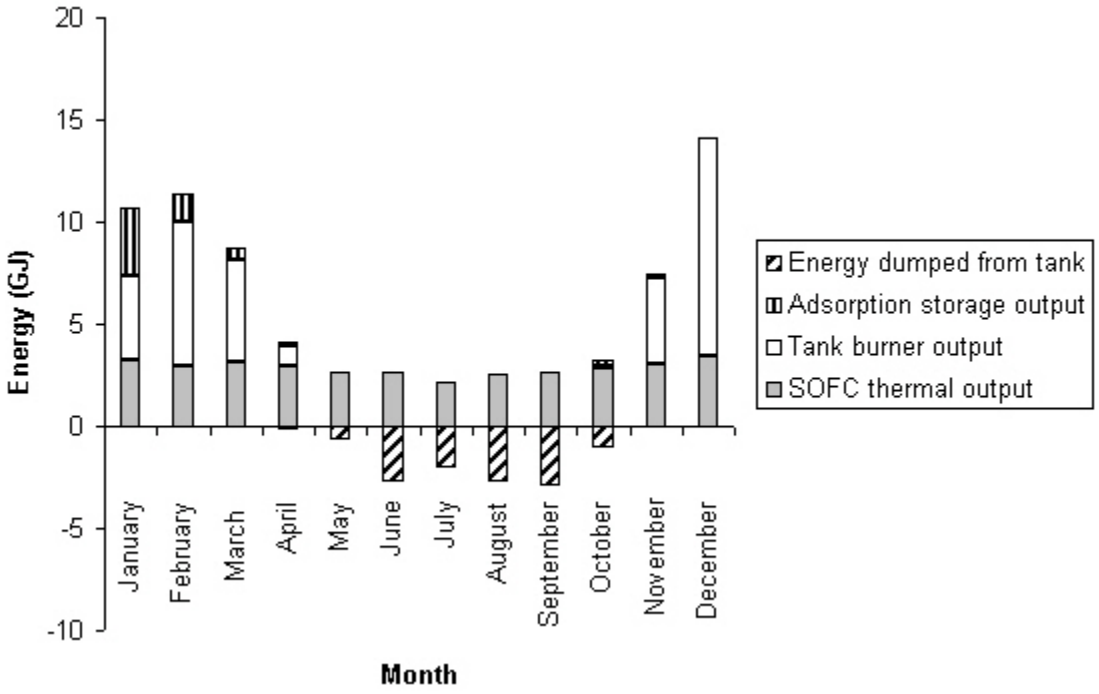

Figure 5.15 Monthly thermal energy balance on water tank for Case 3A

Therefore, for this specific case the SOFC provides 36.5% of the house's thermal requirement while the adsorption storage unit provides 10.0% of the house's thermal requirement.

The total cogeneration efficiency of the system for Case 3A calculated using equation (5.2), is 62.9%, only slightly higher than the cogeneration efficiency calculated for Case 2.

In Chapter 3, the efficiency η_1 of the adsorption storage unit is defined as the ratio of the useful energy retrieved from the unit and the energy required to operate the unit over a complete charging/discharging cycle:

$$\eta_1 = \frac{Q_{discharge}}{Q_{charge} + W_{aux-burner} + W_{pumps} + W_{cond-fan}} \tag{5.3}$$

where $Q_{discharge}$ is the amount of heat transferred from the unit's adsorber to the main water storage tank during the discharge phase [GJ], Q_{charge} is the amount of heat input to the adsorber during the charging phase [GJ], $W_{aux\text{-}burner}$ is the energy consumption of the auxiliary water tank's natural gas burner [GJ], W_{pumps} is the consumption of the circulating pumps B, C and D in Figure 5.2 and $W_{cond\text{-}fan}$ is the consumption of the adsorption unit's condenser fan.

A complete charging/discharging cycle for the annual simulation considered in this analysis would be between May 1 and December 31. The efficiency η_1 of the adsorption storage unit, calculated using equation (5.3), is 39.8%.

It should be kept in mind that the power draw of the circulating pumps and condenser fan were all assumed and may not represent the actual characteristics of the components. Also, it is assumed that the auxiliary water tank is maintained at a temperature above 40°C for the entire period during which discharging of the adsorption storage unit is permitted so that low-temperature heat required at the unit's evaporator is always available. A more efficient method of providing the low-temperature heat at the evaporator should be investigated in future work.

The efficiency η_2, initially defined in Chapter 3, considers the amount of energy that is saved in terms of the energy rejected by the water storage tank's safety device, because of the adsorption storage unit:

$$\eta_2 = \frac{Q_{heat-dump-no-storage} - Q_{heat-dump-with-storage}}{Q_{aux-burner} + W_{pumps} + W_{cond-fan}} \tag{5.4}$$

where $Q_{heat\text{-}dump\text{-}no\text{-}storage}$ is the amount of energy that is rejected from the main water storage tank by the safety device [GJ] for the case where the plant does not contain an adsorption storage unit (case 2) and $Q_{heat\text{-}dump\text{-}with\text{-}storage}$ is the amount of energy that is rejected from the main water storage tank [GJ] for the case where the plant does contain an adsorption storage unit (case 3).

The efficiency η_2 is 7.0%, suggesting that the amount of energy that is saved by the presence of the adsorption storage unit, in terms of the energy rejected by the safety device, is only a small amount of the additional amount of energy required to operate the unit. The efficiency η_2 is very low because of the small amount of energy that is stored in the adsorption storage unit during the summer for the particular set of operating conditions considered in this study.

The efficiency η_3, initially defined in Chapter 3, considers the energy savings in terms of the energy consumed by the water storage tank's natural gas burner, because of the adsorption storage unit:

$$\eta_3 = \frac{Q_{main-burner-no-storage} - Q_{main-burner-with-storage}}{Q_{aux-burner} + W_{pumps} + W_{cond-fan}} \quad (5.5)$$

where $Q_{main\text{-}burner\text{-}no\text{-}storage}$ is the heat output of the backup natural gas burner in the main water storage tank [GJ] for the case where the plant does not contain an adsorption storage unit (case 2) and $Q_{main\text{-}burner\text{-}with\text{-}storage}$ is the heat output of the backup natural gas burner [GJ] for the case where the plant does contain a storage unit (case 3).

The efficiency η_3 is 3.4, signifying that 3.4 times the additional amount of energy required to operate the unit is saved in terms of the energy output of the water storage tank's natural gas burner.

The temperature of the water tank during a typical day in winter (January 6) when the adsorption storage unit operates in discharge mode is depicted in Figure 5.16. The adsorption storage unit is switched into its discharge mode of operation when the temperature in the water storage tank drops below 65°C for more than 25 minutes. The discharging process ends when the temperature in the water storage tank reaches 75°C.

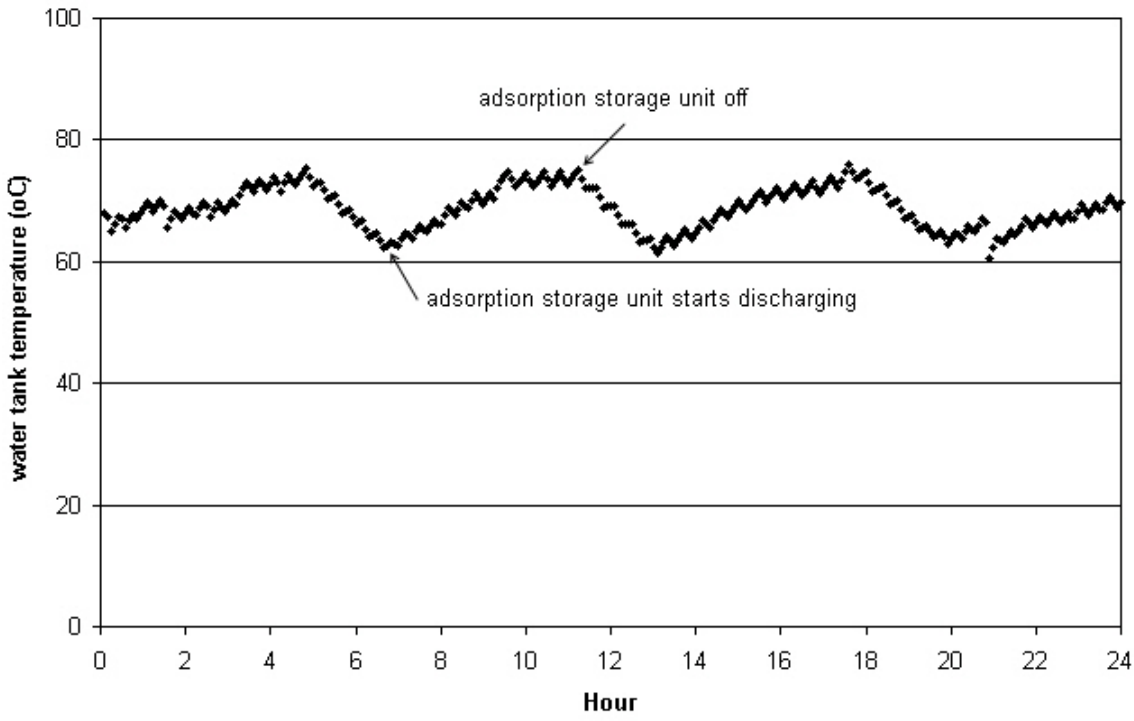

Figure 5.16 Temperature of water in storage tank on January 6 (Case 3A)

On a winter day when the space heating and DHW demands are high, the adsorption storage unit may not provide sufficient thermal output to the water tank and the tank's natural gas burner must provide additional heat. Such a case occurs on January 15 and is depicted in Figure 5.17. The natural gas burner cycles on frequently during the day, more so between 7h00 and 14h00 when space heating and DHW loads are greater.

Figure 5.18 presents the thermal state of the water storage tank on October 16 when the adsorption storage unit is discharged only for several hours in the morning. The remainder of the day the SOFC's thermal output is in balance with the house's space heating and DHW load.

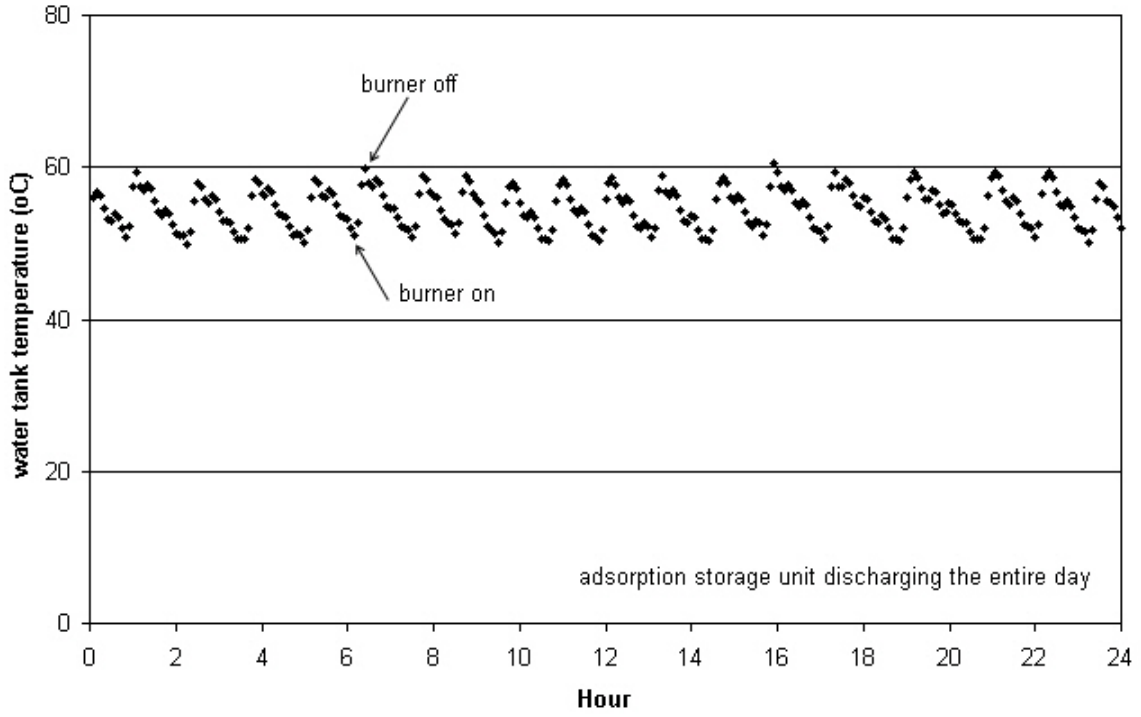

Figure 5.17 Temperature of water in storage tank on January 15 (Case 3A)

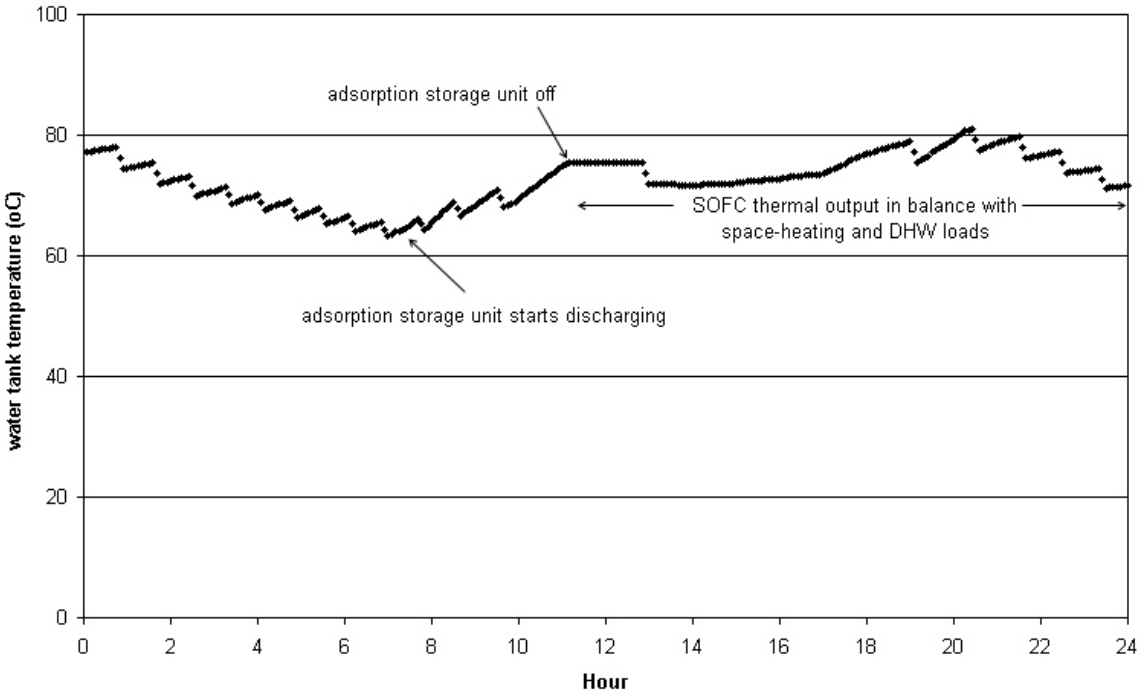

Figure 5.18 Temperature of water in storage tank on October 16 (Case 3A)

The temperature of the water storage tank during a typical day in the spring (May 1) when the adsorption storage unit is permitted to operate in charging mode is depicted in Figure 5.19. The adsorption storage unit is switched into its charging mode of operation when the temperature in the water storage tank is above 65°C for more than 25 minutes and the temperature on the water-side of the SOFC's exhaust-to-water heat exchanger is less than the adsorber's maximum temperature. The charging process ends when the temperature in the water storage tank drops below 55°C.

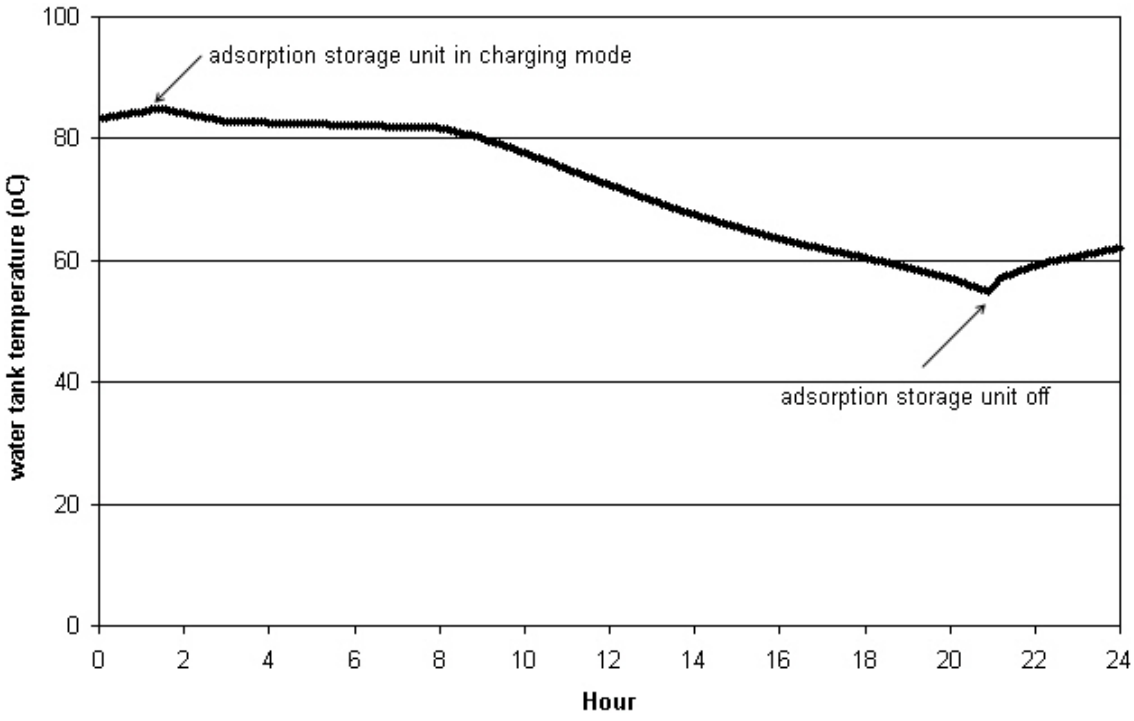

Figure 5.19 Temperature of water in storage tank on May 1 (Case 3A)

5.2.3.2 Case 3B: Mass of adsorbent = 22500 kg

The effect of increasing the capacity of the adsorption storage unit on the performance of the overall system is investigated in this section. In particular, the mass of adsorbent within the unit's adsorber is increased threefold, to 22500 kg (representing an adsorber volume of 25.2 m^3).

For Case 3B, ESP-r predicts the house's annual energy consumption to be 135.9 GJ, 7.8% less than the annual energy consumption predicted for Case 3A. The monthly energy consumption for Case 3B is presented in Figure 5.20.

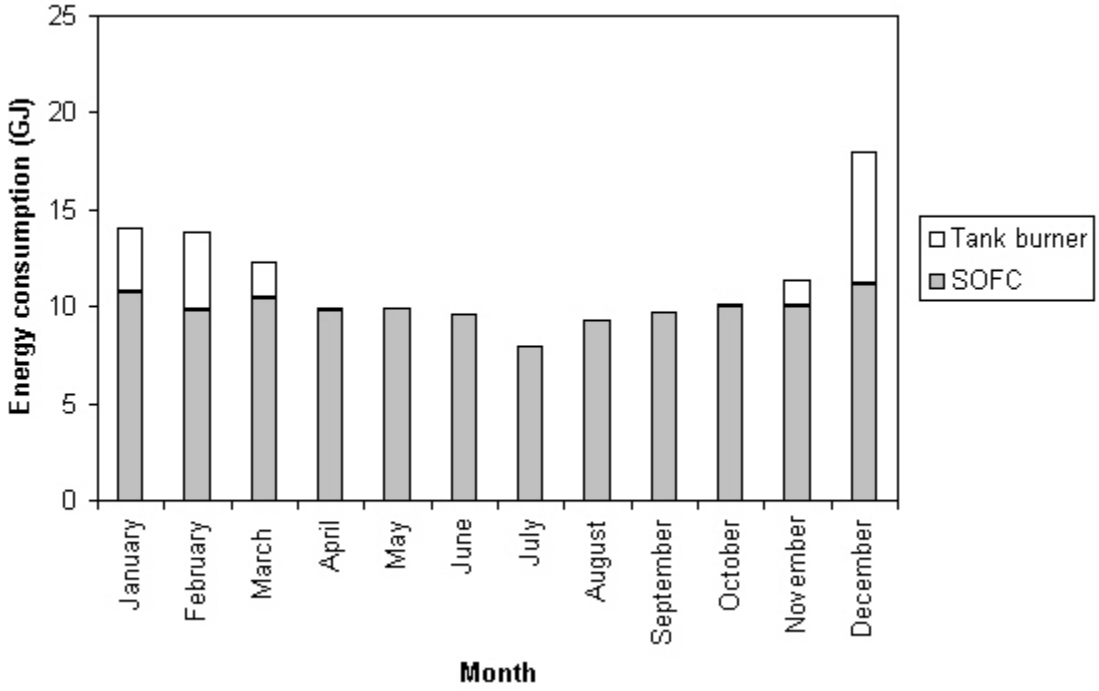

Figure 5.20 Monthly energy consumption for Case 3B

The house's annual natural gas consumption also decreases by 7.8% for Case 3B, to 3789.1 m^3 (based on a LHV of 35.9 MJ/m^3). The monthly natural gas consumption for Case 3B is presented in Figure 5.21.

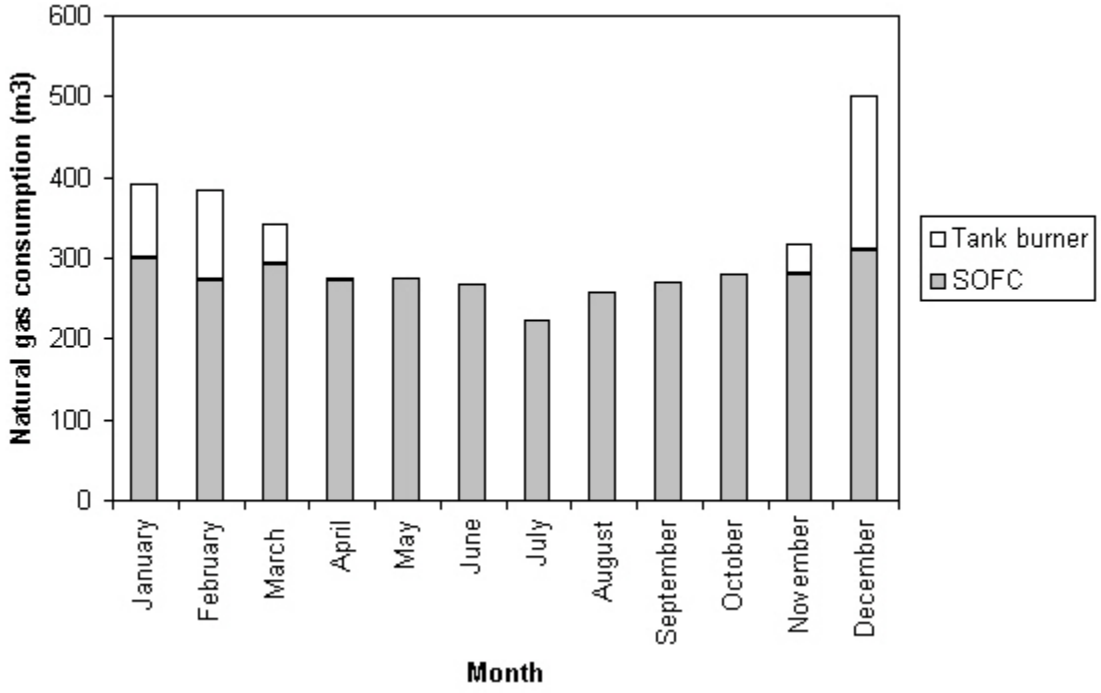

Figure 5.21 Monthly natural gas consumption for Case 3B

Figure 5.22 presents the energy flows into and out of the adsorption storage unit for each month. The adsorption storage unit delivers 11.3 GJ of energy to the water storage tank during the heating season, an increase of 88.3% from Case 3A. However, for Case 3B, the adsorption storage does not store any surplus thermal output from the SOFC during the cooling season.

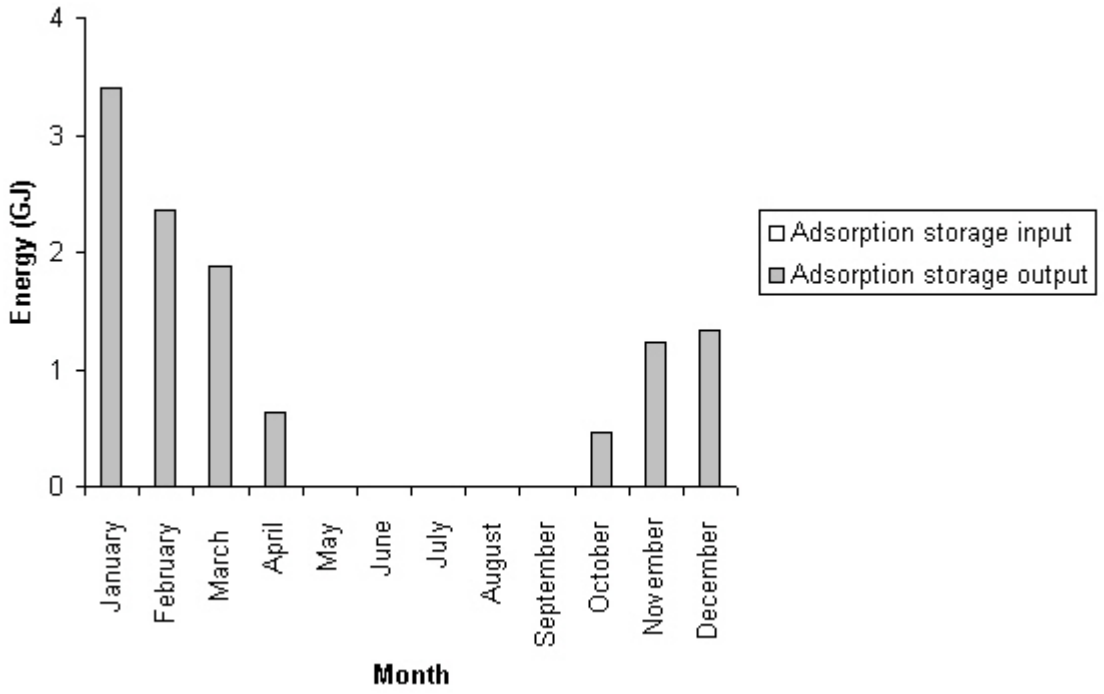

Figure 5.22 Monthly energy flows into and out of the adsorption storage unit (Case 3B)

The adsorption storage unit is available for discharge between January and April and delivers 8.3 GJ of thermal energy to the water storage tank during this time. An examination of the simulation results shows that on April 30, the temperature of the adsorber has dropped to 101.4°C, suggesting that the adsorption storage unit is not depleted of its stored thermal energy.

Charging of the adsorption storage unit is permitted between May and September. However, although surplus thermal energy is available from the SOFC during this time, the temperature of the fluid leaving the SOFC's heat exchanger is below the adsorber temperature (101.4°C) and therefore no thermal energy is stored in the unit.

In October to December, the adsorption storage unit discharges 3.0 GJ of thermal energy to the water storage tank. On December 31, the temperature of the adsorber is 85.1°C.

Figure 5.23 presents the thermal energy added to the water tank by the SOFC, the thermal energy added to the water tank by the natural gas burner, the thermal energy added to the water tank by the adsorption storage unit and the thermal energy rejected from the tank by the safety device on a monthly basis.

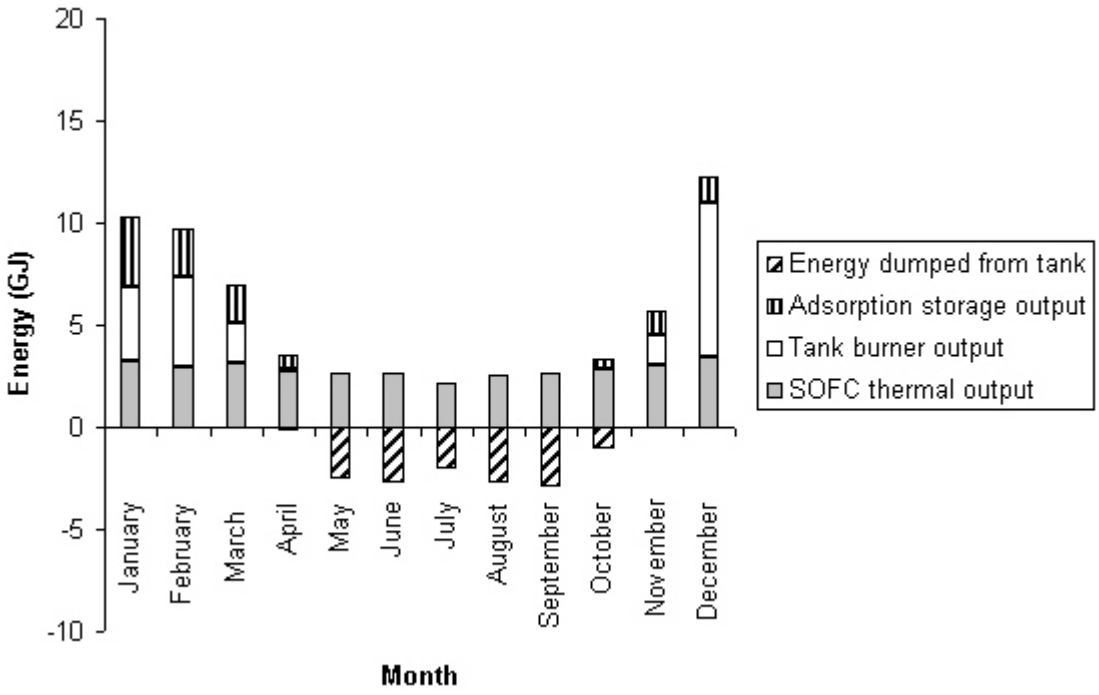

Figure 5.23 Monthly thermal energy balance on water tank for Case 3B

The SOFC delivers 34.0 GJ of thermal energy to the water tank over the year. However, 14.3 GJ of energy is rejected from the water tank to maintain the temperature in the water tank below its maximum set-point temperature. Therefore, the SOFC's net thermal

contribution is 19.7 GJ. The water tank's burner must provide 19.2 GJ of thermal energy during the year to maintain the water in the tank above its minimum set-point temperature. The adsorption storage unit provides 11.3 GJ of thermal output to the tank. Therefore, for this specific case the SOFC provides 39.2% of the house's thermal requirement while the adsorption storage unit provides 22.5% of the house's thermal requirement.

The total cogeneration efficiency of the system for Case 3B, calculated using equation (5.2), is 61.0%, slightly less than the value calculated for Case 3A. This is because of the increased amount of energy rejected from the water storage tank's safety device for Case 3B versus Case 3A. An analysis of the simulation results shows that more thermal energy is rejected from the water storage tank for Case 3B in May for two reasons: (1) no heat can be stored in the adsorption storage unit and (2) the temperature of the water storage tank on May 1 is higher.

The efficiency η_1 of the adsorption storage unit, calculated using equation (5.3), is irrelevant for Case 3B since the unit does not undergo a complete charging/discharging cycle. Similarly, the efficiency η_2 of the adsorption storage unit, calculated using (5.4), is not a good performance indicator of the unit since no energy is saved, in terms of the energy rejected by the safety device, for this case.

The efficiency η_3, defined by equation (5.5), is 5.0, signifying that five times the additional amount of energy required to operate the adsorption storage unit is saved, in terms of the energy consumed by the water storage tank's natural gas burner.

Although the amount of thermal energy available from the adsorption storage unit during the winter increased for Case 3B, as one would expect, the unit is idle during the summer since the temperature of the adsorber's heat source (water leaving the SOFC's heat exchanger) is not at a high enough temperature. This emphasizes the importance of taking into account not only the quantity of heat available for charging the adsorption storage unit but also the temperature of the heat source.

5.2.4 Comparison and discussion of simulation results

The annual simulation results for all of the cases considered are summarized in Table 5.6.

The residential SOFC cogeneration system, with or without an adsorption storage unit, surpasses the energy performance of the conventional natural gas-fired heating system if the primary energy consumption of the latter is considered and electric power is generated from oil. If power is generated from a hydro-electric source, the SOFC cogeneration system surpasses the energy performance of the conventional natural gas-fired heating system only if it includes an adsorption storage unit with a volume of 25.2 m^3 (representing an adsorber containing 22500 kg of zeolite-13X adsorbent).

Table 5.6 Annual simulation results

	Case 1			Case 2	Case 3	
	Secondary	Primary			A	B
		Hydro	Oil			
Energy consumption (GJ/yr)	127.2	138.5	275.9	164.6	147.4	135.9
Difference with Case 1[1]	-			+18.8%	+6.4%	-1.9%
Difference with Case 2	-			-	-10.4%	-17.4%
Difference with Case 3A	-			-	-	-7.8%
Natural gas consumption (m^3/yr)	1769.6[2]			4591.3[3]	4110.9 [3]	3789.1[3]
Difference with Case 1[1]	-			+159.5%	+132.3%	+114.1%
Difference with Case 2	-			-	-10.5%	-17.5%
Difference with Case 3A	-			-	-	-7.8%
Tank burner output (GJ/yr)	n/a			50.6	32.1	19.2
Difference with Case 2	-			-	-36.6%	-62.1%
Difference with Case 3A	-			-	-	-40.2%
Energy dumped from tank (GJ/yr)	n/a			12.9	12.4	14.3
Difference with Case 2	-			-	-3.9%	+10.9%
Difference with Case 3A	-			-	-	+15.3%
Average system efficiency η_{sys-1} (%)	90.7	83.4	41.8	n/a	n/a	
Cogeneration efficiency η_{cogen} (%)	n/a			62.6	62.9	61.0

[1]Primary energy consumption for Case 1 assuming hydro-generated power.
[2]Natural gas only fuels space-heating equipment (furnace).
[3]Natural gas used to meet all energy requirements.

The adsorption storage unit improves the performance of a SOFC cogeneration system by reducing the natural gas consumption of the main water storage tank's backup burner. However, little or no energy is saved in terms of the energy rejected from the water storage tank by its safety device during the summer. As indicated in the preceding sections, the reason for this is that the temperature of the water leaving the SOFC's heat exchanger is not high enough to permit sufficient, or any, charging of the adsorption

storage unit during the summer. This result is specific to the operating conditions considered in this study and it is recommended that different operating conditions be investigated in future work to obtain the optimal performance of the adsorption storage unit during the summer. In particular, the pump flow rates for loops A and B (Figure 5.2) should be optimized since they affect the temperature of the water leaving the SOFC's heat exchanger. Also, it may be feasible to control the SOFC to operate at a constant electrical output during the summer – this will increase both the electrical and thermal output of the SOFC, which will lead to higher exhaust gas temperatures.

Increasing the capacity of the adsorption storage unit threefold resulted in a better performance of the system during the winter since thermal energy provided by the adsorption storage unit reduced the amount of energy required by the water storage tank's natural gas burner. However, increasing the capacity of the adsorption storage unit leads to an increase in the energy rejected from the water storage tank in the summer. The unit was idle during the summer since the temperature of the adsorber's heat source (the water leaving the SOFC's heat exchanger) was less than the temperature of the adsorber at the beginning of the charging season for the operating conditions considered in this study. Also, an examination of the simulation results that the temperature of the water storage tank at the beginning of the charging period (May 1) for case 3B is greater than for case 3A, leading to the increase in the amount of energy rejected in May for the former case. The poor performance of the adsorption storage unit in the summer leads to a reduction in terms of the overall cogeneration efficiency of the system.

6 CONCLUSION

The stated objective of this research is to investigate the feasibility of an adsorption storage system for the seasonal storage of heat in residential buildings. This study looks at the case whereby the surplus thermal output from a solid oxide fuel cell (SOFC) cogeneration system is stored in an adsorption storage unit in the summer and is recovered in the winter.

In order to meet the stated objective, a mathematical model of an adsorption storage system was developed. The system's components (adsorber, condenser and evaporator) were each represented by a separate control volume and governing equations (conservation of mass and energy) were applied to each control volume.

The mathematical model of the adsorption storage system was implemented in the ESP-r simulation program, in which the system is represented as an explicit plant component. The adsorption storage unit can be connected to other plant component models that are available within ESP-r to form a complete heating, ventilation and air-conditioning (HVAC) plant network. A new controller algorithm was also implemented in ESP-r to operate the adsorption storage unit (in charging or discharge mode) depending on the sensed plant conditions.

The mathematical model of the adsorption storage unit and its implementation in ESP-r were validated by comparing simulation results obtained for two sets of operating

conditions to published data. A sensitivity analysis was also performed to verify the model and its implementation in ESP-r.

The energy performance of a residential SOFC cogeneration system coupled to an adsorption storage unit for the seasonal storage of heat was determined for a certain set of operating conditions, within the ESP-r simulation environment, taking into account the dynamic electrical and thermal loads of the house. The energy performance of the aforementioned case was compared to the energy performance of two alternate systems: (1) the case where a conventional natural gas-fired furnace meets the house's space-heating load and the utility grid meets the house's electrical requirements and (2) the case where a residential SOFC cogeneration system meets both the electrical and thermal requirements of the house but there is no provision for the seasonal storage of heat.

For the set of operating conditions considered in this study, the adsorption storage unit was able to improve the energy performance of the overall SOFC cogeneration system in the winter by reducing the energy consumption of the backup heating system. However, the adsorption storage unit did not improve the energy performance of the SOFC cogeneration system in the summer since the temperature of the unit's heat source, the water leaving the SOFC's exhaust gas-to-water heat exchanger, was not at a high enough temperature to fully charge the unit.

If it is assumed that the power supplied by the utility grid is generated from oil, the energy performance of the overall SOFC cogeneration system, with or without an

adsorption storage system, surpasses the energy performance of the conventional system (considering the latter's primary energy consumption), whereby a natural gas-fired furnace supplies the house's space-heating load and the utility grid supplies the electric requirements of the house. However, if it is assumed that the power supplied by the utility grid is generated from a hydro-electric source, the energy performance of the overall SOFC cogeneration system only surpasses the energy performance of the conventional case if it is coupled to an adsorption storage unit with an adsorber volume of 25.2 m^3, which may be unreasonable for a residential application in which the volume of the storage space is limited.

Two different sizes are considered for the adsorption storage unit in this study. In the first instance, an adsorber volume of 8.4 m^3 is considered, which may be feasible for a residential application. In the second instance, the adsorber volume is increased threefold to 25.2 m^3 in order to determine the impact of the unit's capacity on the energy performance of the overall system. The energy performance of the overall system did improve in the winter with the larger-sized adsorption storage unit since more thermal energy was available from the storage unit. However, the performance of the overall system did not improve in the summer since the temperature of the adsorption storage unit's heat source was not high enough to charge the unit. This finding underlies the importance of considering both the quantity of energy that is available to charge a seasonal heat storage system and the quality, or temperature, of the energy.

6.1 Recommendations for future work

The recommendations for future work that were made in Chapters 1 to 5 are summarized in this section.

In this study, zeolite-water was selected as the adsorbent-adsorbate pair, respectively, for the adsorption storage unit. However, other adsorbent-adsorbate pairs identified as having potential for seasonal storage applications should be investigated in future work. Namely, (Nùñez et al., 1999) suggest selective water sorbents (modified silica gels) and commercial silica gels as suitable adsorbents to be paired with water for heat storage applications.

The feasibility of using an adsorption storage unit to store solar heat or surplus heat from other types of cogeneration systems on a seasonal basis should be investigated in future work. In this study, the adsorption storage unit was configured to store the surplus thermal output available from a SOFC cogeneration system.

In this study, it is supposed that the heat of condensation available from the adsorption storage unit during the charging cycle is rejected to the outdoors. The possibility of recovering the low-temperature heat available from the condenser for heating of domestic hot water or other uses should be investigated in future work.

A more efficient method of supplying the heat that is required by the adsorption storage system's evaporator during the discharge cycle should be investigated in future work. In

the HVAC configuration investigated in this study, the low-temperature heat required to evaporate the liquid adsorbate is supplied by an auxiliary water tank that is maintained at 50°C. Ideally, the low-temperature heat can be supplied by the SOFC, by the house's exhaust air or from a renewable energy source, such as the sun.

In this work, it is assumed that pressurized water is used as the heat exchanger fluid to transfer heat between the SOFC and the water storage tank, the SOFC and the adsorption storage unit (during the charging cycle) and the adsorption storage unit and the water storage tank (during the discharge cycle) in order to permit temperatures greater than 100°C to be considered. Pressurized water may not be the most efficient heat exchanger fluid and other fluids should be considered in future work.

For the simulations carried out in Chapter 5, the heat losses from the adsorption storage system's components to the ambient are ignored. It is recommended that in future feasibility studies, the heat losses be taken into account, preferably using actual experimental data to characterize the overall heat transfer coefficients for each of the components (this type of data are not available in the published literature). Also, it is not known how, in the actual operation of an adsorption storage system, the adsorber pressure is kept constant when heat losses occur from the adsorber to the ambient. This should be determined and accounted for in the model in future work.

An adsorption storage unit operates much like an adsorption heat pump except that in the former case the operation of the unit is not continuous - the charging (or regeneration)

phase is separated from the discharge phase (or adsorption phase) by the storage period. The model parameters can be modified in future work in order to permit the plant component model implemented in ESP-r to represent an adsorption heat pump.

A new modelling feature has recently been added to the ESP-r simulation program to permit continuous multi-year simulations and simulations that cross over January 1 (Ferguson, 2005). It is suggested that the model of the adsorption storage system implemented in ESP-r be improved by taking into account the degradation of the system's performance due to repeated charging and discharging cycles and that multi-year simulations be carried out to investigate the importance of the system degradation over time. The new multi-year simulation feature can also be used to investigate the performance of the adsorption storage system over a complete charging/discharging cycle since simulations can start at the beginning of the cooling season and end at the end of the heating season (for example, simulations can be performed for the period May 1 – April 30).

As discussed in Chapter 5, the simulation time for the house models containing an adsorption storage unit were very long – an annual simulation was completed in 30 hours on a computer with 1.5 GB of RAM and a CPU speed of 3 GHz. A review of the FORTRAN 77 code that was added or modified for the implementation of the adsorption storage model within ESP-r did not identify any obvious errors that were inadvertently introduced. The cause of the long simulation time should be investigated further and modifications made within the ESP-r source code to reduce it.

For the set of operating conditions that were considered in this study, it was found that the adsorption storage unit's heat source, that is the pressurized water leaving the SOFC's exhaust-to-water heat exchanger, was not at a high enough temperature to significantly charge the unit in the summer. Several operating conditions should be modified in future work to increase the temperature of the pressurized water leaving the SOFC's exhaust-to-water heat exchanger and thereby potentially improve the performance of the unit in the summer. Firstly, the thermal output of the SOFC can be increased. This can be done by increasing the electrical output of the SOFC during the summer (the SOFC's thermal output is proportional to its electrical output) – either by having it respond to a greater electrical load (in the present study the SOFC cogeneration system is controlled to follow the house's electrical load) or by controlling the SOFC to operate at its maximum electrical output. Secondly, the flow rates of the pumps circulating pressurized water through the SOFC's exhaust-to-water heat exchanger should be decreased, thereby increasing the temperature difference between the heat exchanger's inlet and outlet and leading to an increase in the temperature of the water leaving the heat exchanger. In the present study, the pump flow rates were selected based on a previous study of a residential fuel cell cogeneration system (Beausoleil-Morrison et al., 2002a).

The characteristic data that were used to describe the adsorption storage system in this study were obtained from published data for adsorption heat pumps. Actual experimental data obtained for an adsorption system used in a storage application would be helpful to both validate the model developed for this work and properly characterise the system for future feasibility studies.

Finally, the operating parameters for each of the system components (SOFC, adsorption storage system, water storage tanks, pumps, etc.) that will lead to the optimal performance of the overall system should be determined in future work. In this study, only one set of operating conditions is considered and the conclusions made as to the feasibility of an adsorption storage system to store the surplus thermal output from a residential SOFC cogeneration system seasonally are specific to the operating conditions considered.

REFERENCES

Aasem, E.O., Clarke, J.A., Hensen, J.L.M., Kelly, N.J., MacQueen, J. and Negrao, C.O.R. (1994), 'Current Building Systems Modelling Potential of ESP-r', *Proceedings of the 4th International Conference on System Simulation in Buildings*, Liège, Belgium.

ASHRAE (2001), *Fundamentals*, SI Edition, American Society of Heating, Refrigerating and Air-Conditioning Engineers Inc, Atlanta USA.

Bach, P. and Haije, W. (1999), 'Storage and transformation of waste heat', *IEA Annex 10, Phase Change Materials and Chemical Reactions for Thermal Energy Storage, Fourth Workshop*, Benediktbeuren, Germany.

Ballard Power Systems Inc. (2004), Website http://www.ballard.com/.

Beausoleil-Morrison, I. (2001), 'The Incorporation of a Fuel Cell Explicit Plant Component Model into ESP-r/HOT3000', *CANMET Energy Technology Centre (CETC) Internal Report*, Natural Resources Canada.

Beausoleil-Morrison, I., Cuthbert, D., Deuchars, G. and McAlary, G. (2002a), 'The Simulation of Fuel Cell Cogeneration Systems Within Residential Buildings', *Proceedings of eSim 2002*, Montréal, Canada, 40-47.

Beausoleil-Morrison, I. (2002b), 'Design of Storage Tank Component Models for FCT project', *CETC Internal Report*, Natural Resources Canada.

Bourdouxhe, J-P., Grodent, M. and Lebrun, J. (1998), *Reference Guide for Dynamic Models of HVAC Equipment*, American Society of Heating, Refrigerating and Air-Conditioning Engineers, Research Project 738-RP.

Brunberg, E.A. (1980), 'The TEPIDUS System for Seasonal Heat Storage and for Cooling', *Proceedings of the International Seminar on Thermochemical Heat Storage*, Edited by Wettermark, G., Stockholm, Sweden.

Cacciola, G., Hajji, A., Maggio, G., Restuccia, G. (1993), 'Dynamic simulation of a recuperative adsorption heat pump', *Energy*, 18, 11, 1125-1137.

Cacciola, G. and Restuccia, G. (1995), 'Reversible adsorption heat pump: a thermodynamic model', *International Journal of Refrigeration*, 18, 2, 100-106.

Casarin, C. and Ibanez, J.G. (1993), 'Experimental Demonstration of the Principles of Thermal Energy Storage and Chemical Heat Pumps', *Journal of Chemical Education*, 70, 2, 158-162.

Chahbani, M.H., Labidi, J. and Paris, J. (2002), 'Effect of mass transfer kinetics on the performance of adsorptive heat pump systems', *Applied Thermal Engineering*, 22, 23-40.

Chahbani, M.H., Labidi, L. and Paris, J. (2004), 'Modeling of adsorption heat pumps with regeneration', *Applied Thermal Engineering*, 24, 431-447.

Clarke, J.A. (2001), *Energy Simulation in Building Design*, (2nd Edn), Butterworth Heinemann.

De Maria, G., D'Alessio, L., Coffari, E., Paolucci, M. and Tiberio, C.A. (1985), 'Thermochemical Storage of Solar Energy With High Temperature Chemical Reactions', *Solar Energy*, 35, 5, 409-41.

Dinçer, I. and Rosen, M.A., ed, (2002), *Thermal energy storage systems and applications*, John Wiley & Sons, New York, U.S.A.

Dubinin, M.M. (1967), 'Adsorption in Micropores', *Journal of Colloid and Interface Science*, 23, 487-499.

Energy Systems Research Unit (ESRU) (2002), *The ESP-r System for Building Energy Simulations: User Guide Version 10)*, ESRU Manual U02/1, University of Strathclyde, Glasgow, U.K.

Environment Canada (2005), Government of Canada, State of the Environment Infobase, http://www.ec.gc.ca/soer-ree/English/Indicator_series/new_issues.cfm?issue_id=4&tech_id=15#bio_pic

Ervin, G. (1977), 'Solar Heat Storage Using Chemical Reactions', *Journal of Solid State Chemistry*, 22,51-61.

Ferguson, A. (2005). Personal communication.

Fischer, S., Hauer, A. (1998), 'Space Heating and Cooling with a Thermochemical Storage System in the District Heat Net of Munich', *Proceedings of IEA Annex 10 Phase Change Materials and Chemical Reactions for Thermal Energy Storage, Second Workshop,* Sofia, Bulgaria.

Fuel Cell Technologies (FCT) Ltd. (2004), Website http://www.fct.ca.

Gregg, S.J. and Sing, K.S.W. (1982), *Adsorption, Surface Area and Porosity*, Second Edition, Academic Press Inc. (London) Ltd.

Gui, Y.B., Wang, R.Z., Wang, W., Wu, J.Y., Xu, Y.X. (2002), 'Performance modeling and testing on a heat-regenerative adsorptive reversible heat pump', *Applied Thermal Engineering*, 22, 309-320.

Ham, Ph. J. (1984), 'Mollier-h/x-diagrammen voor vochtige lucht, geoconstrueerd door middle van de computer', *Klimaatbeheersing*, 13, 8, 269-274; as cited in ESP-r source code.

Hauer, A. (2002), 'Thermal Energy Storage with Zeolite for Heating and Cooling Applications', *Proceedings of IEA ECES IA Annex 17: Advanced Thermal Energy Storage Through Phase Change Materials and Chemical Reactions- Feasibility Studies and Demonstration Projects, 3rd Workshop*, Tokyo, Japan.

Hensen, J.L.M. (1991), *On the Thermal Interaction of Building Structure and Heating and Ventilation System*, PhD Thesis, Eindhoven University of Technology, The Netherlands.

International Association for the Properties of Water and Steam (IAPWS) (1992), *Revised Supplementary Release on Saturation Properties of Ordinary Water Substance*, St.Petersburg, Russia.

International Association for the Properties of Water and Steam (IAPWS) (1996), *Release on the IAPWS Formulation 1995 for the Thermodynamic Properties of Ordinary Water Substance for General and Scientific Use*, Fredericia, Denmark.

Kato, Y., Minakami, A., Guangzhe, L., Yoshizawa, Y. (2001), 'Operability of a Thermally Driven Magnesium Oxide/Water Chemical Heat Pump', *The Canadian Journal of Chemical Engineering*, 79, 4, 536-541.

Lachance, D. (2003), *Étude expérimentale et modélisation d'une pompe à chaleur à adsorption*, Mémoire du diplôme de maîtrise ès sciences appliquées, École Polytechnique de Montréal.

Lachance, D., Bernier, M., Castaing-Lasvignottes, J. and Meunier, F. (2002), 'Simulation dynamique d'une machine à adsorption: application à un cycle cascade bi-étage', *Proceedings of eSim 2002*, Montréal, Canada, 71-77.

Lang, R., Roth, M., Stricker, M. and Westerfeld, T. (1999), 'Development of a modular zeolite-water heat pump', *Heat and Mass Transfer*, 35, 229-234.

Leong, K.C. and Liu, Y. (2004a), 'Numerical modeling of combined heat and mass transfer in the adsorbent bed of a zeolite/water cooling system', *Applied Thermal Engineering*, 24, 2359-2374.

Leong, K.C. and Liu, Y. (2004b), 'Numerical study of a combined heat and mass recovery adsorption cooling cycle', *International Journal of Heat and Mass Transfer*, 47, 4761-4770.

Lund, P. (1996), 'Solar Thermal Storage Systems', *Proceedings of EuroSun '96, International Solar Forum,* Volume 1.

Métivaud, V., Ventolà, L., Andreu, J., Mondieig, D., Calvet, T. and Cuevas-Diarte, M.A. (2005), 'Latent heat thermal energy storage systems for space heating of buildings', *Proceedings of the 8th Workshop of the IEA, ECES IA Annex 17, Advanced thermal energy storage through phase change materials and chemical reactions- feasibility studies and demonstration projects*, Kizkalesi, Turkey.

Mittelbach, W. and Henning, H.M. (1997), 'Seasonal Storage for Solar Space Heating based on Adsorption Processes', *Proceedings of North Sun '97, International conference on Solar Energy at High Latitudes and Solar Exhibition*, 286-293.

Mittelbach, W., Nùñez, T., Luginsland, F. and Henning, Henning, H.M. (2000), 'Solid sorption thermal energy storage for solar heating systems', *Proceedings of Terrastock 2000, 8th International Conference on Thermal Energy Storage*, 1, 415-420.

National Institute of Standards and Technology (NIST) Chemistry Webbook (2003), NIST Standard Reference Database Number 69, available on-line at http://webbook.nist.gov/chemistry/.

Natural Resources Canada (NRCan) (2001), Government of Canada, Energy Use Data Handbook 2001, http://oee1.nrcan.gc.ca/corporate/statistics/neud/dpa/data_e/handbook05/chapter2.cfm?attr=0

Natural Resources Canada (NRCan) (2005), Government of Canada, *R-2000 Standard – 2005 Edition*, http://www.oee.nrcan.gc.ca/residential/personal/new-homes/r-2000/standard/current/purpose.cfm?attr=4

Nùñez, T., Mittelbach, W., and Henning, H.M. (1999), 'Performance Evaluation and Characterisation of Solid Sorbents for Thermal Energy Storage', *Proceedings of IEA Annex 10: Phase Change Materials and Chemical Reactions for Thermal Energy Storage, 4th Workshop,* Benediktbeuren, Germany.

Ogura, H., Yamamoto, T. and Kage, H. (2003), 'Efficiencies of $CaO/H_2O/Ca(OH)_2$ Chemical Heat Pump for Heat Storing and Heating/Cooling', *Energy*, 28, 1479-1493.

Poyelle, F., Guilleminot, J.J., Meunier, F., Canal, P., Soidé, I. and Klemsdal, E. (1997), 'Experimental Tests of a Gas Fired Adsorption Air Conditioning System', *Proceedings of the IGU-20th World Gas Conference*, Copenhagen, Denmark, 441-451.

Press, W.H., Flannery, B.P., Teukolsky, S.A. and Vetterling, W.T. (1986), *Numerical Recipes: The Art of Scientific Computing*, Cambridge University Press.

Restuccia, G. and Cacciola, G. (1999), 'Performances of adsorption systems for ambient heating and air conditioning', *International Journal of Refrigeration*, 22, 18–26.

Restuccia, G., Recupero, V., Cacciola, G. and Rothmeyer, M. (1988), 'Zeolite Heat Pump for Domestic Heating', *Energy*, 4, 333-342.

Ruthven, D.M. (1984), *Principles of Adsorption and Adsorption Processes*, John Wiley and Sons Inc.

Saha, B.B., Akisawa, A. and Kashiwagi, T. (2001), 'Solar/waste heat driven two-stage adsorption chiller: the prototype', *Renewable Energy*, 23, 93-101.

Sami, S.M. and Tribes, C. (1996), 'An improved model for predicting the dynamic behaviour of adsorption systems', *Applied Thermal Engineering*, 16, 2, 149-161.

Seewald, F., Pollei, A., Kraume, M., Mittelbach, W. and Lang, J. (1999), 'Numerical Calculation of the Heat Transfer in an Adsorption Energy Storage with KARDOS', *ZIB Technical Report SC 99-04*.

Solar Energy Laboratory (SEL) (1994), *TRNSYS, A Transient System Simulation Program: Reference Manual*, Volume 1, University of Wisconsin-Madison, Madison, USA.

Srivastava, N.C. and Eames, I.W. (1998), 'A review of adsorbents and adsorbates in solid-vapour adsorption heat pump systems', *Applied Thermal Engineering*, 18, 707-714.

Stritih, U. (2003), 'Heat transfer enhancement in latent thermal storage system for buildings', *Energy and Buildings*, 35, 1097-1104.

Tather, M., Tantekin-Ersolmaz, B. and Erdem-Şenatalar, A. (1999), 'A novel approach to enhance heat and mass transfer in adsorption heat pumps using the zeolite-water pair', *Microporous and Mesoporous Materials*, 27, 1-10.

Thorstensen, B. (2001), 'A parametric study of fuel cell system efficiency under full and part load operation', *Journal of Power Sources*, 92, 9-16.

Ülkü, A.S. and Mobedï, M. (1989), 'Adsorption in Energy Storage', *Energy Storage Systems, NATO ASI Series E: Applied Sciences*, 167, 487-507.

U.S. Department of Energy (DOE) (1982), *DOE-2 Engineers Manual*, Version 2.1A, Part 1 of 2, United States Department of Energy, USA.

U.S. Department of Energy (DOE) (2000), *Fuel Cell Handbook*, Fifth Edition, National Energy Technology Laboratory, Morgantown, USA.

U.S. Department of Energy (DOE) (2001), *EnergyPlus Engineering Document: The Reference to EnergyPlus Calculations*, Morgantown, USA.
http://www.eere.energy.gov/buildings/energyplus/documentation.html

Visscher, K. and Veldhuis, J.B.J. (2005), 'Comparison of Candidate Materials for Seasonal Storage of Solar Heat Through Dynamic Simulation of Building and Renewable Energy System', *Proceedings of Building Simulation 2005, 9th International IBPSA Conference*, Montréal, Canada, 1285-1292.

Wentworth, W. E. and Chen, E. (1976), 'Simple Thermal Decomposition Reactions for Storage of Solar Energy', *Solar Energy*, 18, 3, 205-214.

Wolk, Ronald H. (1999), 'Fuel cells for homes and hospitals', *IEEE Spectrum*, 36, 5, 45-52.

Wu, J.Y., Wang, R.Z. and Xu, Y.X. (2000), 'Dynamic simulation and experiments of a heat regenerative adsorption heat pump', *Energy Conversion and Management*, 41, 1007-1018.

Yong, L. and Sumathy, K. (2002), 'Review of mathematical investigation on the closed adsorption heat pump and cooling systems', *Renewable and Sustainable Energy Reviews*, 6, 305–337.

Zmeureanu, R. (2005). Personal communication.

APPENDIX A

The model input values that are used to validate the model of the adsorption storage unit and its implementation in ESP-r are provided below. Table A.1 presents the model inputs for the comparison of the simulation results to (Lachance, 2003) in section 4.1.1. Table A.2 presents the model inputs for the comparison of the simulation results to (Leong and Liu, 2004a) in section 4.1.2. Table A.3 presents the model inputs for the sensitivity analysis carried out in section 4.2.

Table A.1 Model inputs for comparison with (Lachance, 2003)

Adsorption storage unit	
Mass of adsorbent (kg)	7.21
Specific heat of adsorbent (J/kgK)	850.83
Coefficient Wo of D-A equation (m^3/kg)	0.148E-03
Coefficient D of D-A equation (-)	0.15563E-06
Coefficient n of D-A equation (-)	2
Mass of adsorber vessel (kg)	40.24
Specific heat of adsorber vessel (kg)	544
Mass of adsorber heat exchanger (kg)	0
Specific heat of adsorber heat exchanger (J/kgK)	0
Enthalpy of adsorption (J/kg)	0.32E+07
Surface area of adsorber (m^2)	0
Thickness of adsorber insulation layer (m)	.025
Thermal conductivity of adsorber insulation (W/mK)	0.04
Overall heat transfer coefficient adsorber-surroundings (W/m^2K)	10
Condenser pressure (kPa)	8
Condenser heat exchanger effectiveness (-)	0.7
Mass flow rate of air entering condenser (kg/s)	0.05
Surface area of condenser (m^2)	0
Overall heat transfer coefficient condenser-surroundings (W/m^2K)	10
Condenser fan power rating (W)	200
Temperature of air entering condenser (°C)	8.3

Evaporator pressure (kPa)	1.5
Evaporator heat exchanger effectiveness (-)	0.5
Surface area of evaporator (m^2)	0
Overall heat transfer coefficient evaporator-surroundings (W/m^2K)	10
Temperature of heat source to evaporator (°C)	40
Delta T for determining dX/dT (°C)	0.05
Ambient temperature (°C)	20
Temperature of heat source (°C)	180
Adsorber-fuel cell heat exchanger effectiveness (-)	0.5
Pressure of adsorber-fuel cell heat exchange loop (kPa)	2000
Minimum temperature of heat source for charging unit (°C)	170
Temperature of heat sink (°C)	40
Adsorber-water tank heat exchanger effectiveness (-)	0.5
Pressure of adsorber-water tank heat exchange loop (kPa)	2000
Minimum temperature difference between adsorber and heat sink/source (°C)	0
Temperature of liquid adsorbate (°C)	35
Circulating pumps	
Component total mass (kg)	5
Mass weighted average specific heat (J/kgK)	2250
UA modulus from wall to environment (W/K)	0.2
Rated total absorbed power (W)	150
Rated volume flow rate (m^3/s)	0.3E-03
Overall efficiency (-)	0.7
Pressure (kPa)	2000
Water volume flow rate/adsorber-heat source (m^3/s)	0.00004
Water volume flow rate/adsorber-heat sink (m^3/s)	0.00004
Water volume flow rate/evaporator-heat source (m^3/s)	0.00009
Circulating pipes	
Component total mass (kg)	2
Mass weighted average specific heat (J/kgK)	2250
UA modulus from wall to environment (W/K)	2
Hydraulic diameter of pipe (m)	0.015

Length of pipe section (m)	5
Cross-sectional face area (m^2)	0.1767E-03
Pressure (kPa)	2000

Table A.2 Model inputs for comparison with (Leong and Liu, 2004a)

Adsorption storage unit	
Mass of adsorbent (kg)	17
Specific heat of adsorbent (J/kgK)	836
Coefficient Wo of D-A equation (m^3/kg)	0.311E-03
Coefficient D of D-A equation (-)	0.18023E-06
Coefficient n of D-A equation (-)	2
Mass of adsorber vessel (kg)	0
Specific heat of adsorber vessel (kg)	0
Mass of adsorber heat exchanger (kg)	0
Specific heat of adsorber heat exchanger (J/kgK)	0
Enthalpy of adsorption (J/kg)	0.32E+07
Surface area of adsorber (m^2)	0
Thickness of adsorber insulation layer (m)	.025
Thermal conductivity of adsorber insulation (W/mK)	0.04
Overall heat transfer coefficient adsorber-surroundings (W/m^2K)	10
Condenser pressure (kPa)	9.53
Condenser heat exchanger effectiveness (-)	0.7
Mass flow rate of air entering condenser (kg/s)	0.1
Surface area of condenser (m^2)	0
Overall heat transfer coefficient condenser-surroundings (W/m^2K)	10
Condenser fan power rating (W)	200
Temperature of air entering condenser (°C)	8.3
Evaporator pressure (kPa)	1
Evaporator heat exchanger effectiveness (-)	0.3
Surface area of evaporator (m^2)	0
Overall heat transfer coefficient evaporator-surroundings (W/m^2K)	10
Temperature of heat source to evaporator (°C)	20
Delta T for determining dX/dT (°C)	0.05
Ambient temperature (°C)	20
Temperature of heat source (°C)	210

Adsorber-fuel cell heat exchanger effectiveness (-)	0.5
Pressure of adsorber-fuel cell heat exchange loop (kPa)	2000
Minimum temperature of heat source for charging unit (°C)	100
Temperature of heat sink (°C)	25
Adsorber-water tank heat exchanger effectiveness (-)	0.5
Pressure of adsorber-water tank heat exchange loop (kPa)	2000
Minimum temperature difference between adsorber and heat source (°C)	10
Minimum temperature difference between adsorber and heat sink (°C)	20
Temperature of liquid adsorbate (°C)	20
Circulating pumps	
Component total mass (kg)	5
Mass weighted average specific heat (J/kgK)	2250
UA modulus from wall to environment (W/K)	0.2
Rated total absorbed power (W)	150
Rated volume flow rate (m^3/s)	0.3E-03
Overall efficiency (-)	0.7
Pressure (kPa)	2000
Water volume flow rate/adsorber-heat source (m^3/s)	0.00004
Water volume flow rate/adsorber-heat sink (m^3/s)	0.000035
Water volume flow rate/evaporator-heat source (m^3/s)	0.0002
Circulating pipes	
Component total mass (kg)	2
Mass weighted average specific heat (J/kgK)	2250
UA modulus from wall to environment (W/K)	2
Hydraulic diameter of pipe (m)	0.015
Length of pipe section (m)	5
Cross-sectional face area (m^2)	0.1767E-03
Pressure (kPa)	2000

Table A.3 Model inputs for sensitivity analysis

Adsorption storage unit	
Mass of adsorbent (kg)	20
Specific heat of adsorbent (J/kgK)	800
Coefficient Wo of D-A equation (m^3/kg)	0.311E-03
Coefficient D of D-A equation (-)	0.18023E-06
Coefficient n of D-A equation (-)	2
Mass of adsorber vessel (kg)	40
Specific heat of adsorber vessel (kg)	540
Mass of adsorber heat exchanger (kg)	50
Specific heat of adsorber heat exchanger (J/kgK)	540
Enthalpy of adsorption (J/kg)	0.32E+07
Surface area of adsorber (m^2)	60
Thickness of adsorber insulation layer (m)	0.250
Thermal conductivity of adsorber insulation (W/mK)	0.1E-01
Overall heat transfer coefficient adsorber-surroundings (W/m^2K)	4
Condenser pressure (kPa)	10
Condenser heat exchanger effectiveness (-)	0.5
Mass flow rate of air entering condenser (kg/s)	0.01
Surface area of condenser (m^2)	2
Overall heat transfer coefficient condenser-surroundings (W/m^2K)	4
Condenser fan power rating (W)	200
Temperature of air entering condenser (°C)	8.3
Evaporator pressure (kPa)	1
Evaporator heat exchanger effectiveness (-)	0.5
Surface area of evaporator (m^2)	30
Overall heat transfer coefficient evaporator-surroundings (W/m^2K)	4
Temperature of heat source to evaporator (°C)	40
Delta T for determining dX/dT (°C)	0.05
Ambient temperature (°C)	20
Temperature of heat source (°C)	200
Adsorber-fuel cell heat exchanger effectiveness (-)	0.5
Pressure of adsorber-fuel cell heat exchange loop (kPa)	2000
Minimum temperature of heat source for charging unit (°C)	100
Temperature of heat sink (°C)	40

Adsorber-water tank heat exchanger effectiveness (-)	0.5
Pressure of adsorber-water tank heat exchange loop (kPa)	2000
Minimum temperature difference between adsorber and heat sink/source (°C)	5
Temperature of liquid adsorbate (°C)	20
Circulating pumps	
Component total mass (kg)	5
Mass weighted average specific heat (J/kgK)	2250
UA modulus from wall to environment (W/K)	0.2
Rated total absorbed power (W)	150
Rated volume flow rate (m^3/s)	0.3E-03
Overall efficiency (-)	0.7
Pressure (kPa)	2000
Water volume flow rate (m^3/s)	0.00004
Circulating pipes	
Component total mass (kg)	2
Mass weighted average specific heat (J/kgK)	2250
UA modulus from wall to environment (W/K)	2
Hydraulic diameter of pipe (m)	0.015
Length of pipe section (m)	5
Cross-sectional face area (m^2)	0.1767E-03
Pressure (kPa)	2000

APPENDIX B

The input parameters that are specified for the adsorption storage unit in Chapter 5 are provided in Table B.1.

Table B.1 Model inputs for adsorption storage unit in Chapter 5

Mass of adsorbent (kg)	Case 3A	Case 3B
	7500	22500
Specific heat of adsorbent (J/kgK)	800	
Coefficient Wo of D-A equation (m^3/kg)	0.311E-03	
Coefficient D of D-A equation (-)	0.18023E-06	
Coefficient n of D-A equation (-)	2	
Mass of adsorber vessel (kg)	20	
Specific heat of adsorber vessel (kg)	540	
Mass of adsorber heat exchanger (kg)	50	
Specific heat of adsorber heat exchanger (J/kgK)	540	
Enthalpy of adsorption (J/kg)	0.32E+07	
Surface area of adsorber (m^2)	0 (heat losses neglected)	
Thickness of adsorber insulation layer (m)	0.025	
Thermal conductivity of adsorber insulation (W/mK)	0.04	
Overall heat transfer coefficient adsorber-surroundings (W/m^2K)	10	
Condenser pressure (kPa)	10	
Condenser heat exchanger effectiveness (-)	0.5	
Mass flow rate of air entering condenser (kg/s)	0.1	
Surface area of condenser (m^2)	0 (heat losses neglected)	
Overall heat transfer coefficient condenser-surroundings (W/m^2K)	10	
Condenser fan power rating (W)	200	
Evaporator pressure (kPa)	1	
Evaporator heat exchanger effectiveness (-)	0.5	
Surface area of evaporator (m^2)	0 (heat losses neglected)	
Overall heat transfer coefficient evaporator-surroundings (W/m^2K)	10	
Delta T for determining dX/dT (°C)	0.05	
Adsorber-fuel cell heat exchanger effectiveness (-)	0.5	
Pressure of adsorber-fuel cell heat exchange	2000	

loop (kPa)	
Minimum temperature of heat source for charging unit (°C)	60
Adsorber-water tank heat exchanger effectiveness (-)	0.5
Pressure of adsorber-water tank heat exchange loop (kPa)	2000
Minimum temperature difference between adsorber and heat sink/source (°C)	5
Temperature of liquid adsorbate (°C)	20